Faculty of Electrical Engineering

Department of Microelectronics

Biosensors Based on Nanocrystalline Diamond

Ing. Václav Procházka

DOCTORAL THESIS

Doctoral Study Programme: P2612 Electronics and Informatics
Doctoral Study Field: 2612V015 Electronics

Doctoral Thesis Supervisor: Ing. Pavel Kulha, Ph.D.
Doctoral Thesis Supervisor Specialist: doc. Ing. Alexander Kromka, DrSc.

Prague, 2022

Declaration

Student's name: Ing. Václav Procházka

Title of the doctoral thesis: Biosensors based on nanocrystalline diamond.

I hereby declare that this doctoral thesis is my work and effort written under the guidance of Ing. Pavel Kulha, Ph.D., and doc. Ing. Alexander Kromka, DrSc.

All sources and other materials used have been quoted in the list of references. All the co-authors on the referred publications have been acknowledged with equal authorship part. The doctoral thesis was written with the support of the projects: P108/12/G108, 15-33018A, LM2018110, TK02020094, SGS15/159/OHK3/2T/13, SGS17/136/OHK4/2T/13, and SGS19/112/OHK4/2T/13

In Prague on

Ing. Václav Procházka

Acknowledgements

First, I would like to thank my supervisors, namely doc. Ing. Alexander Kromka, DrSc. at the Institute of Physics of the Czech Academy of Sciences and Ing. Pavel Kulha, Ph.D., at the Czech Technical University in Prague for their careful guidance, for providing help and expertise throughout my studies, and for giving me opportunities for my personal growth and expansion of my knowledge in scientific activities.

My gratitude belongs to all my colleagues from the Institute of Physics of the Czech Academy of Sciences, who have been co-workers on various parts of my research and who provided me with technical assistance (SEM, AFM, Raman measurements, diamond depositions, etc.) and valuable suggestions. I would like to mention namely:
Ing. Tibor Ižák, Ph.D.; Ing. Marián Varga, Ph.D.; Ing. Štěpán Potocký, Ph.D.; Ing. Rajisa Jackiv; Mgr. Pavla Bauerová; Ing. Mária Domonkos, Ph.D.; RNDr. Pavla Štenclová, Ph.D.; Ing. Kateřina Aubrechtová Dragounová, Ph.D.; Mgr. Ekaterina Shagieva; Ing. Marie Krátká, Ph.D.; Mgr. Oleg Babčenko, Ph.D.; Ing. Ondrej Szabó, Ph.D.; Mgr. Jitka Libertínová; Dr. Egor Ukraintsev; prof. RNDr. Bohuslav Rezek, Ph.D. (currently at CTU); Kateřina Faltysová and Martin Faltys

Furthermore, I would like to express my gratitude to the Department of Microelectronics for their goodwill and for many opportunities to get valuable knowledge. In addition to my supervisor and other department members, I would like to thank namely: prof. Ing. Miroslav Husák, CSc.; Ing. Adam Bouřa, Ph.D.; Ing. Michal Kočí; doc. Ing. Václav Prajzler, Ph.D. and Ing. Alexandr Laposa, Ph.D.

Finally, I want to thank my family, which always supported me and provided me with a great deal of understanding and patience.

Abstract

This work deals with nanocrystalline diamond (NCD) thin films for biosensor studies and it is composed from authors peer-reviewed articles. It shows the basic ways to utilise and modify NCD for cell culture sensing, tissue sensing, and adhesive protein sensing. This research describes living matter interfacing bioelectronic sensors. Its goal is to develop a workflow from fabrication to the measurement and understanding of living material interaction on diamond-based biosensors represented by three different principles.

The first study deals with measuring the viability of the yeast cells (*Saccharomyces cerevisiae*) using the diamond SGFET sensor. The transfer characteristics of the SGFETs exhibit negative shifts of the gate voltage by –26 mV and –42 mV for sucrose and yeast peptone dextrose (YPD) with cells compared to blank solutions without the cells. This effect is explained by the local pH change in the close vicinity of the H-functionalised diamond channel due to the metabolic processes of the yeast cells. This approach paved the way for using NCD SGFET with new types of cell cultures (bacterial/fungi cells).

The second study focuses on sensing the viability of adult stem cells by NCD-coated impedance sensor employing interdigitated electrodes (IDT). For usability evaluation, the experiment has been done in parallel with the commercially used laboratory equipment to observe the difference in sensitivity. It was found that the diamond sensor is more sensitive during the initial phase of the cell growth, while the control system is more sensitive during the second ASC's growth phase. This work serves as a basis to stable surface functionalisation of the diamond, which enables the modification of cell cultures adhesion to the surface and opens the way for various new types of functional coatings.

The third study (diamond-based QCM sensor), which was until now used only as a gas sensor, investigates variation in adhesion of proteins on the NCD-coated quartz crystal microbalance (NCD-QCM). The serial resonance shifts of the sensor were analysed, and the level of adhesion of two fibrillar and globular proteins was evaluated by measurements. As follows, two types of surface terminations were compared, namely hydrophobic hydrogen termination and hydrophilic oxygen termination. Above that, the different time-dependent behaviour of protein adhesion on the O-NCD and H-NCD QCMs was observed. The study described the protein/NCD interface explaining the response of the NCD-QCM sensors and deepened the general knowledge of protein conformation on the surface based on its wettability.

This thesis verifies that diamond is an exciting material thanks to the combination of biocompatibility and vast possibilities of surface modification, which allows tuning electrical and chemical properties depending on the specific use in biology.

Keywords: nanocrystalline diamond, biosensors, surface modification

Abstrakt

Tato práce se zabývá tenkými vrstvami nanokrystalických diamantů (NCD) pro studie bio-senzorů a je tvořena komentovaným souborem autorových publikací. Ukazuje základní způsoby, jak využít a modifikovat NCD pro snímání buněčné kultury, tkáňových kultur a savčích adhezivních proteinů. Tento výzkum popisuje, jak živá hmota interaguje s diamantovým povrchem bio-senzorů. Jejím cílem je vyvinout pracovní postup od výroby po měření a porozumění interakci živých materiálů s bio-senzory na bázi na diamantu reprezentované třemi různými funkčními principy.

První studie se zabývá měřením životaschopnosti kvasinkových buněk (*Saccharomyces cerevisiae*) pomocí SGFET senzoru na bázi NCD. Přenosové charakteristiky SGFET senzorů vykazují negativní posuny napětí hradlové elektrody o hodnotu –26 mV a –42 mV pro sacharózu a kvasinkovou peptonovou dextrózu (YPD) s buňkami ve srovnání se stejnými roztoky bez buněk. Tento efekt je vysvětlen lokální změnou pH v těsné blízkosti vodíkem modifikovaného diamantového kanálu v důsledku metabolických procesů kvasinkových buněk. Tento přístup otevírá cestu pro použití SGFET senzorů na bázi diamantu s novými typy buněčných kultur (bakteriální buňky, buňky hub, části virů).

Druhá studie se zaměřuje na snímání životaschopnosti savčích kmenových buněk pomocí impedančního senzoru (IDT) pokrytého NCD. Pro hodnocení použitelnosti byl experiment proveden paralelně s komerčně používaným laboratorním zařízením pro otestování rozdílu v citlivosti. Bylo zjištěno, že diamantový senzor je citlivější během počáteční fáze růstu buněk, zatímco kontrolní systém je citlivější během druhé růstové fáze ASC. Tato práce přispívá k prokázání stability, biokompatibility odolnosti a univerzálnosti diamantového povrchu, který dále umožňuje modifikaci adheze buněčných kultur na povrch a otevírá cestu pro nové typy funkčních povlaků.

Třetí studie, zaměřená na senzor QCM pokrytý NCD, který byl dosud používán pouze jako senzor plynu, zkoumá adhezi proteinů na NCD v závislosti na smáčivosti povrchu. Byly analyzovány posuny sériové rezonanční frekvence senzorů a na jejich základě byla vyhodnocena míra adheze fibrilárních a globulárních proteinů. Senzory byly modifikovány dvěma typy povrchových zakončení, v prvním případě hydrofobní funkcionalizací vodíkem a v druhém případě hydrofilní funkcionalizací kyslíkem. Dále byla pozorována různá časově závislá adheze proteinů na O-NCD a H-NCD QCM. Tento výzkum popisuje rozhraní proteinu/NCD pomocí odezvy senzorů NCD-QCM a prohlubuje obecnou znalost konformace proteinů na povrchu na základě jeho smáčivosti.

Tato práce prokazuje, že diamant je vhodným materiálem, který kombinací biokompatibility a širokých možností modifikace povrchu, umožňuje ladění elektrických a chemických vlastností v závislosti na specifickém použití v biologických vědách.

Klíčová slova: nanokrystalický diamant, bio-senzorika, povrchová modifikace

List of acronyms

3D	Three Dimensional
AFM	Atomic Force Microscopy
ASC	Adult Stem Cells
BDD	Boron Doped Diamond
bioMEMS	bio Micro Electro Mechanical System
BSA	Bovine Serum Albumin
BVA	Bionic Vision Australia
CNT	Carbon Nano Tube
CVD	Chemical Vapour Depositon
DIW	DeIonized Water
DMEM	Dulbecco's Modified Eagle Medium
DNA	DeoxyriboNucleic Acid
ECM	ExtraCellular Matrix
EGFET	Extended-Gate Field Effect Transistor
FBS	Fetal Bovine Serum
FFF	Fused Filament Fabrication
FGF	Fibroblast Growth Factor
FN	Fibronectin
H-NCD	Hydrogen Nanocrystalline Diamond
HeLa	Human Cervical Carcinoma Cell Line (abbreviation from Henrietta Lacks)
HF CVD	Hot Filament Chemical Vapour Deposition
HIV	Human Immunodeficiency Virus
HNCD	Hydrogen Nanocrystalline Diamond
HPHT	High Pressure High Temperature
IDT	Inter-Digital Transducer
ITO	Indium Tin Oxide
JGS	Jain Glass Solutions
JGS	Jain Glass Solutions
MCD	Micro-Crystalline Diamond
ME-CVD	Microwave Enhanced Chemical Vapour Deposition
MEA	Micro-Electrode Array
MEMS	Micro ElectroMechanical System
MW	MicroWave
NCD	Nano-Crystalline Diamond
NCD-QCM	Nanocrystalline Diamond-based Quartz Crystal Microbalance
NEMS	Nano Electro Mechanicall Sensor
NV	Nitrogen Vacancy
O-NCD	Oxygen Nanocrystalline Diamond
PA-CVD	Plasma Assisted Chemical Vapour Deposition
PBS	Phosphate Buffered Saline
PCB	Printed Circuit Board
PCD	Poly-Crystalline Diamond

PDMS	PolyDiMethylSiloxane
QCM	Quartz Crystal Microbalance
RNA	RiboNucleic Acid
RT	Room Temperature
SaOS-2	Sarcoma osteogenic cells
SAW	Surface Accoustic Wave
SCD	Single Crystal Diamond
SEM	Scanning Electron Microscopy
SGFET	Solution-Gated Field Effect Transistor
SLA	StereoLithography
SRF	Serial Resonance Frequency
Tat	Trans-Activator of Transcription
UNCD	Ultra-Nano-Crystalline Diamond
UV	Ultra-Violet
YPD	Yeast Peptone Dextrose

List of figures

Table of Contents

1. Introduction

The presented doctoral thesis deals with the nanocrystalline diamond-based biosensors and their use with living matter to further describe the processes taking place during the interaction of cells and macromolecular proteins with the hydrophobic and hydrophilic surface of nanocrystalline diamond.

Diamond is considered a perspective material in cells and tissue-oriented life sciences. In addition to unique mechanical, thermal, and electrical properties, diamond is also biocompatible and exhibits two-dimensional hole-like surface conductivity, which is highly sensitive to changes in the surrounding environment due to the surface transfer doping mechanism [1,2]. Modern biosensors must be very sensitive and selective, easy to use and fabricate, portable, cheap, reliable, and optimally detect biological events in real-time. In the case of a diamond, the very best advantage lies in the possibility of durable and straightforward surface termination, which enables the adaptation of its properties to specific sensing needs.

The submitted thesis dissertation takes the form of a set of publications as per Article 1, paragraph 3 of the Dean's Directive for Defence of Dissertation Theses at Czech Technical University, Faculty of Electrical Engineering. It consists of 4 publications published in peer-reviewed journals and 7 contributions at international and national conferences in the field of biosensors in the last 6 years. The publications present the complete life cycle of the sensors from the design and fabrication across their use for living matter to the measurement, signal analysis and finally, the discussion and interpretation of the accumulated results.

As a result of this thesis, I have utilised a specific type of diamond (nanocrystalline) applicable for biosensors. There are three characteristic/representative sensor-working principles on which are demonstrated the usefulness and the great potential of diamond as a unique functional layer in biosensors. However, this work aims not only to prove the use of the diamond but its goal is also to demonstrate the possibilities of surface functionalisation of nanocrystalline diamond-based sensor elements. Sensors described in this thesis were designed, fabricated, and the sensor testing experiment elaborated as a proof-of-concept for future use of diamond films as label-free bio-electronic sensors working in real-time. Sensors were successfully tested in laboratory conditions to monitor the viability and motility of living cells and to investigate the properties of adhesive proteins depending on the wettability of the surface, and experimental findings were discussed and explained, and relevant results were published in peer-reviewed scientific journals.

Presented work was done within the scope of the projects listed in section 7.4 of this thesis.

1.1. Structure of the thesis

At the start, a concise theoretical introduction is provided to the topic of different forms of carbon. Since this work deals exclusively with the nanocrystalline diamond (NCD) in a thin-film form, the reader gets acquainted with different types of diamond and selected (bio-) sensors. Both topics are summarised in the state of the art research. Fusing those two broad areas of expertise results in a field of study focused on the sensing applications of diamonds.

In the experimental part, the reader gets acquainted with the utilisation of NCD in the form of diamond-based electrical biosensors for biological research. Sections 4.1 to 4.3 of the experimental part describe the detailed fabrication procedures. Following sections 4.4 to 4.6 describe laboratory uses of fabricated sensors in the biomedical research as the summary of published articles (integration text), further extended by the text describing the author's contribution and summarizing the novelty of the publications to the current state of the topics. The conclusion of the thesis summarises achieved goals and gives the reader an idea about the author's prospects. Full texts of the referred author’s articles are enclosed in the appendix.

1.2. Objectives

The main goal of this thesis is to generate new scientific knowledge on the interaction of nanocrystalline diamond (NCD) thin films with different types of living matter and to show the novel potentials of diamond thin films and their surface functionalisation in new ways not yet described. For the author to follow the line of research, multiple steps are necessary to achieve the main goal. First, suitable sensor principles must be selected. Also, the grown diamond layer must be compatible with the used technology to withstand the fabrication conditions. All the above is demanding on technological implementation, which is one of the goals of this dissertation. As suitable, the three diamond-based sensor types were found, each employing a different working principle.

Previous studies have already focused on the utilisation of semiconductive properties of diamonds in the form of SGFET. In this matter, I extended the present state of the art with my experimental findings by involving the non-adhesive living organisms, which differ from mammal cell interactions used until now.

The second suitable type is the impedance sensor in the form of the interdigitated transducer electrode (IDT, also called comb electrode). Although this sensor with gold electrodes has been already commercially used for sensing mammal cell cultures, it has not been used in such matter with superficially functionalised NCD thin film coating.

The third type of sensor is an acoustic sensor, specifically quartz crystal microbalance. In this case, an opportunity arises to use NCD thin film as an interfacing layer that can be easily and steadily functionalised with various molecular groups.

Other types of sensors are to be issued but to maintain the clear scope of the thesis; it covers only research to highlight significant achievements and findings. The main objectives can be summarised as follows:

- Conceptualise new use of existing and new types of NCD based biosensors
- Fabricate nanocrystalline diamond in sufficient quality for biosensors use
- Fabricate multiple sensors with different working principles and enhance their properties by using NCD
- Design and perform novel experiments with fabricated diamond sensors and biomaterial to discuss its “in-vitro” usability
- Expand the use of the developed SGFET sensors to other types of live organisms like bacteria or viruses
- Create a “proof of concept” using living cells and cultures on nanocrystalline diamond-based biosensors
- Discuss the measured results and propose a model describing ongoing effects to achieve new knowledge
- Based on the results, adjust a fabrication procedure, and update the design of the sensors to overcome their disadvantages

2. Motivation

2.1. Advantages of using diamond thin films

The most advantageous properties of the diamond are usually connected with its biocompatibility on the level of cellular interaction. Diamond in any form is biocompatible, where the level of biocompatibility is highly dependent on the content of the sp^2 phase of carbon and other (possibly toxic) contaminating molecules. In biosensors, the diamond's biocompatibility is assessed based on such purity. The motivation for my research is not limited strictly to biocompatibility; the main reason behind choosing diamond as a functional layer is the combination of optical transparency and the great possibility of surface modification of the diamond. Thanks to its carbon cubical lattice, diamond is perfect for bonding multiple types of molecules on its surface, all changing its chemical, macroscopic, and microscopic properties.

2.1.1. Surface termination

The diamond acts as an excellent carrier for surface functionalisation by atoms or atomic groups, aptamers, or other types of functional (bio-) molecules. In section 4.6, these properties were used to examine a protein adhesion to the terminated NCD.

2.1.2. Biocompatibility

One of the main topics of this thesis is the utilisation of the NCD and its biocompatibility in biosensors studies. In section 4.5. the properties of the diamond were utilised to monitor adipose-derived stem cells (ASC) and their growth from inoculation through confluency to the formation of additional layers. In addition, the inertness of the diamond is a great advantage when using it as a sensing material in section 4.4.

2.1.3. Morphology modulation

NCD offers excellent possibilities for surface morphology modification by changing the deposition time, the gas composition, or after-growth treatment. Cells differ in size and shape, and NCD can be morphologically adapted to suit the properties of cell cultures and living tissues.

2.1.4. Electrochemical window

Boron doped diamond (BDD) can act as an excellent electrode because of the diamond's very broad electrochemical window (highest of any known material, see Table 3.1). That means the wide potential range combined with the conductivity of BDD is predicting this type of diamond for use as a sensory implant, which enables us to use higher power levels before causing oxidation or reduction at the surface of the electrode.

2.2. Originality and novelty

The motivation of my thesis is to employ multiple of the abovementioned properties of the NCD to create a novel biosensor or use an existing diamond-based biosensor in a novel way. I intend to utilise the biocompatibility of the NCD, the chemical inertness with living organisms, the wide electrochemical window of NCD, the surface conductivity induced by hydrogen termination and most importantly, the stability and ease of surface functionalisation under room conditions.

2.2.1. NCD as a platform for biosensors

There are sensing principles that have not been used with NCD before as a biosensor for detecting living culture. For example, the IDT electrode (electrical sensing) is widely used to monitor mammal cell culture growth, but such a sensor is based solely on gold electrodes, which may expose the culture to higher currents than being coated with NCD.

Piezoelectric principles offer such possibilities in the form of acoustic sensors such as QCM or SAW sensors. Generally, acoustic sensors are often overcoated with a functional layer to increase sensitivity and specificity. With thin NCD film on the sensor's surface, a variety of surface modifications can be added among the abovementioned benefits.

Amongst other principles, it is worth mentioning optical biosensors. This field promises exciting possibilities, although the use of NCD in this field is currently in the phase of theoretical considerations. Regarding my field of study, this work is focused on electrical sensors.

2.2.2. Novel use of NCD-based biosensors

There are NCD based sensors that have already been under research in past years, e.g., SGFET sensor which has been used to monitor sarcoma osteoblast (SaOS-2) and HeLa culture, but never as the tool for monitoring the viability of nonadherent cells as yeast cells or other types of bacteria/fungi. One of my goals is to investigate NCD-based SGFET under the influence of nonadherent cell culture and understand the relation between modulation of SGFET’s characteristics and cell culture viability. Moreover, I intend to extend my research on SGFET by modifying the conductive channel with functional molecules (aptamers, carbonyl, and others).

As diamond can act as an insulator and semiconductor at once, it can be used for multisensory purposes, where it combines stimulator in the form of SGFET or IDT electrodes with applied voltages on and QCM measurement in a single sensor chip.

3. State of The Art

3.1. Carbon Forms

All life forms on Earth consist of many atoms of most of the elements on the periodic table. Some of the atoms play an essential role in metabolic mechanisms, and some are, despite being present in small amounts, redundant or even toxic, and some as carbon, are essential in every role we can think of. Carbon is essential for all forms of life on Earth and is without a doubt one of the most important natural elements in the periodic table. It is the 17th most abundant element in the Earth's lithosphere and the 2nd most abundant element in the human body [3].

Carbon can perform various bonding hybridisations and forms, enabling the existence of life (combined with other elements) as we know it. Its variability predetermines the diamond as the element around which the world is turning around. Whether it is the circulation of CO_2 in the atmosphere and through the biomass of all living things or the energy we use every day in the form of oil, coal, or gas, carbon has many utilisations for modern society. We are slowly learning to use carbon in other ways than burning it to produce energy as it was for long years.

Allotropes of carbon have also received considerable attention due to their usefulness in material science [4]. Generally, there is a need for materials that shows almost ideal physical characteristics in any physical way. Carbon allotropes of all dimensionalities are known, but there is no consensus on how many are defined at present. Moreover, other new forms are predicted (e.g., Me-graphene, 2020) [5]. The most well-known allotropes of carbon are graphite (1917), fullerene (1970), nanotube (1991), graphene (2004), nanobud (2006) (Figure 3.1), (nano-)diamond, nanofoam, nanoribbon, nano-horn, nanosheet and others [6].

This structural diversity allows many different types of scientific and technological utilisation. Carbon forms are suitable for all kinds of applications, depending only on molecular conformation, whether it is superconductivity at room temperature (graphene), high thermal conductivity, biocompatibility (diamond), molecular charge transport (CNT), or the possibility to carry functional molecules inside (C60 – C540).

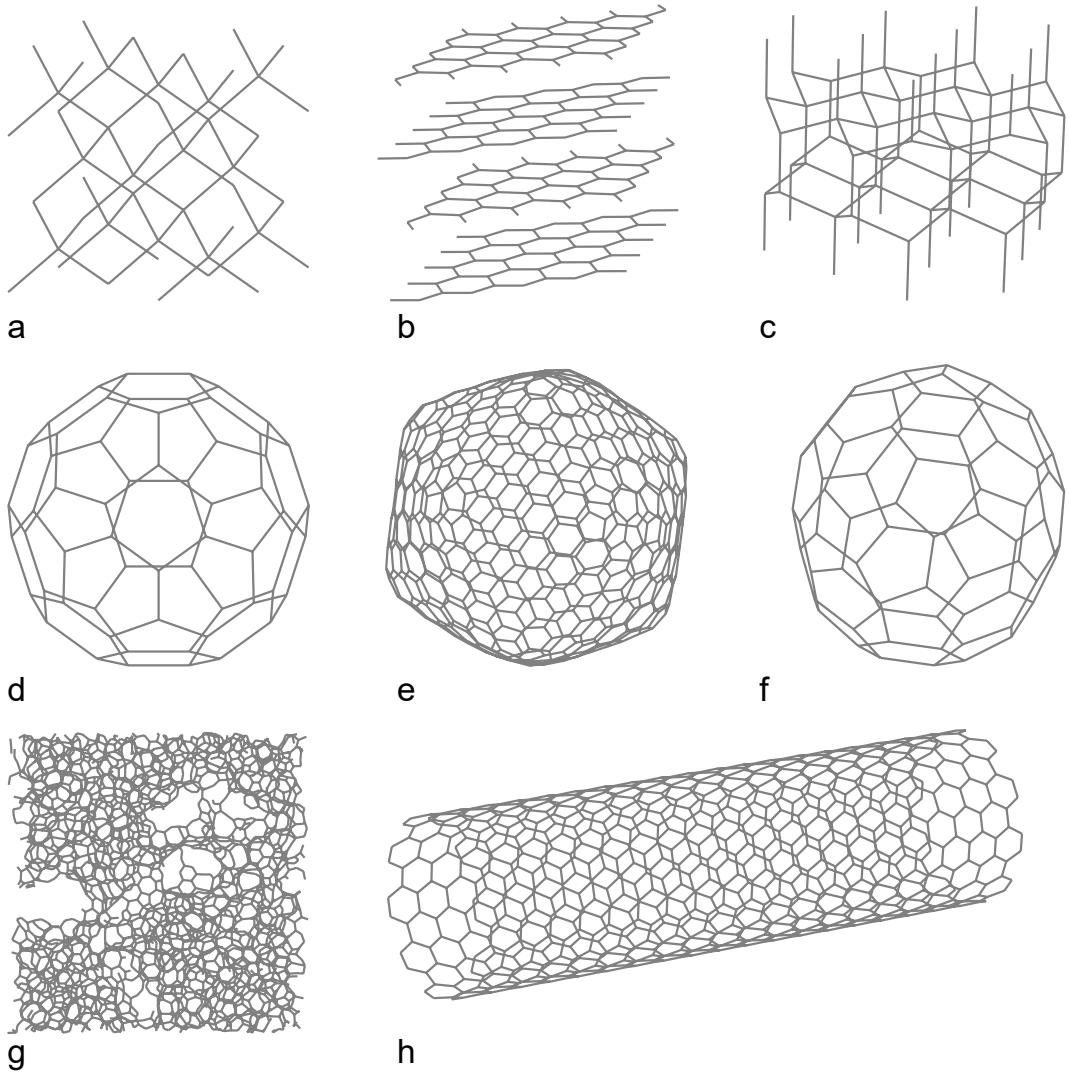

Figure 3.1 a) Diamond: b) Graphite, c) Lonsdaleite, d) C60 buckyball, e) C540, f) C70, g) Amorphous carbon, and h)single-walled carbon nanotube [4].

The extreme and well-defined conditions, as well as the purity of reactants, have to be secured, causing some molecular conformations to be challenging to achieve, which is apparent from the carbon phase (pressure/temperature) diagram in Figure 3.2. This transformation is a field of science of its own, and this thesis is concerned exclusively with the fabrication of diamond which is indisputably the most biocompatible form of all carbon-based materials. Plenty of studies focused on the use of its unique extreme properties as it is also partly the focus of the presented thesis.

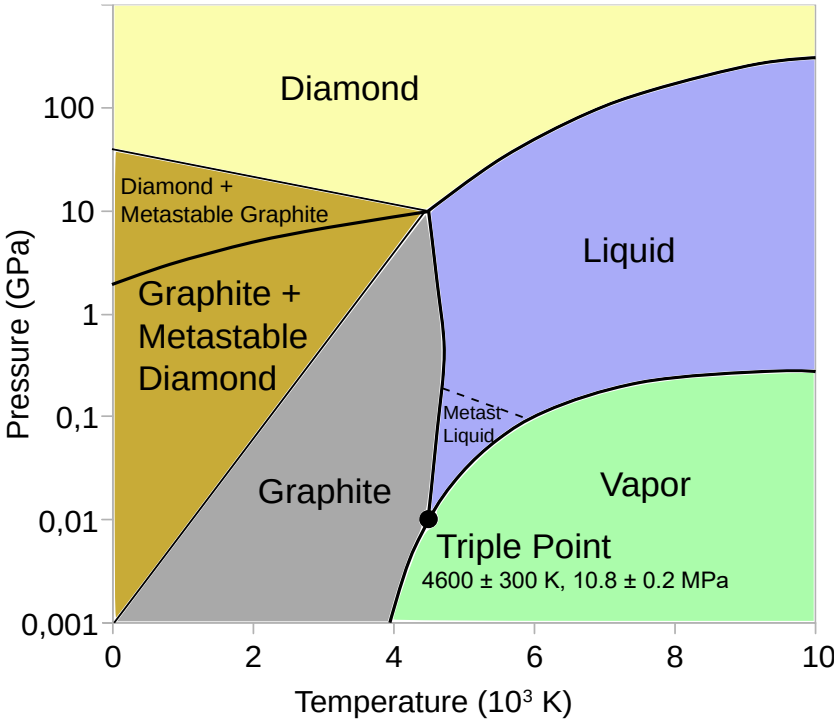

Figure 3.2 Phase diagram of carbon [7]

The neutral carbon atom bears six electrons – two tightly bound (1s) close to the nucleus and four as valence electrons (two in the 2s subshell and two in the 2p subshell) [8]. The ground-state electron configuration of carbon ($1s^2 2s^2 2p^2$) allows it to bond in three different ways (single, double, and triple bonds) and with many different elements. For this reason, carbon manifests itself in many different allotropic forms with entirely different properties [9]. All of them have the same building block, the carbon atom, but their crystalline structure is different. The three basic carbon allotropes with an integer degree of carbon bond hybridisation are carbine, graphite, and diamond, corresponding to sp, sp^2 and sp^3 hybridisation of the atomic orbitals (Figure 3.3) [10,11].

- sp hybridisation (linear): one s-orbital hybridises with one of the p-orbitals to make two sp-hybridized orbitals. The angle between these new orbitals is 180°, and the carbon atom bonds by a diagonal symmetry.
- sp^2 hybridisation (trigonal planar): one s-orbital is mixed with two p-orbitals to form three hybridised orbitals with a trigonal symmetry and characteristic 120° angles between them [10].
- sp^3 hybridisation: each carbon atom is arranged tetrahedrally. Each tetrahedron combines with four other tetrahedra and forms a strongly bonded, entirely covalent face-centred cubic crystal structure (Figure 3.1a). Diamond can also exist in a hexagonal (lonsdaleite) form [12].

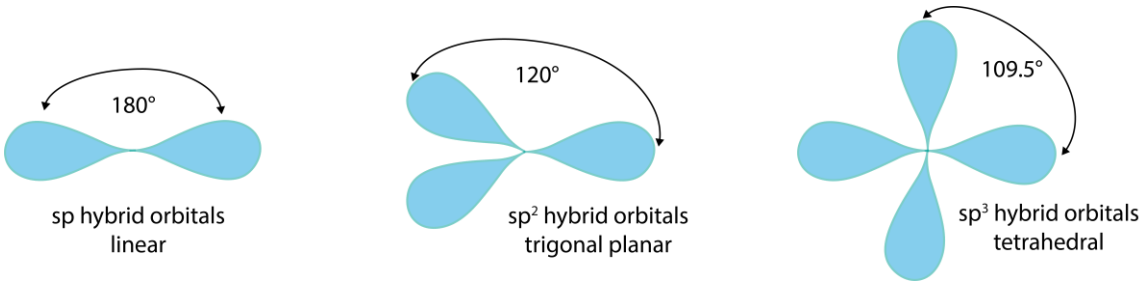

Figure 3.3 Drawing of sp, sp2, and sp3 hybrid orbital [10].

Diamond

Diamond (Figure 3.1) is an allotrope of carbon that is being considered for use in several medical applications. Its crystal exhibits a higher atomic density ($1.76 \cdot 10^{23}$ cm^{-3}) than any other solid. The high bond energy between two carbon atoms (83 $kcal \cdot mol^{-1}$) and the directionality of tetrahedral bonds are the main reasons for the high strength of the diamond. Diamond demonstrates the highest Vickers hardness value of all materials (10 000 $kg \cdot mm^{-2}$). The coefficient of friction of polished diamond is 0.07 in argon and 0.05 in humid air. Diamond is resistant to corrosion at temperatures over 800 °C, except in an oxygen atmosphere. Also, some types of diamond have the highest thermal conductivity of all materials (20 $W \cdot cm^{-1}K^{-1}$ at room temperature). See summarisation in Table 3.1. Diamond is considered a perspective material in cells and tissue-oriented life sciences. Related to that, it is an ideal substrate for surface functionalisation thanks to the vast and known carbon-based chemistry [13]. In addition to unique mechanical, thermal, and electrical properties, diamond is also biocompatible and exhibits surface conductivity which is highly sensitive to changes in the surrounding environment due to the surface transfer doping mechanism and no need for a gate dielectric layer. Recently, a new generation of bio-electronic devices is being developed based on the p-type surface conductivity (superficial functionalisation with H), or B for p-type and P for n-type doping of the diamond thin film [1]. The primary division of the diamond materials is from the top level as monocrystalline and polycrystalline; in this thesis, I focus exclusively on the nanocrystalline diamond thin film, which is polycrystalline.

Table 3.1 The physical properties of chemical vapour deposited (CVD) diamond [14–18]

Properties	CVD Diamond
Hardness	10 000 $kg \cdot mm^{-2}$
Thermal conductivity	20 $W \cdot m^{-1} \cdot K^{-2}$ (at 300 K)
Electron mobility	4500 $cm^2 \cdot V^{-1} \cdot s^{-1}$
Hole mobility	3800 $cm^2 \cdot V^{-1} \cdot s^{-1}$
Bandgap	5.47 eV
Density	3.52 $g \cdot cm^{-3}$
Melting point	4027 °C

Resistivity	10^{20} Ω·cm
Bond length	1.54 Å
Bond angle	109.47°
Bonding	sp^3
Dielectric constant	5.7
Refractive index	2.41 (at 591 nm)

3.2. Polycrystalline diamond (PCD)

Polycrystalline diamonds can be further divided according to the process of growth and the resulting size of crystals.

3.2.1. Microcrystalline diamond (µCD or MCD)

Microcrystalline diamond (MCD) is commonly prepared by chemical vapour deposition (CVD). Its fabrication is done by ionisation of gases in microwave plasma of methane in which the carbon is highly represented. MCD occurs in specific conditions when nanocrystalline diamond (NCD) thin film is deposited for a long time without re-nucleation. Strong re-nucleation results in the evolution of small grain sizes, causing nanocrystalline of ultra-nanocrystalline growth, see Figure 3.4 [20]. Large crystals can be divided into smaller pieces depending on the application after fabrication. It can be accomplished using molten iron and aluminium at high temperatures and pressure [19]. The diamond can be further polished with various methods and processes summarized in [20].

3.2.2. Nanocrystalline diamond (NCD)

Nanocrystalline diamond thin films are usually referred to as diamonds with a grain size of less than 0.5 µm with suppressed re-nucleation. NCD-based thin films or grains embedded in binder are widely used in industry as a coating for hard material cutting tools. The nanocrystalline diamond offers an interesting compromise joining the properties of bulk diamond in the thin layer embodiment. It exhibits good enough electron/hole mobility and thermal conductivity, which is mainly limited by the scattering of electrons/holes on grain boundaries [21,22].

First, it is necessary to distinguish between the use of NCD in the form of individual nanoparticles or a thin film.

In biology and medicine, the use of NCD nanoparticles is researched as one of the progressive methods for drug delivery and tracking pathways of molecules. The particle's surface is grafted with a functional molecule on its surface and serves as the selective point, which binds with a target molecule, concentrating nanocrystalline particles at a specific location [23,24]. Another use of diamond nanoparticles is fluorescence imaging. If nitrogen-vacancy centres are introduced into a nanoparticle,

some cellular biomolecules display autofluorescence. The emission intensity is well above the background signal [25].

In the form of NCD as the thin film, the research activities are broader (passivation layer, functional layer, layer for MEMS, and others). For example, the study where the NCD coated steel and titanium substrates were colonised with bacteria revealed exciting results on their biocompatibility. NCD exhibited the highest resistance to the process of bacterial colonisation. It was found that the rate of biofilm formation is firmly dependent on the presence of adhesive proteins in the medium [26]. In another study, the adhesion of platelets was tested to investigate the suitability of NCD for use as a coating for medical applications. The platelets did not attach to the NCD surface, but they did attach in spots with low homogeneity of NCD thin film [27,28]. The main idea is to use NCD as a functional coating for medical implants, but the problems with poorly defined effects on the interface, homogeneity and delamination remain. For those reasons, there is a need to develop new ways of surface treatment.

3.2.3. Ultra-nanocrystalline diamond (UNCD)

The smallest grain size diamond film is called ultra-nanocrystalline. Its grain size is less than 10 nm, and because it is easier made on metal substrates than NCD, it is a very suitable material for implantable medical devices [29]. Thus, it is more appropriate for the fabrication of bio-MEMS and retinal implants. UNCD is fabricated by a similar procedure as NCD diamond, usually at a lower temperature, approx. 200 – 400 °C with a higher concentration of CH_4. A higher concentration of argon gas (Ar) or nitrogen gas (N_2) is injected. Its exact amount is dependent on deposition temperatures and substrates [20]. The structural difference between MCD, NCD, and UNCD is shown in Figure 3.4. and Figure 3.5. As shown, during deposition of UNCD occurs continuous re-nucleation in layers.

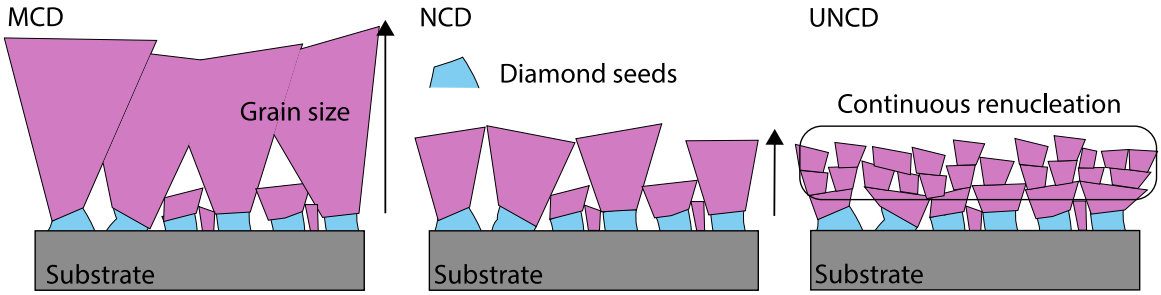

Figure 3.4 Left: MCD structure, Middle: NCD structure, right: UNCD structure of diamond [32].

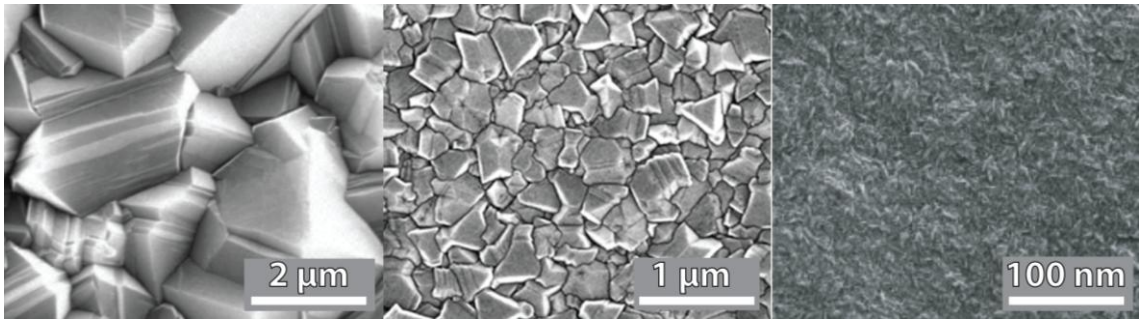

Figure 3.5 Scanning electron microscopy images of a) microcrystalline diamond, b) nanocrystalline diamond and c) ultra-nanocrystalline diamond. Notice the scale [30–33]

3.3. Fabrication of diamond

There are two basic methods to induce the growth of the synthetic diamond (not to mention natural diamonds creation)

The oldest and most straightforward is the fabrication of diamonds using high pressure and high temperature (HPHT) or detonation nano-diamond (DND). Those methods applied high pressure (in order of GPa) and high temperature to obtain a synthetic diamond. The HPHT method is used usually to produce a monocrystalline diamond. However, due to uncontrollable conditions during this type of diamond fabrication, the diamond particles, as well as diamond thin layers and flakes, are produced. The DND method of fabrication is used to produce diamond particles.

3.3.1. The technology of NCD fabrication

The other type of technology procedure used to fabricate diamonds is chemical vapour deposition (CVD).

CVD low-pressure deposition is performed in two types of equipment, which differ in how plasma is spread in the deposition chamber and in how plasma is generated, as shown in Figure 3.6.

The standard methods according to the way how plasma is generated are plasma jet, dc discharge (presently used less often), hot filament (HF) CVD (producing diamond in lesser purity) and microwave enhanced/assisted (ME) CVD producing a diamond thin film of a higher purity in compare with HF-CVD.

In the scope of my research, I focused on ME-CVD, which we can further divide by how plasma is spread during deposition. Linear microwave-frequency plasma (Figure 3.6a) is most often used for deposition of diamond on substrates or larger area ($> 15 \times 15$ mm^2), while elliptical focused plasma and bell resonator focused plasma (Figure 3.6 b and c) is rather used for smaller substrates, faster growth and for effective surface functionalisation. The process of diamond growth is done as follows [15,34].

1. Activation into radicals
2. Gas-phase chemical reactions
3. Gas-phase chemical reactions between activated species
4. Reaction with the substrate
5. Nucleation and growth of individual crystallites [35]

The most used method is currently a low-pressure synthesis of the diamond through plasma-enhanced chemical vapour deposition (PE-CVD), which uses a mixture of gases (CH_4, CO_2 and H_2 for non-diamond phases purification) ionised by microwave antennas, which as a source of energy creates plasma (other sources can be thermal, optical, etc.). The proper procedure creates a diamond phase near the substrate's surface, binding with the present nucleation centre to the substrate that eventually grows into a continuous diamond layer. A specific description of microwave PE-CVD reactors and the generic conditions used during my research can be found below.

Low-temperature CVD reactor (Diffusion plasma)

During this type of deposition, the growth rate is much slower than in high-temperature plasma, but the deposition area is bigger and the temperature lower than with focused plasma. This is especially beneficial for big planar substrates, where the high homogeneity of large deposition areas can be achieved. The temperature during deposition lies between 350 °C – 550 °C, which enables deposition on a surface with relatively higher thermal expansion, such as microscopy glass, or common substrates with low thermal expansion, such as Corning Eagle XG®, borosilicate glass, or JGS® grade A, B [36].

High-temperature CVD reactor (Focused plasma)

This type of deposition progresses in a much smaller volume of plasma but with much greater intensity and growth speed. Therefore, it is suitable for thicker diamond depositions with excellent homogeneity and resulting purity of the diamond. Nevertheless, this technology can be used only with substrates that can resist high temperatures during deposition, such as Corning Eagle XG®, JGS Grade A, B®, and the effective area of the deposition is much smaller. The temperature may vary from 600 °C to roughly 1500 °C, depending on the deposition chamber, microwave power, and heat conductivity of the sample and the holder [37].

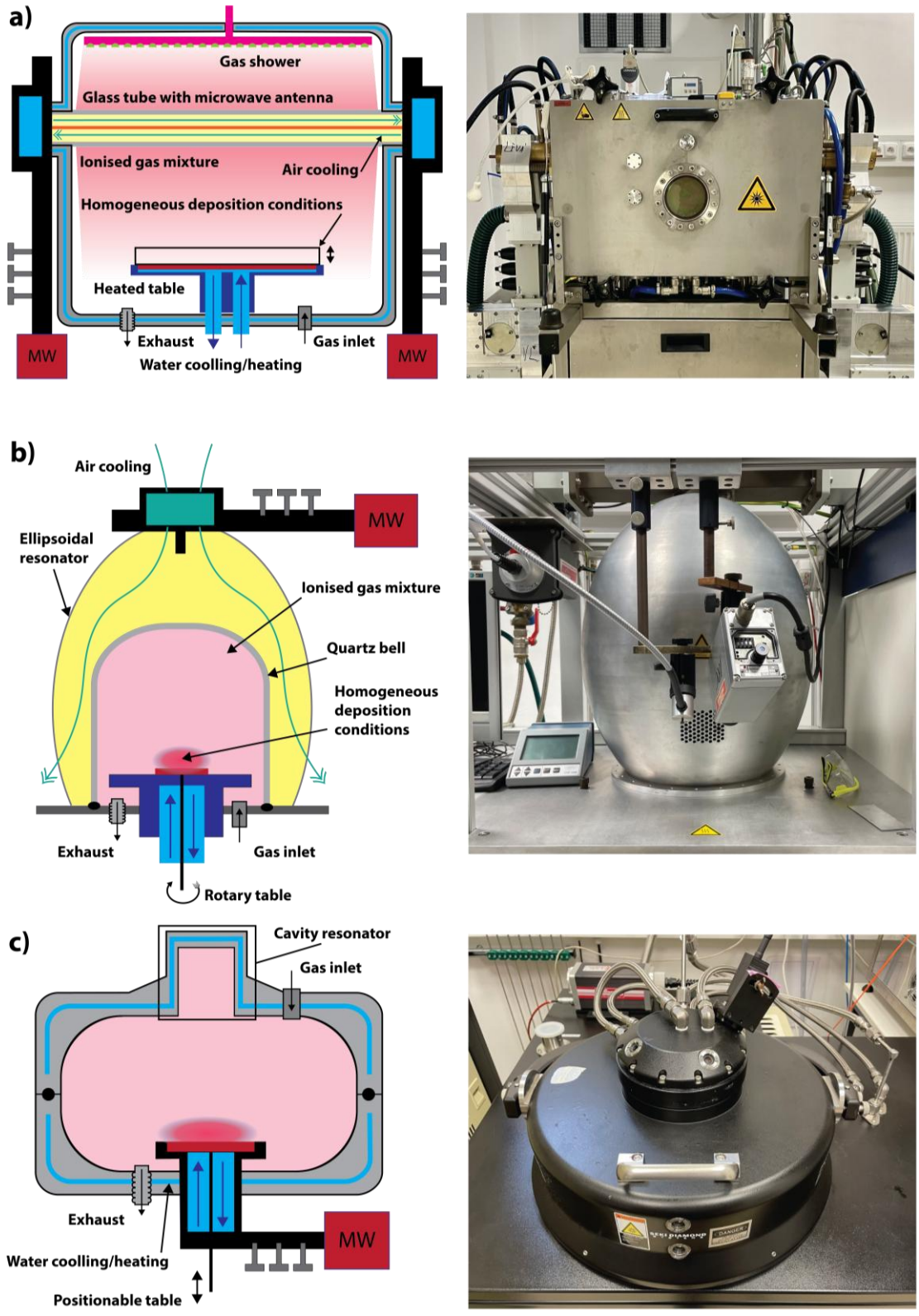

Figure 3.6 a) Linear deposition chamber (Roth&Rau® AK400), b) Ellipsoidal deposition chamber with focused plasma (Aixtron®), c) Bell resonator deposition chamber with focused plasma (SEKI®) [42]

3.3.2. Deposition conditions and standard procedures

The generic deposition conditions used to fabricate nanocrystalline diamonds are described in this section, which has been referred to further in the text. NCD is fabricated for biosensors, and it was utilised to monitor living cultures and characterise protein adhesion and cell culture adhesion on NCD surfaces. Each of the sensors appeals to the different properties of a nanocrystalline diamond as the main advantage of such an enhanced sensor.

SGFET sensors were made on quartz glass substrates. Corning Eagle XG® glass substrates (in the size of $10 \times 10 \times 1$ mm^3) were ultrasonically cleaned in isopropyl alcohol and deionized water (DIW). Subsequently, they were immersed for 10 minutes in an ultrasonic bath with a colloidal suspension of diamond nano-powder with a nominal particle size of approx. 5 nm. This process formed a 5 to 25 nm thin layer of diamond powder necessary to initiate the diamond growth in a thin film. NCD thin films were grown in a microwave ellipsoidal cavity reactor by chemical vapour deposition (CVD) process for 4.5 hours, at the following conditions: gas pressure 30 bar, gas mixture 1 % CH_4 in H_2, and microwave power 1000 W. The deposition temperature was in the range of $550 \div 600$ °C. These deposition parameters led to the growth of approx. 450 nm thick diamond film with grain sizes approx. 250 nm [21]. Diamond films on glass substrates were hydrogenated in the same microwave plasma reactor at 600 °C in a microwave-induced hydrogen plasma for 10 minutes to induce surface conductivity. After surface treatment, the chamber was slowly filled with nitrogen (N_2) to maintain H-termination on the substrate surface.

Metal composite inter-digitated electrodes form the interdigitated transducer sensor (IDTs, 10 nm Ti and 80 nm Au) deposited on a quartz substrate (Corning Eagle XG®, $15 \times 15 \times 1$ mm^3 in size). The width/gap of electrode periodicity was set to 100 µm. Samples with IDTs were coated with a diamond layer approx. 100 nm thick, using a linear antenna pulsed microwave plasma chemical vapour deposition system [38]. The deposition conditions were as follows: microwave power 2×1700 W, pressure 0.1 mbar, gas mixture 200 / 5 / 20 sccm of H_2 / CH_4 / CO_2, temperature 400 °C, and process time 50 h. After deposition, the active sensor area was homogenously covered with a fully closed NCD film. The diamond character of the deposited film is confirmed after deposition by Raman spectroscopy [39].

QCMDs were made from both-side polished AT-cut (35° 15') quartz crystal plates with a diameter of 14 mm and thickness of 170 µm. Two key-hole-shaped electrodes with diameters of 5 mm were deposited on both sides by vacuum deposition. The electrodes were composed of a 30 nm Cr adhesion layer and a 100 nm. top Au layer. The mass-sensitive area is situated in the central part of the resonator, covering the area where the two electrodes are overlapped, thus creating the thickness-shear mode resonator (See Figure 4.6) [40]. The effective sensing area on the gold electrode is

25 mm^2. QCMs were nucleated by ultrasonic seeding with diamond powder in deionized water, grown by pulsed linear antenna microwave plasma chemical vapour deposition system [41] at a temperature lower than 400 °C. Such deposition conditions were used (microwave power 1700 W, pressure 0.1 mbar, gas mixture 100 / 5 / 20 sccm of H_2 / CH_4 / CO_2), which resulted in a diamond film thickness of approx. 200 ÷ 300 nm. Afterwards, the diamond surfaces were hydrogen and oxygen-treated by appropriate plasma procedures to obtain hydrophobic or hydrophilic character.

3.4. Diamond-based sensors

Sensors using diamond layers have been the target of the research for about 30 years now. In medicine and biotechnology, there is a need to characterise biomaterials, for example, different kinds of proteins, their hydrophilicity, and change of conformation. The characterisation of structural changes of macromolecules contributes to a more profound knowledge of biomolecular processes. The most significant advantage of diamond-based sensors is that living culture can be monitored "in vivo" without its destruction, and the diamond surface can be easily tailored for any application. The cells and tissues can be cultivated directly on the sensor, and they can be non-destructively monitored and stimulated. As further described, the use of the diamond is not limited only to a biosensor study, but its use is expanded to many more sensory fields.

3.4.1. Electrochemistry

In the pure state, an intrinsic diamond is an excellent insulator. When properly doped, the diamond excels as an electrode in the field of electrochemistry. Thus, for this purpose, it must be doped with boron to achieve p-type conductivity with high carrier mobility. The benefits of using a diamond in electrochemistry are mainly the wider potential window and lower background currents in aqueous solutions. Another type of treatment which customises diamond as an electrode is the surface functionalisation with hydrogen. After this treatment, the diamond electrode is highly sensitive to the ionic strength of the solution and pH [42,43]. The boron-doped diamond (BDD) has been extensively used in water treatments as it can effectively generate ozone and hydroxyl radicals with minimal degradation of the BDD electrode [44]. More detailed electrochemical properties of diamond are out of the scope of this thesis, but a reader with more profound interest is pointed to [45–47].

3.4.2. Mechanical sensor, nanomechanical sensing, and quantum nano-sensors

When we are talking about the use of the diamond as a mechanical sensor, we discover that the piezo resistance of the diamond is utilised in most work published in the field

of diamond mechanical sensing. Boron doped diamond will change electrical resistance with strain (piezo-resistance), meaning it can be used as a strain gauge on rugged electronic microsensors for pressure and acceleration sensing at high temperatures up to 170 °C or 250 °C [48–50]. From the measurement of the macroscopic properties, diamond also found its way to measure nanomechanical properties of sample molecules in nano electro-mechanical systems (NEMS). Nitrogen vacancy (NV) centres in diamonds are being used to locate single elementary charges. Embedded NV in diamond offers a great perspective for quantum sensors [51] and nano-sensing applications. Recent discoveries in the field of quantum sensing shifted the spotlight of diamond research to one area, which is the area of quantum computing. The diamond is being extensively tested for new emerging quantum technology. Diamond is a very attractive material with a long coherence time. NV centre in a diamond can perform as a qubit at room temperature. Photoelectrically read NV centre in a diamond can be utilized as a bridging device between basic quantum processor unit and nanoscale electronic, enabling photoelectric quantum gate operations [52–54].

3.4.3. Gas sensors

Diamond can be used as a sensitive layer for detecting the single-molecule substances and macromolecular and even the whole organism, just by a change of structure and surface functionalisation (e.g., SGFET). Sensors based on the diamond are recently used as gas detectors and sensors sensitive to specific gases such as hydrogen, water vapour [55], ammonia, and carbon dioxide [40,56]. A similar application is found in the pH sensitivity of SGFET transistor based on hydrogen-terminated diamond [57]. Termination with hydrogen offers sensitivity to the surrounding gas environment due to induced surface conductivity [58]. With the use of surface functionalisation, a broad spectrum of gas sensing applications can be found [59–62].

3.4.4. Deoxyribonucleic acid (DNA) and protein sensors

DNA sensors based on diamond thin films are another subject of research with great perspective. Existing sensors often use amine, carboxyl, or thiol termination necessary for biomolecule immobilisation. The detected biomolecule is immobilised on the surface of the biosensor and forms a layer. There is high capacitive binding between layers of the solid surface channel and liquid electric double layer on the surface. This enables the detection of DNA aptamers influenced by the distance between layers and polarity of the molecule [63]. Another type of detection is the fluorescence of DNA binding on diamonds [34]. In another study, enzyme-modified field-effect transistors were realised using acetylcholinesterase and penicillinase as detection layers of specific enzymatic reactions [64]. The surface of the diamond sensor can also be chemically modified by organic layers, which again serve as linking biomolecules of solid surface

and specific protein [65]. The biomolecular layer leads to changes in the conductivity of the interface, altering the conductivity of the diamond thin film [66].

3.4.5. Cell culture sensors

In the field of direct electrical measurement of living cells, several approaches are used to investigate the properties of the cell membrane and cell/surface interface. One of the common techniques is direct impedance measurement of cells by microelectrode array (MEA) or Interdigitated Transducer (IDT) electrode [67–69]. The patch-clamp contacting the cell by microelectrode is the method for measuring living cells' surface potentials [8] and estimating the cell's behaviour “in vivo”. However, it is a technological challenge whether the excitable or non-excitable cells are used [70–73]. Another study was performed by observation of the cell aggregation influence on impedance spectrum, measured between microelectrodes and one referent electrode [74]. A possible way is a measurement by patch-clamp technique, more explicitly monitoring of cell viability as was described in [75].

From all the above, I found a solution-gated field-effect transistor with functionalised diamond suitable for the measurement of cellular electrostatic effects. These devices, so-called solution-gated field-effect transistors (SGFETs), have found vast use in the study of solution/cell-surface interactions, living microorganisms, and tissue cells as biocompatible sensors [76]. Most of the experiments focused on the adherent type of cells are aimed to describe the influence of the functionalised diamond on cell cultures and its common interaction [77,78]. The surface wettability can be tailored during fabrication by specific termination (by hydrogen and oxygen or its combination). Effects such as the dependence of the conductivity on the grain size [79], pH sensitivity of SGFETs [66], protein adsorption [80], and disruption of the semiconductive properties by adhesive proteins were described [81].

3.4.6. Tissue sensors

The functionalised diamond was used in several studies for the pattern-guided formation of glial and retinal neuron networks. It was found that the function of the adhesive cell growth on the diamond surface was not disturbed [82,83]. This makes a diamond perfect solution for a photosensitive retinal prosthesis and neural interfacing device [84]. In advance, nonconventional boron-doped nanocrystalline diamond (B-NCD) was used as an interfacing device [85]. Diamond-based biosensors are not limited only to excitable neuron cells. It can be used in situations when the tissue cannot be observed by conventional techniques (optically, exposing the cell culture to light), and its condition must be monitored without any invasion in the sterile incubator. Such a sensor should be biocompatible in the long term, and it should not electrically influence the measured sample. The interdigital transducer (Figure 3.11) is perfectly

suitable for this kind of application. In this research, adult stem cells (ASC) were used as a sample for impedance characterization "in vivo", as described in section 4.5. Monitoring cell settlement, proliferation and differentiation in the body-like conditions is one of the targets of future work. The application of diamonds is summarised in Figure 3**.7**, with the main division between therapeutic use and diagnostic use.

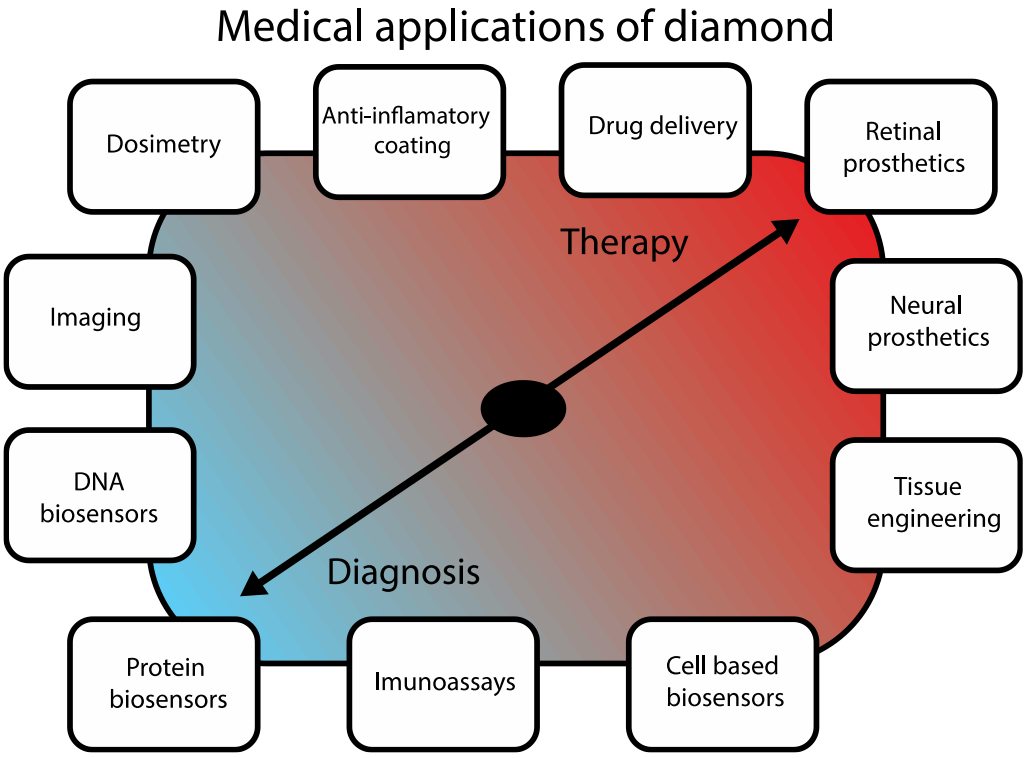

Figure 3.7 Applications of diamond thin films and diamond nanoparticles in biomedicine [13]

3.5. Biosensors

Nowadays, in biotechnology and molecular biology, most of the methods are based on biochemical processes, dyes, and optical observation. These methods are often destructive and based on subjective evaluation methods. There is a need for non-destructive, objective, and simple to use cell / tissue monitoring techniques. Biosensors have great yet unfulfilled potential in live sciences. Its properties characterise each sensor according to the form of energy domain they transform, the type of signal they produce, or the properties of such signal. Although it is necessary to know how the sensor works and what modulates the signal it produces, we often distinguish between time and frequency signals or different characteristics. Every biosensor has specific selectivity and specificity. The combination of these determines how the sensor behaves in a defined environment. Other properties can characterise the function of the sensor based on the output signal. It can be divided into static parameters (transfer, linear, load characteristics, precision, resolution, sensitivity, specificity, stability, hysteresis, reproducibility) and dynamic parameters (transfer function, frequency,

impulse response). Functional materials are used to achieve exact specificity and selectivity, not to mention other important properties of the sensor.

Biosensors based on nanocrystalline diamond thin films functionalised by surface termination are the focus of the presented doctoral thesis. In the Experimental part, three types of sensors were developed and tested with cell culture and proteins.

3.5.1. Solution Gated Field Effect Transistor

There are many types of diamond-based bio-electronic devices of a new generation. They differ in the type of diamond (intrinsic or boron-doped polycrystalline diamond in the form of thin films deposited on different substrates, mainly glass or robust single-crystalline diamond substrates) as well as a working principle. The working principle of devices for direct electrical measurement of cell activity and for the study of the cell-cell or cell-substrate interactions differs for individual device configuration and specific applications such as impedance measurements, field-effect transistor configuration, and others. For example, both impedance and conductivity measurement techniques employ microelectrode arrays (MEAs) as described in [85,86].

MEAs found application in the study of immune system response efficiency [87], direct monitoring of cardiac action potentials of cells [85] as shown in Figure 3.8, or for action potential recording and stimulation of neural networks for both “in vitro” applications (rigid substrate) as well as for “in vivo” retinal prostheses (flexible biocompatible substrate) [88]. Interdigital transducer electrodes (IDT) based on the hydrogen-terminated diamond on glass substrates were found prospective as optically transparent devices for real-time monitoring of cellular activity (incubation, cultivation, adhesion, and others) [89].

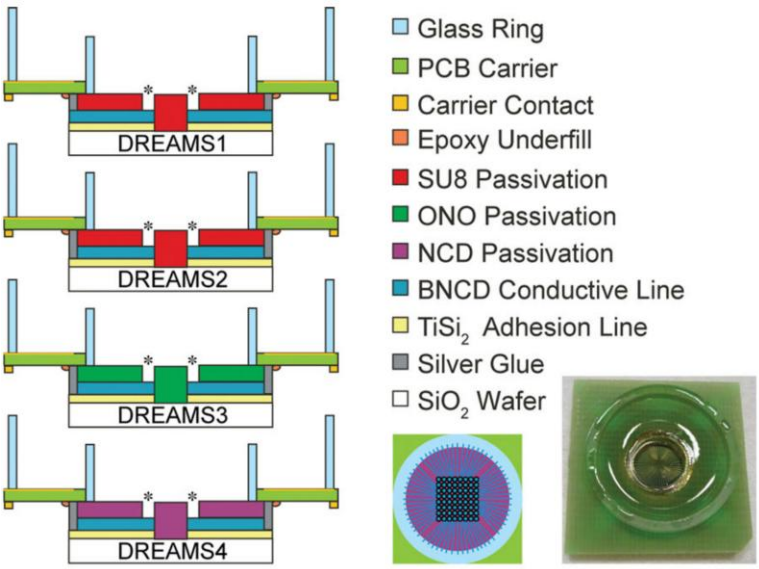

Figure 3.8 The cross-section view of MAE sensor for monitoring of action potentials of cardiac cells [85]

In contrast to impedance-based devices, solution-gated field-effect transistors (SGFETs) with hydrogen-terminated diamond surfaces allow the study of a single cell with minimum load currents. They have found use in research of solution/cell-surface interactions, living microorganisms, and tissue cells as biocompatible sensors. The properties of diamond SGFETs, such as the influence of the diamond thin film morphology [90], pH [91], protein adsorption [92], or membrane adsorption and disruption [93] on the electrical characteristics, have been well described. In another study, enzyme-modified field-effect transistors were applied to detect enzymatic reactions [65] or to measure the surface potential of living cells [94]. Micro and nanoscopic field SGFETs have the potential for the study of electrodynamic cellular behaviour, which is theoretically predicted [95] yet challenging to detect [96]. The functionalised diamond surface was used in several studies for the pattern-guided formation of glial and retinal neuron networks [78,97], and it was also demonstrated as the perfect solution for photo-sensitive retinal prosthesis and neural interfacing devices [98] (See Figure 3.9).

However, most of the studies were focused on the interactions of mammal adherent cells or excitable cells with surface potential. There is a lack of studies focused on the interactions of non-adherent, non-excitable cells.

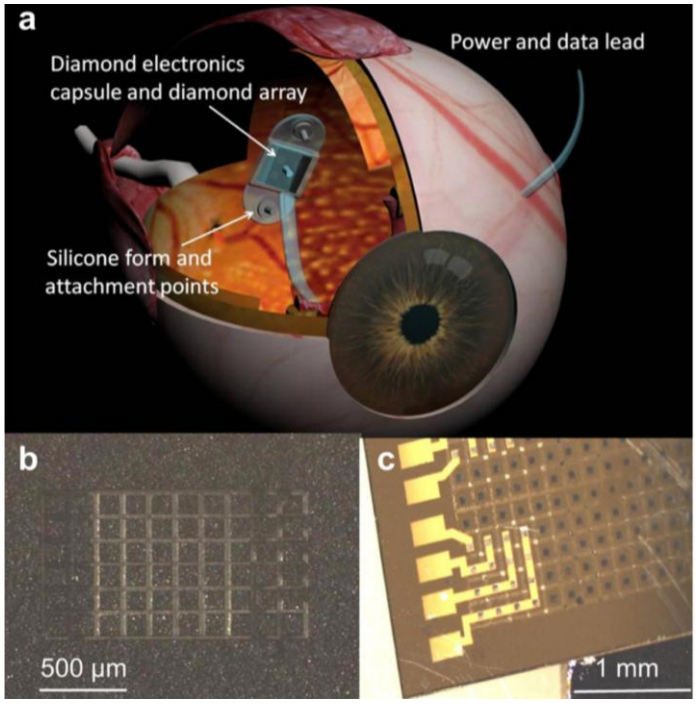

Figure 3.9 (a) Medical illustration of the form for the Bionic Vision Australia (BVA) epiretinal device, tacked in position over the macula, (b) Micrograph of the external face of a diamond feed-through array. The black squares are conducting N-UNCD, and the lighter lines are exposed PCD through which light is transmitted. Some light through the array is blocked by evaporated wires on the reverse side. (c) The interior face of the feedthrough array with evaporated metal wires contacting some feed-throughs [98].

Thus in the presented work, I focused on yeast cells (*Saccharomyces cerevisiae*), which are widely used as the basic model of eukaryotic cells in molecular biology and genetics [99]. Yeast cells are the subject of various genetic engineering techniques and strict functional analyses of proteins. They are non-polar, non-excitable, and non-adherent cells. Their inner and surface structures are well defined and understood. They have a stable negative surface charge with very weak pH dependency, which determines their behaviour in the solution [100,101]. In general, yeast cells are known as non-adherent cells, although some yeasts such as *Saccharomyces cerevisiae*, *Candida albicans* and *Candida glabrata* can adhere to plastic surfaces [102,103].

The yeast cell adhesion to plastic substrates depends on hydrophobic interaction [105]. Novel methods for attachment and cultivation of precisely positioned single yeast cells on a microelectrode surface employ a weak electrical potential (−0.2 and −0.4 V) [104] (See Figure 3.10). It was reported that the yeast cells attached to the negative potential-applied indium tin oxide (ITO) electrodes showed normal cell proliferation.

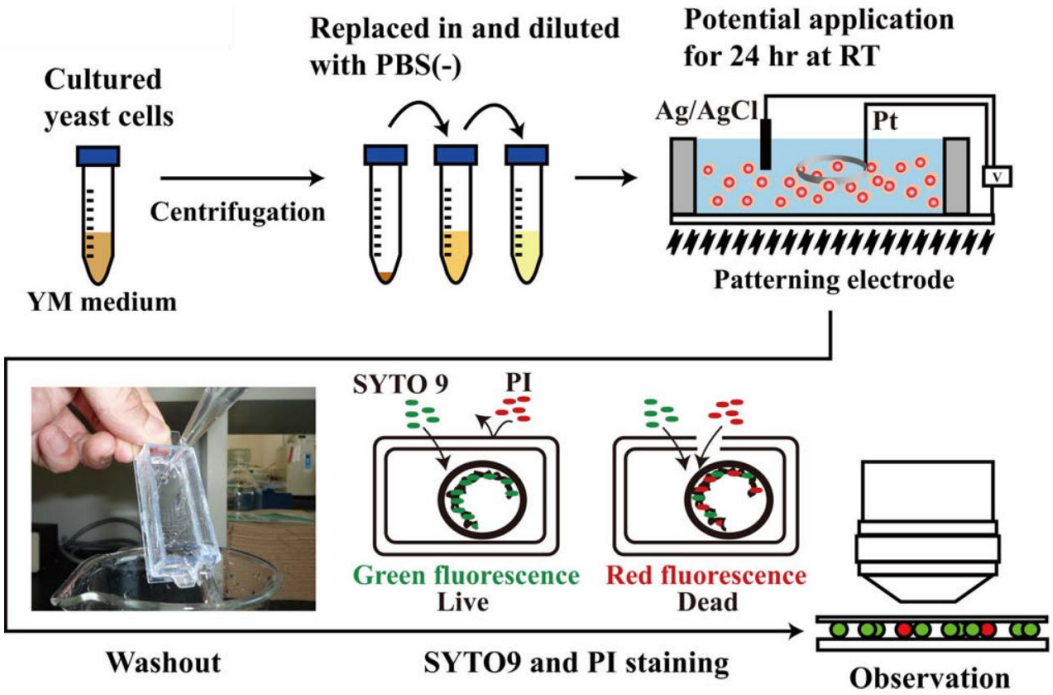

Figure 3.10 The procedure of attachment and cultivation precisely positioned yeast cells [104].

The influence of different solutions (sucrose and yeast peptone dextrose (YPD) without or with yeast cells) on the H-diamond SGFET electrical characteristics is studied. The interactions of the yeast cells and cell culture solutions with the H-terminated diamond surface on the transistor gate and other interesting findings are discussed in section 4.4.

3.5.2. Interdigitated Transducer Sensor

Bioelectrical sensors are of high interest due to their non-invasive label-free use for "in-vitro" monitoring of biological events and simplicity and fast response in real-time. Presently, there are two analytic approaches that employ either optical or electronic signal processing [106]. Both these approaches reached state of the art in a transducer type that converts a stimulus-induced cellular response into the quantifiable signal (i.e., biosensor signal). From the broad family of electronic systems, impedance measurement seems to be one of the simplest and most powerful methods for monitoring cellular signals during cell cultivation [107]. The main reason for its wide application is that the monitored impedance signal is sensitive not only to ionic currents but also to cell growth stages, i.e., cell attachment, spreading, shape, proliferation, differentiation, and communication [106,108]. Diamond is proposed as a promising material for life science and regenerative medicine due to its biocompatibility, chemical stability, and favourable combination of optical, mechanical, and electrical properties [109]. In addition, its surface can be covalently terminated by specific atoms or molecules which control the cell occupation, adhesion, proliferation, and cell differentiation [80]. In previous studies, a surface-conductive diamond thin film was already introduced as a functional layer in impedance sensors for biological studies [89] and for the recognition of gas and chemical molecules [110]. It was proven that intrinsic diamond thin film could be used as a biocompatible biosensor for "in-situ" electronic monitoring of cells behaviour in cultures [89]. In that case, the sensing principle of the diamond-based impedance sensor was based on impedance measurements employing conductive hydrogen-terminated surface regions as in-plane electrodes that were separated by resistive oxidized surface regions.

The diamond thin film was deposited on the quartz substrate, and thereby, it was fully transparent in the visible range, including low fluorescence background. Moreover, any possible and unwanted geometrical effects of metal electrodes (like steep edges) were avoided as purely surface atom modifications defined and induced the p-type diamond surface conductivity [111]. The surface-conductive H-functionalised diamond channels were also applied in the case of solution-gated field-effect transistors to study the interactions of human osteoblast-like *SaOS-2* cells with the diamond surface [112].

In this thesis, impedance sensors with a functional diamond layer deposited on gold interdigitated electrodes are employed to monitor the growth and activity of adipose tissue-derived stem cells (ASCs) electrically and optically. ASCs were chosen because, together with human bone marrow mesenchymal stem cells, they became the most popular adult stem cells used in tissue engineering, cell therapy, and studies on cell differentiation towards various phenotypes [113]. For example, the differentiation of ASCs towards adipocytes and osteoblasts was successfully quantitatively monitored in real-time by impedance sensing [71]. Generally, cell

differentiation is preceded by cell adhesion, spreading, and proliferation, and these cell functions are also used for expanding the ASCs into desirable quantities, needed for further studies on various properties of these cells and for their biomedical applications. Therefore, in this research, I have focused on the investigation of cell adhesion, spreading, and proliferation by impedance sensing with diamond-based impedance sensors.

The results are compared with impedance measurements provided using a commercially available gold interdigitated electrodes array (xCELLigence® RTCA system, Roche Applied Science®). The concept of the diamond enhanced IDTs is schematically described in Figure 3.11

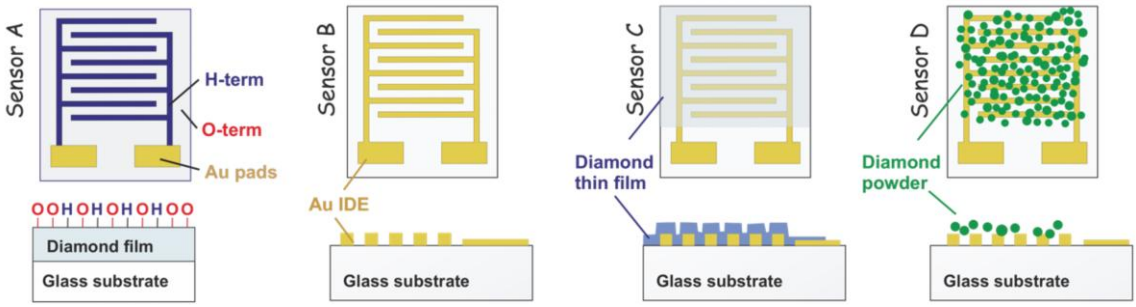

Figure 3.11 Four types of IDT sensor configuration for measurement of living cells [89].

3.5.3. Quartz Crystal Microbalance

The quartz crystal microbalance (QCM) sensor is based on the piezoelectric effect. It is a high-resolution mass sensing technique with sensitivity at the picogram level and has been widely used in many fields such as surface chemistry, biochemistry, and biomedical engineering [114]. Several works have shown that QCM is suitable for detection of multiple types of substances, such as pollutant molecules in the air [115,116], antibodies, allergens [117,118], proteins [119], DNA sequence [120,121], bacteria [116,122,123] and cell culture layer [123]. Its certain advantages are low cost and relatively easy fabrication. However, bare QCMs (i.e., with SiO_2 or gold sensing surface) have low selectivity and are fragile in terms of mechanical properties. On the other hand, a wide range of surface modifications or functionalisation can improve sensitivity and selectivity.

Generally, immunological detection methods are based on surface functionalisation by specific antibodies that immobilise the detected substance to the sensor's surface by direct binding via a functional group or Key-Lock system, as shown in Figure 3.12 [124,125]. For example, for DNA detection, a complementary synthetic DNA sequence (oligonucleotide probe) is usually used with a grafting point on the sensor surface. In the case of bacteria detection, common chemical compounds are applied, which are produced by the investigated organisms [126]. For example, the *Escherichia coli* detection was realised using the O157:H7 sequence [127], and for the detection

of *Salmonella enteritidis* and *Chlamydia trachomatis* bacteria, thin layers of polyethyleneimine bound with glutaraldehyde and cysteamine were applied, respectively [122]. A proper and long-term stable surface functionalisation of the QCM sensors is vital for biosensor applications. As known, the basic configuration of the QCM device consists of circular-shaped quartz crystal, which is covered with a planar gold electrode on both sides.

Thus, when the surface functionalisation of the QCMs is mentioned, it primarily means the surface functionalisation of those gold electrodes. However, as it was already confirmed, the stability of (e.g.) gold–thiol functionalisation is questionable for long-term monitoring of pathogens or other critical areas where a false negative signal could be a real threat to the evaluation of the measured data.

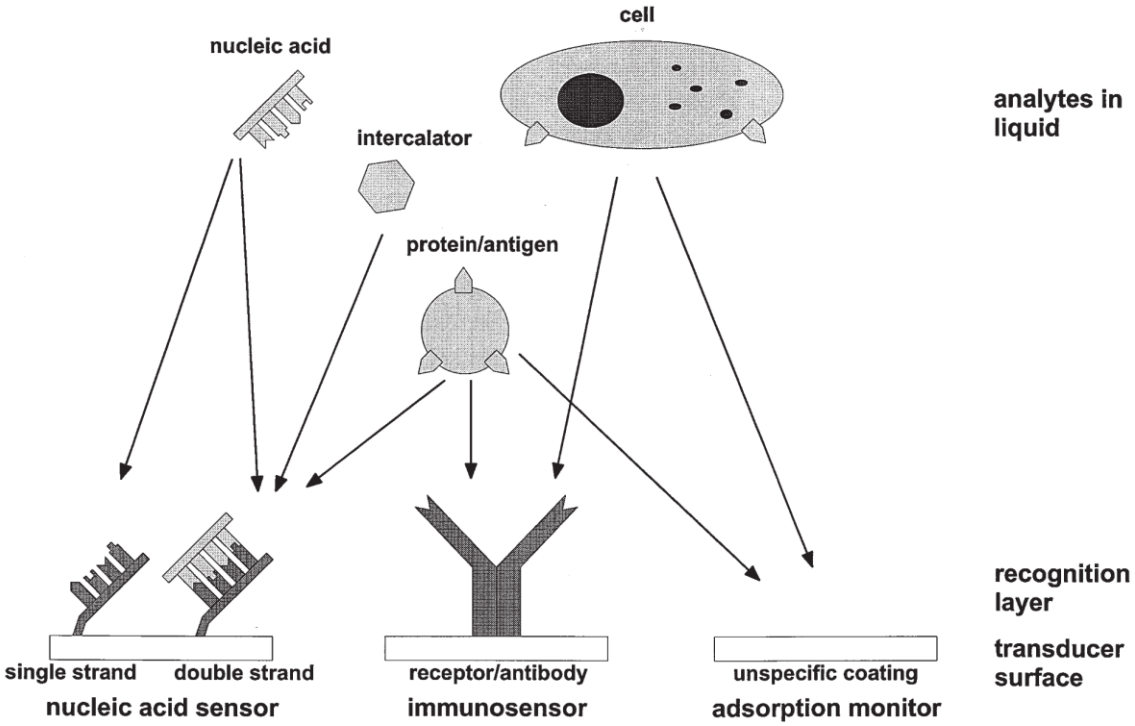

Figure 3.12 Biosensing interfaces with typical applications. Sensor surfaces can be coated with single or double-stranded DNA. Single-stranded DNA recognises complementary strands in solution by hybridisation. Furthermore, unspecific adsorption processes of proteins or cells with surfaces can be monitored [125]

In contrast to that, the stability of the diamond surface is unrivalled [2]. Diamond, due to its properties, provides the possibility to obtain stable surface bonds using standard chemical or physical methods. The idea of coating the QCM with a diamond thin film is not new, but unfortunately, the Curie point of quartz (573 °C) is lower than the deposition temperature of conventional diamond growth processes (600–1000 °C). Thus, the deposition of diamond on QCM was not widely utilised due to the loss of piezoelectric properties of the quartz exposed to high temperatures. Nevertheless, some success has been already obtained by bonding a free-standing

diamond to the QCM [128]; but these experiments resulted in a significant reduction of quality factor Q, and this solution was not commercially viable due to the desired thickness of the free-standing diamond layer (> 20 µm). One way how to overcome the problems with the low Curie point of quartz was the use of high melting point piezoelectric crystals such as langasite (no phase transition up to the melting point at 1500 °C) and gallium phosphate (950 °C) [129,130]. However, these materials are more expensive than quartz. In the last decade, there have been many attempts to decrease the temperature of diamond film deposition [128]. This was successfully achieved by the development of surface wave plasma [36] or linear antenna microwave plasma deposition systems [38,131] (See Figure 3.6a). These methods allow the deposition of diamond films even at temperatures as low as 250 °C [132]. A linear antenna microwave plasma system was already successfully applied for deposition of a homogeneous diamond film on QCMs without loss of its piezoelectric properties [40]. These diamond-coated QCM sensors, developed by our research group, were further successfully applied for a proof-of-concept study in gas sensor applications [40,133]. This thesis is building on the gained knowledge regarding low-temperature NCD diamond deposition and aims to demonstrate the novel use of diamond-coated QCM for label-free protein detection of two standard proteins: bovine serum albumin (BSA) and fibronectin (FN). The results of this research are presented in section 4.6.

4. Experimental part

The experimental part of this thesis consists of authors' publications with a connection to conference papers and proceedings related to the topic. This thesis dealt with three types of electrical sensing principles. Firstly, a solution gated field-effect transistor with a nanocrystalline diamond (NCD) conductive channel was used to characterise the non-adherent non-polar yeast cells' viability. In another study, the conductive channel is modified to sense the HIV-1 Tat protein responsible for HIV infectivity. The second, the interdigitated transducer (IDT) electrode with NCD coating, was employed for "in-vitro" monitoring of live adipose-derived stem cells (ASCs), and the comparison with a commercially used solution is offered. The third sensor is NCD coated quartz crystal microbalance (QCM), which was used for label-free protein sensing. This section covers everything from the fabrication of the sensors to published results.

4.1. Solution-Gated Field Effect Transistor (SGFET)

The first of the sensors is a solution-gated field-effect transistor used for the detection of yeast cells settled on its gate. This type of sensor is sensitive to pH. The study described in detail in section 4.4 deals with the detection of yeast cells. The cells settle in the opening of the sensor, and then the transfer characteristics are measured, and the shifts are recorded with reference to the solution without cells.

4.1.1. Fabrication of SGFET sensor

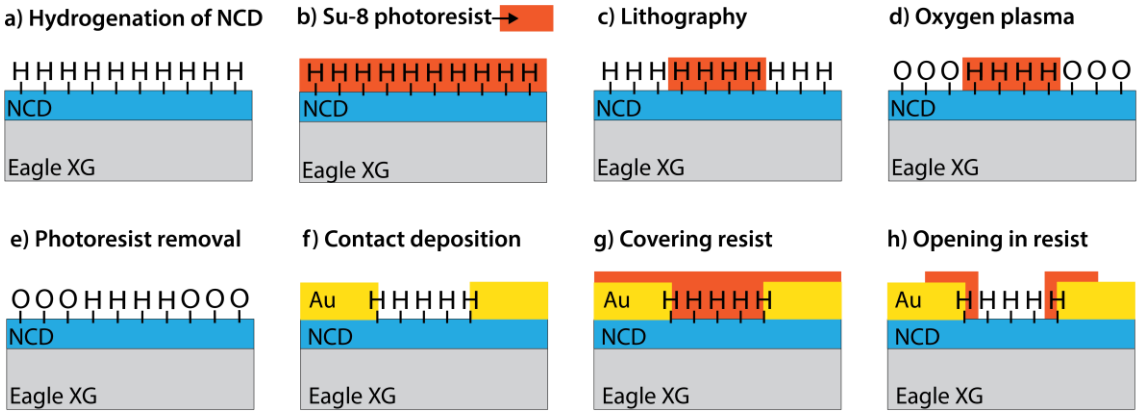

Figure 4.1 Cross-sectional scheme of H-diamond SGFET fabrication procedure [77]

As shown in Figure 4.1, photolithographic masks were applied on H-terminated NCD films using a positive ma-P1215 photoresist to define conductive channels and contacts. The NCD films were treated in oxygen radio-frequency plasma (300 W, 3 min. exposition time) to generate insulating O-terminated areas, which surround the H-terminated channels (5 µm wide and 60 µm long stripes) connecting

source and drain contacts. The source and drain contacts were prepared by thermal evaporation (10 nm of Ti and approx. 50 nm of Au), followed by the lift-off technique.

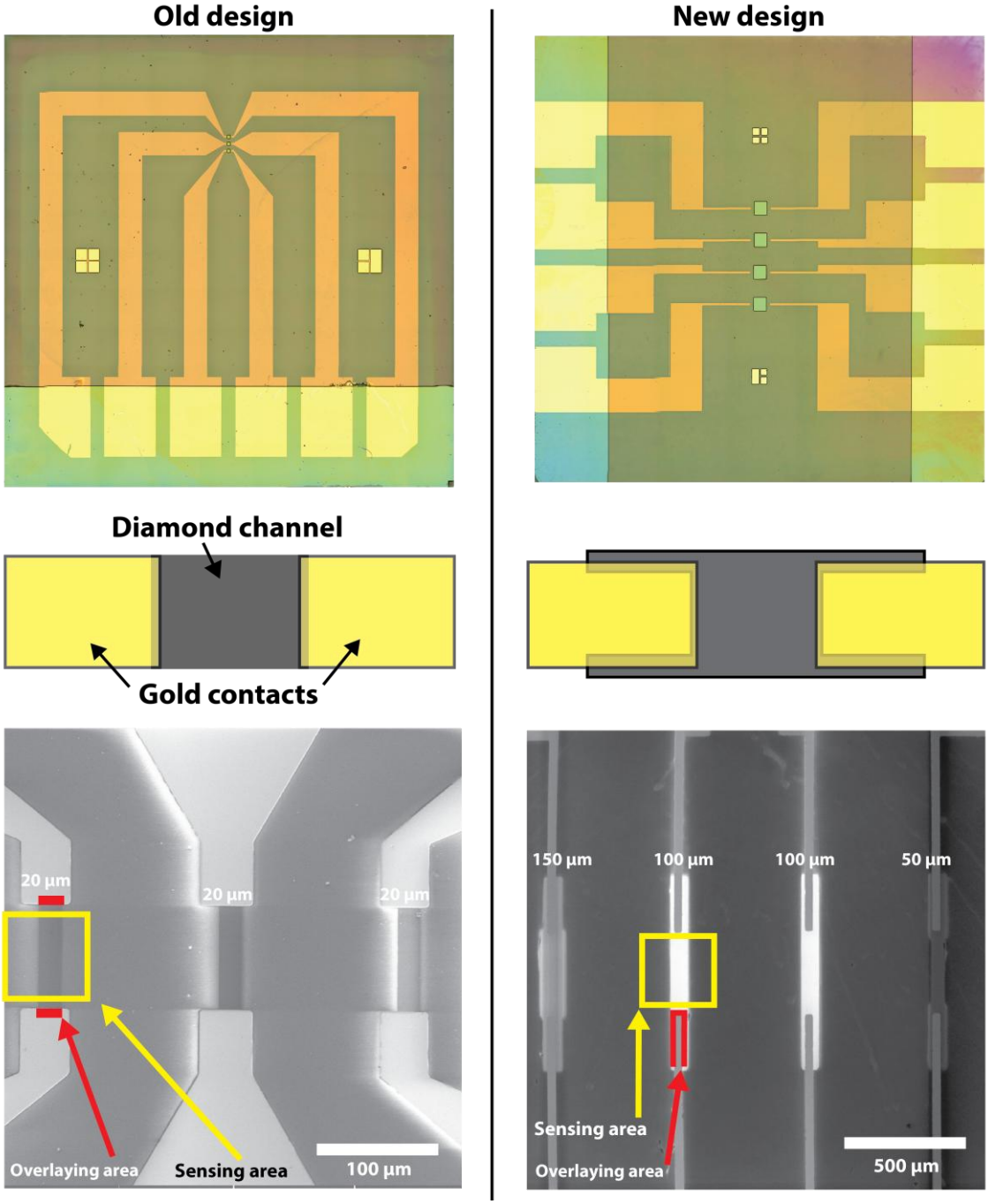

Figure 4.2 SGFET sensors (left) according to old design with rectangular hydrogenated NCD and decentred narrower channels, (right) according to new design with bone-like hydrogenated NCD area and centred wider channels [134].

The samples were cleaned in acetone and photoresist stripper (mr-REM 660). The area between contacts was covered with a negative photoresist SU-8 (thickness 4 µm). With the final photolithographic step, openings were created (60 µm × 60 µm) to define the active gate area [23]. The resulting sensors are shown in Figure 4.2.

Based on previous experience with unreliable sensors, the new design was created, highly increasing the conductivity and, most importantly, the reliability. The comparison of the designs is also shown in Figure 4.2. The main difference is that the sensitive structure of the channel was changed from a rectangular shape to a bone-like shape to increase the area of Ti/Au electrode in contact with the channel, where the weak spot was observed very often in the past. Another difference is the positioning of the conductive channels in the centre of the substrate. This was done because of the lowest spatial deformation of NCD thin film in the centre during the cooling-down phase after deposition. During cooling, the diamond thin film cracked, causing the disruption of the electrical conductivity. The last enhancement is the widening of the channel resulting in higher and more stable currents through the channel, as shown in Table 4.1. [134]

Table 4.1 The conductivities of the conductive surface channel fabricated according to the old design (light grey) and new design (dark grey)

	OLD	NEW	NEW	NEW
Channel width (µm)	20	50	100	150
Conductivity ($n\Omega^{-1}$) for $U_G = U_{DS} = -0.6V$	7.57±0.07	13.6±0.04	74.2±0.7	76.4±0.5

4.2. Interdigitated Transducer Electrode (IDT)

The second of the sensors is an IDT sensor covered by a nanocrystalline diamond thin film used to detect ASCs growing on its surface. The IDT sensors are most often used as gas sensors offering comprehensive options for coating a sensitive variety of gases and substances. The main principle is based on the fact that the coating or functional material between the electrodes is changing its properties as permittivity and conductivity. This is the reason; we can observe a change in impedance spectrum after performing impedance measurement. Section 4.5 is dedicated to the use of such a sensor for "in-vitro" monitoring of adipose-derived stem cells. In Figure 4.3, the interdigitated transducer (NCD-IDT) is shown with the nanocrystalline diamond coating over the Ti/Au electrodes and openings for gold contacts. The gap between electrodes is 100 µm, and the width of the electrodes is 100 µm. The whole dimension of the sensor's substrate is 15 x 15 x 1 mm^3 to fit the measuring chamber created for this measurement, on which the utility model was filed [ARef:14]. The chamber from polycarbonate serves as the sterile and inert reservoir for measurement with the cell culture in DMEM solution. The chamber preserves optical transparency and is small enough to fit the incubator. Read the complete research in Appendix 8.2.

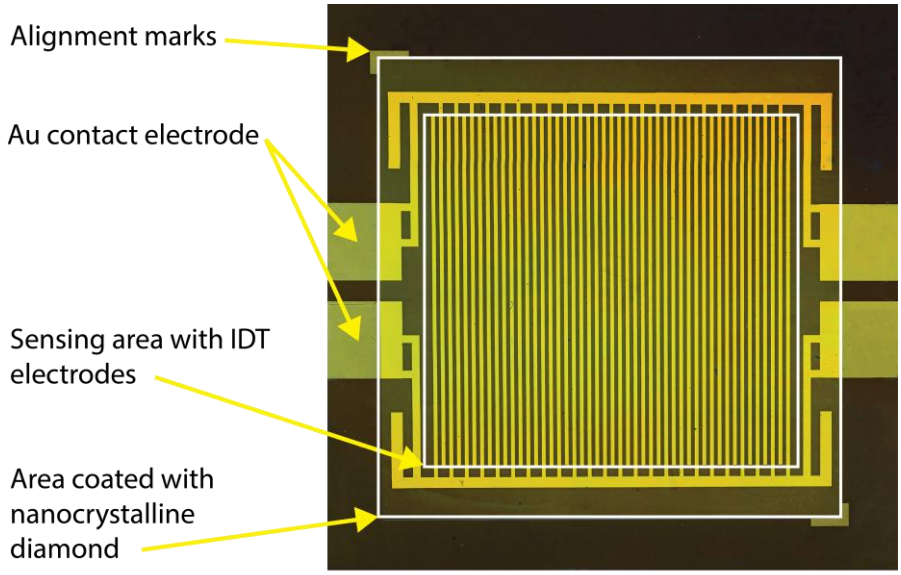

Figure 4.3 NCD based interdigitated transducer sensor developed for in vitro measurements with adipose-derived stem cells

4.2.1. Fabrication of interdigital transducer (IDT) sensors

Lithography steps are shown in Figure 4.4. The sensors are made on JGS glass, which is capable of withstanding high temperatures up to 800 °C before reaching its melting point. The glass is thoroughly cleaned in an ultrasonic bath, and the mixture of acetone and isopropyl alcohol is used to perfectly clean the surface of the substrate from grease and the residues from cutting it to 15 x 15 x 1 mm^3 squares. After the cleaning procedure, the optical lithography is done for the further deposition of the titanium/gold electrodes. Before evaporation, the exposed area of the substrate, which is going to bear the electrodes, needs to be treated in oxygen plasma to clean the rest of the polymer ("plasma ashing"). This step is very important for the adhesion of the gold contacts. The evaporation of the gold electrodes is followed by lift-off in acetone assisted by soft ultrasound treatment. This step leaves us with standard gold IDT structures on glass, not unlike those commercially used by X-Celligence®. After the IDT electrode is fabricated, the second lithography procedure is performed to create a "sandwich-like" structure with the diamond seeds trapped in the initially spin-coated resist and the top resist layer, fixing them through selective nucleation.

After this procedure, the sensors are coated with a nanocrystalline diamond thin film, using the deposition conditions described in subsection 3.3.2. The selective nucleation by the lithographic mask enabled the gold contacts to remain uncoated on the sides of the sensor after deposition, thus without insulating the NCD layer.

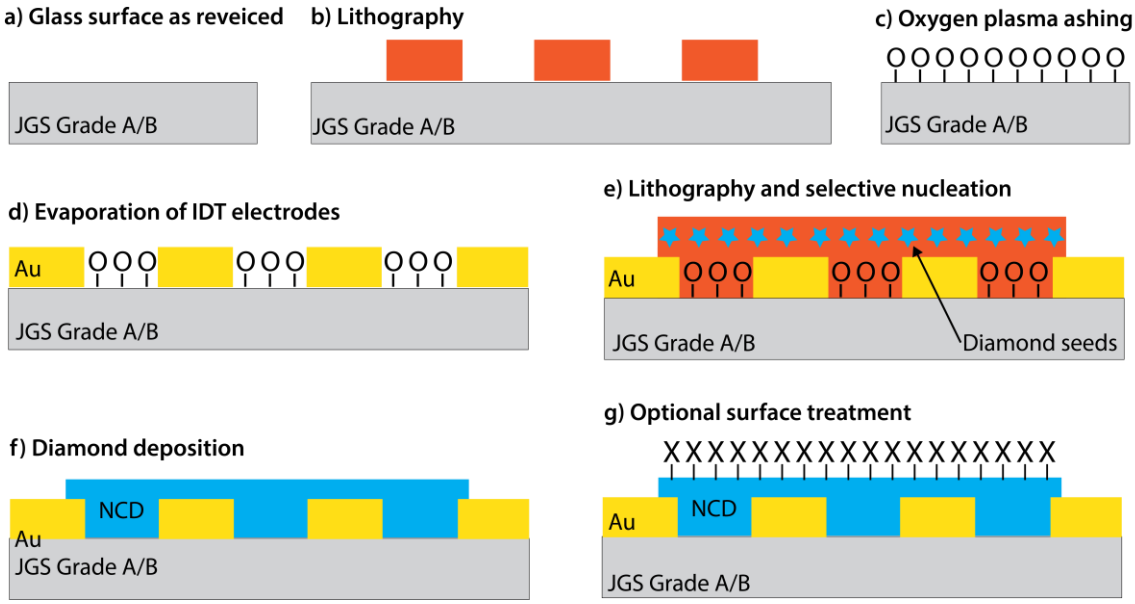

Figure 4.4 Fabrication procedure of NCD coated IDT sensor. a) The JGS glass was formatted to size followed by cleaning, and b) lithography. After c) plasma "ashing" in oxygen, d) gold electrodes were evaporated, and e) selective nucleation using lithography was done. At last, f) diamond deposition was done, resulting in NCD thin film covering the IDT electrodes and leaving the contacts opened.

After the diamond deposition, the surface is exposed to hydrogen plasma to clean its surface further and leave it terminated by hydrogen, which is suitable for our experiments [135]. At the end of fabrication, IDT electrodes are entirely covered with NCD diamond.

4.3. Quartz Crystal Microbalance (QCM)

The third principle gaining the advantages of a diamond is QCM. A nanocrystalline diamond coating grew under low temperature in the CVD chamber to preserve the piezoelectric properties. This approach enables new types of assays and functionalisation of QCM due to the capability of the diamond to bond multiple molecular and atomic groups. As a proof of concept, working samples were provided, and their reaction was measured in response to fibronectin and albumin as seral proteins with adhesive functionality in the mammal body. In this research, the sensor was designed, simulated, and fabricated to be capable of performing label-free measurements. This study contributes to a better understanding of mechanisms that integrin proteins (albumin, fibronectin) are using to adhere to the hydrophobic and hydrophilic surface. In Figure 4.5, the QCM sensor is shown after deposition and on the right side of the socket and holder during the measurement of protein settling on the modified diamond's surface.

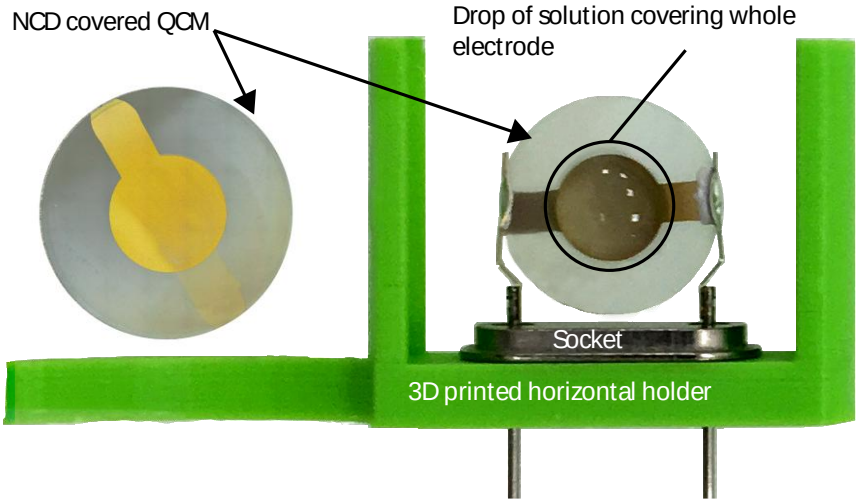

Figure 4.5 The QCM sensor in the socket and holder with a drop of solution covering the whole electrode

4.3.1. Fabrication of QCM diamond-based sensors

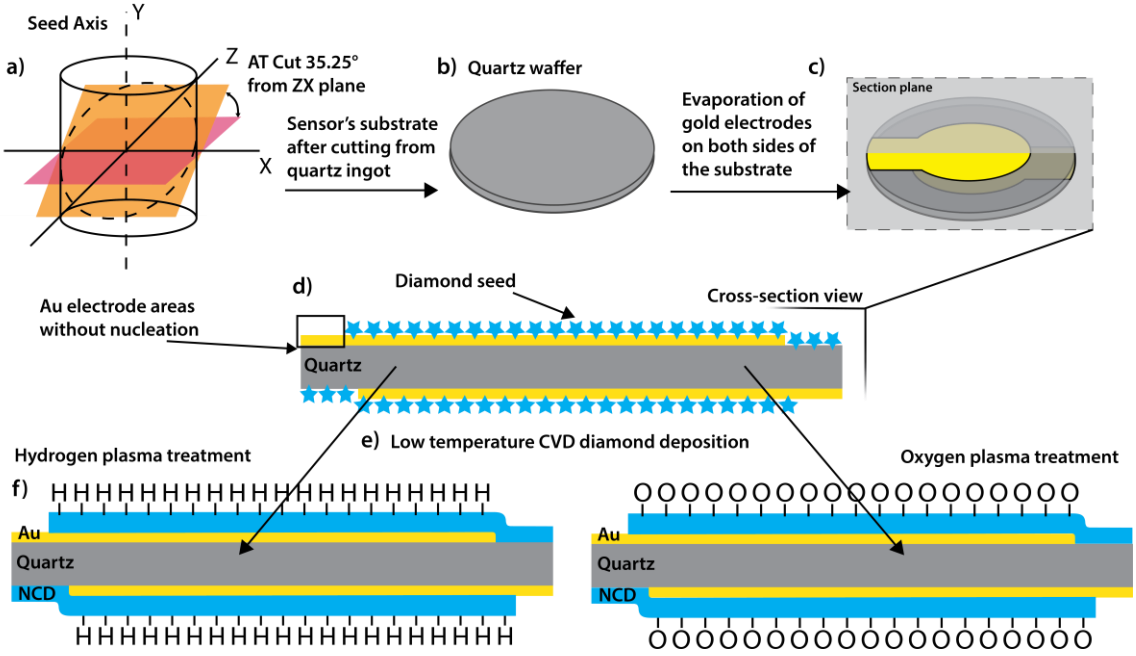

Figure 4.6 The fabrication procedure of the nanocrystalline diamond-coated quartz crystal microbalance sensor. a) Planar AT-cut from quartz ingot resulting in b) quartz wafer is followed by c) evaporation of gold electrodes. For nanocrystalline diamond coating, the QCM sensor is d) nucleated with diamond nanoparticles in a nominal size of 5 nm and e), f) treated in hydrogen or oxygen plasma.

The procedure of DQCM fabrication is at some point like the fabrication of the previous two sensors. The process diagram is shown in Figure 4.6. The substrate is prepared by AT-cut of the homogenous quartz ingot to preserve the specific piezoelectric

properties. After polishing the sensor, gold electrodes are evaporated on both sides, with lead areas pointing to the opposite side of the sensor to be contacted by a vector network analyser later. The sensing area nearby and over the electrode is then nucleated, and the diamond deposition is performed, leaving a nanocrystalline diamond thin film on the sensor's surface. After that, half of the sensors are treated with hydrogen and the other half with oxygen plasma to achieve hydrophobicity and hydrophilicity. There is similar morphology of diamond (as in the case of SGFET and IDT sensors) with termination by hydrogen and oxygen at the end of the fabrication.

As it was described in section 3.3.2, it is crucial not to exceed the Currie point temperature of the quartz during deposition. Doing so would disrupt the piezoelectric properties of the quartz. The maximum temperature during deposition and surface treatment can rise to 350 °C at the peak, and the cooling phase after deposition must be prolonged to maintain the integrity of the quartz crystal lattice.

4.4. Influence of bacterial/fungi cells and RNA aptamers on electrical characteristics of diamond-based field-effect transistors

Based on: Influence of non-adherent yeast cells on electrical characteristics of diamond-based field-effect transistors, published in Applied Surface Science, 2017
DOI: http://dx.doi.org/10.1016/j.apsusc.2016.05.003

Václav Procházka[*,1,2], Michal Cifra[3], Pavel Kulha[1,2], Tibor Ižák[1], Bohuslav Rezek[1,2], Alexander Kromka[2,4]

[1]Faculty of Electrical Engineering, Czech Technical University in Prague, Technická 2, 16627 Prague, Czech Republic
[2]Institute of Physics, The Czech Academy of Sciences, Cukrovarnická 10/112, 162 00 Prague, Czech Republic
[3]Institute of Photonics and Electronics, The Czech Academy of Sciences, Chaberská 57, 182 51 Prague, Czech Republic
[4]Faculty of Civil Engineering, Czech Technical University in Prague, Thákurova 7, 16629 Prague, Czech Republic

4.4.1. Summary

This research explores the new way to use nanocrystalline diamond solution gated field effect transistor as a platform for measuring yeast cells' metabolic activity and detecting HIV-1 Tat protein in the serum sample. The pH sensitivity of the SGFET sensor predestines it to be the perfect tool for monitoring the cells which are changing the pH of the solution by producing acidifying metabolites in their vicinity. The influence of yeast cells (*Saccharomyces cerevisiae*) on electrical characteristics of the diamond SGFETs was studied. Two different cell culture solutions (sucrose and yeast peptone dextrose - YPD) were used, with and without the cells. It was found that transfer characteristics of the SGFETs exhibit a negative shift of the gate voltage by –26 mV and –42 mV for sucrose and YPD with cells in comparison to the blank solutions without the cells. This effect is attributed to a local pH change in the close vicinity of the H-terminated diamond surface due to the metabolic processes of the yeast cells. The pH sensitivity of the diamond-based SGFETs, the role of cell and protein adhesion on the gate surface, and the role of the negative surface charge of yeast cells on the SGFETs electrical characteristics are discussed as well. The simplified model of the cells/diamond interface is shown in Figure 4.7.

Another study dealt with the detection of HIV-1 Tat protein with RNA aptamer-sensing technique. This research investigated the trans-activator of transcription (Tat) protein, a potent viral gene activator that plays a pivotal role in the primary stage of the human immunodeficiency virus type 1 (HIV-1) replication. The interactions of HIV-1 Tat on nanocrystalline diamond extended gate field-effect transistor (NCD-EGFET)-based RNA aptamer sensing surface were monitored and attained the detection down to 10 fM. The linear regression curve set the limit of detection to 6.18 fM.

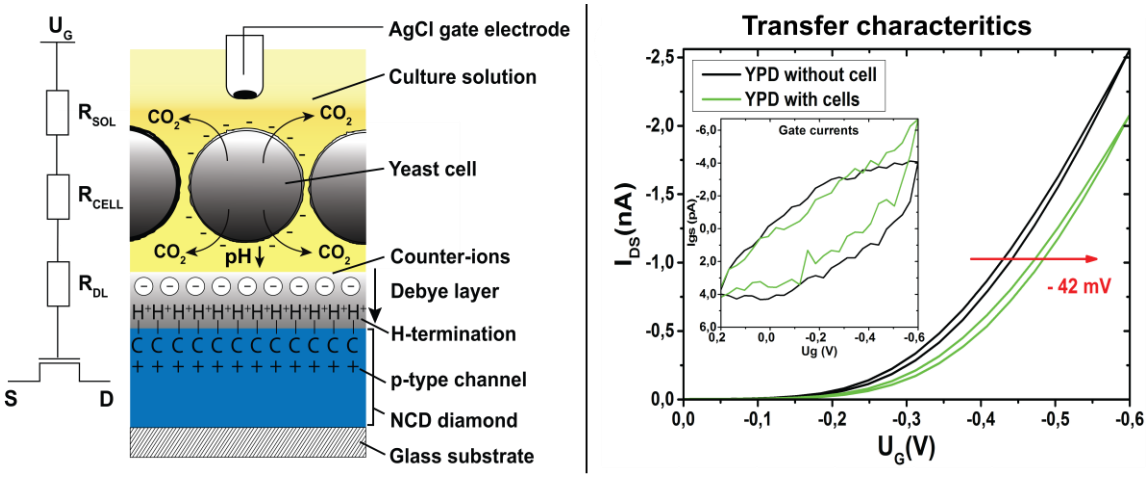

Figure 4.7 Simplified model of effects on the yeast/HNCD interface

The selectivity analysis of NCD-EGFET was conducted with different proteins from HIV (Nef and p24) and bovine serum albumin. Furthermore, to practice in the clinical application, HIV-1 Tat was spiked into the human blood serum, and it displayed a genuine non-fouling interaction with the aptamer. This work presented a new way to use EGFET to detect HIV-1 Tat protein [136]. (See Figure 4.8)

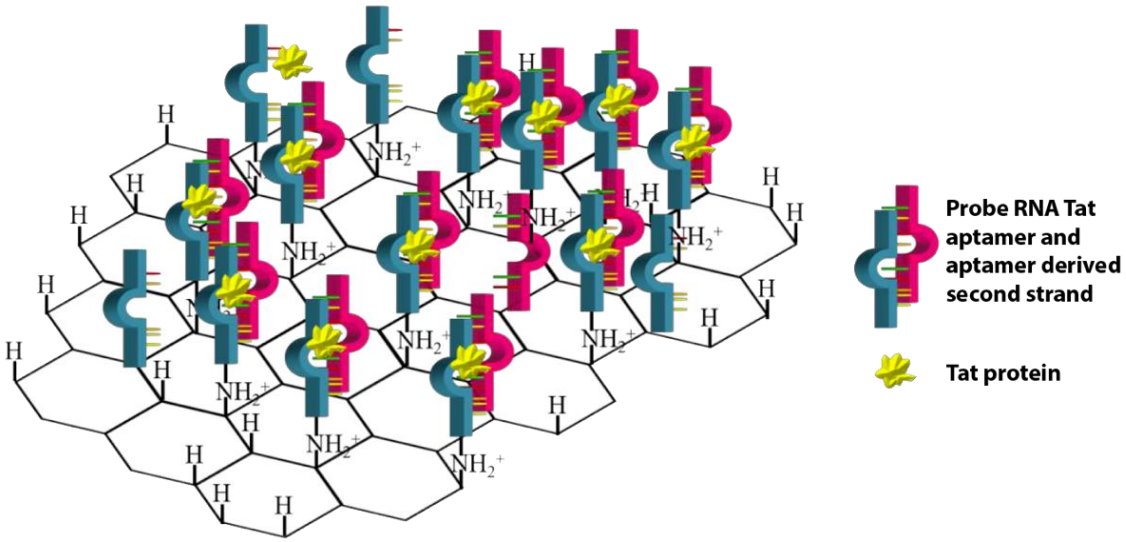

Figure 4.8 The functionalisation of EGFETs channel for detection of HIV-1 Tat protein [136]

4.4.2. Author's contribution

I participated in the research regarding experimental studies on the influence of non-adherent yeast cells on electrical characteristics of diamond-based field-effect transistors by proposing and performing the experiment, including the preparation of samples, solutions, and measurement setup, followed by data collection and analysis, the discussion of the results with co-authors, and the article composure and review. Co-authors participated in the form of the yeast cells culture preparation, the deposition of diamond thin film, consulting, co-writing, and reviewing individual parts of the article.

The author participated in the study regarding detecting HIV-1 Tat protein with NCD-EGFET by fabrication of SGFET sensors on Si/SiO_2 substrates and tutoring the University Malaysia Perlis student regarding the fabrication of SGFETs. He also participated in the deposition of diamond films, conceptualising the experiment, evaluating the sensor's functionality after fabrication, and preparing the text for the experimental part. Co-authors were responsible for the preparation, post-fabrication procedures, analyses, and chemical procedures to achieve stable functionalisation, writing parts of the text depending on the analysis performed and reviewing the article.

4.4.3. The paper's contributions toward the progress of the field

The SGFET sensor has been used since its first introduction with polypyrrole as a chemical sensor [137] and soon after that for its pH sensing capabilities in aqueous solutions [138,139]. As a next step, it has been used in research with specific aptamer functionalisation to detect DNA in multiple forms [140–143], although in most cases, the SGFET sensor was formed by a modified graphene layer. Recently, multiple studies have shown its usability with living cells and cultures. In [112], osteoblastic cells and cancer cells were used, and the mutual influence of the NCD and the cells on the gate electrode surface was described. In another study [144], gamma irradiation was used to investigate the change of the gate currents when irradiating fibroblast culture. In [145], the influence of excitable neural cells was investigated to determine the distortion of graphene SGFETs to large amplitude and the high-frequency signal generated by neural cells. Before this paper [ARef:1], an NCD based SGFET sensor was never used with the culture of *Saccharomyces cerevisiae,* which led to the following. The use of the SGFET sensor with yeast cells laid down a new method of measuring the viability of yeast cells. This research provided an explanation of yeast cells' influences on the sensors transfer characteristics and pointed out the different metabolism activity of yeast cells whether a sucrose or yeast peptone dextrose (YPD) is used as a culture solution. It proposed the model in which yeast cells exclude CO_2 in close vicinity in sufficient amount to change pH and consequently transfer characteristics of NCD based SGFET.

The paper focused on the detection of HIV-1 Tat protein [ARef:3] and presented a new method of nanocrystalline diamond functionalisation with aptamer in order to detect HIV-1 Tat protein (See [136], which enabled the new use of such sensor, and the authors tested its function in laboratory conditions. It was found that the sensor is preserving its sensitivity and low detection threshold in serum, making it sensitive to low concentrations of measured protein in clinical conditions.

4.4.4. Compliance with the objectives of the thesis

The NCD-based SGFET sensor was successfully fabricated on Corning Eagle XG® substrate to preserve optical transparency for monitoring purposes.

In the core study, four solutions were prepared, sucrose and YPD, both with and without yeast cells at the same concentrations. The pH and conductivity of the solutions were monitored to determine the rate of pH change as cells began to metabolise. Multiple measurements with SGFET were performed to show the influence of sensor transfer characteristics.

The technological goal of fabricating the nanocrystalline diamond thin film in high quality was done as the sensors showed good stability and conductivity through the channel.

As an extension of SGFETs usability, new experiments with these diamond sensors functionalised with HIV-1 Tat aptamers were designed, and the experiments focused on the detection of HIV-1 Tat protein has been performed with results published in a peer-reviewed journal. The use of bacterial and viral organisms or their genome fulfilled the goal of expanding the use of the SGFET sensor. A proof of concept was successfully demonstrated.

By this work, it was laid down a new way of measuring non-adhering cells and their viability. It utilised the unique properties of nanocrystalline diamond films. The most important properties utilised by this work were semiconductivity, surface morphology, biocompatibility, optical transparency, and fabricability of SGFET on the quartz or Si/SiO_2 substrate. A simplified model of the interface was proposed. The results contributed to a better understanding of the ongoing effects on the interface nonadherent cell-diamond surface.

4.5. Nanocrystalline diamond-based impedance sensors for real-time monitoring of adipose tissue-derived stem cells

Based on: Nanocrystalline diamond-based impedance sensors for real-time monitoring of adipose tissue-derived stem cells, published in Colloids & Surfaces B: Biointerfaces, DOI: http://dx.doi.org/10.1016/j.colsurfb.2019.01.048

Václav Procházka[1,2], Roman Matějka[3,4], Tibor Ižák[1,2], Ondrej Szabó[1], Jana Štěpanovská[1,4], Elena Filová[3], Lucie Bačáková[3], Vít Jirásek[1] and Alexander Kromka[1,2]

[1]Institute of Physics, Czech Academy of Sciences v.v.i., Cukrovarnická 10, 162 00 Prague 6, Czech Republic
[2]Faculty of Electrical Engineering, Czech Technical University in Prague, Technická 2, 166 27 Prague, Czech Republic
[3]Institute of Physiology, Czech Academy of Sciences v.v.i., Videnska 1083, 14220 Prague 4, Czech Republic
[4]Faculty of Biomedical Engineering, Czech Technical University in Prague, nám. Sítná 3105, 272 01 Kladno, Czech Republic

4.5.1. Summary

In this work, the NCDs electrochemical window was utilized to lower the currents, which burden the cells in the existing X-Celligence® solution. When using nanocrystalline diamond as a coating, a smaller current density near the electrodes was confirmed with simulation. The diamond-based impedance sensor with built-in gold interdigitated electrodes (IDT) is a promising platform for simultaneous electrical and optical monitoring of adipose tissue-derived stem cells (ASCs). The impedance spectra were collected in a wide frequency range (from 100 Hz to 50 kHz) for 105 h of cell cultivation in chambers designed for static cultivation. Whole impedance spectra were analysed in terms of measured frequencies and cell properties monitored by a high-resolution digital camera. These results were confirmed optically by live-cell imaging and comparison with a commercial control system with gold electrodes directly exposed to media (X-Celligence®). The diamond-based sensors were more sensitive for detecting the cell-substrate interaction in the first phase of cell growth, while the control system was more sensitive in the second phase of cell growth. The NCD layer provided a fully biocompatible interface and inert layer, which promoted the cell growth on its surface, which can be easily tailored for a specific function. Impedance measurements combined with simultaneous live imaging showed that we could observe every change in adipose-derived stem cells (ASC) behaviour, whether it is cell attachment and spreading, forming a confluent layer, or forming more layers. The toxicity study with staining was performed to prove the biocompatibility of nanocrystalline diamond thin film fabricated for such a purpose. (See Figure 4.9)

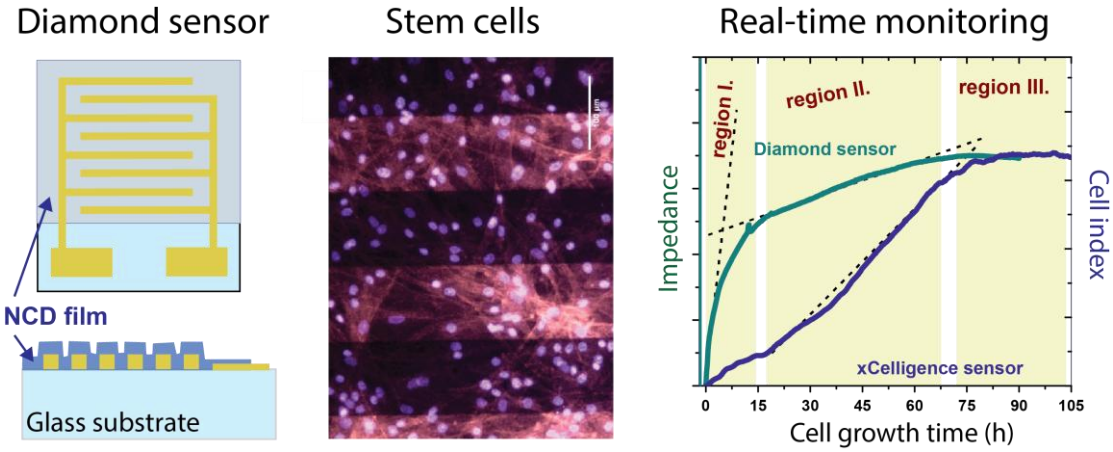

Figure 4.9 The diamond sensor top view and cross-section view (left), fluorescence microscopy image of stem cells growing on NCD IDT sensor (middle), and the response of diamond and gold surface X-Celligence® sensor during 105 hours long growth time(right)

4.5.2. Author's contribution

I participated in this research with the design and fabrication of the impedance sensor, validation of its function, the conceptualization of the experiment, and automation of measurement with adipose-derived stem cells. Also, I participated in data evaluation, discussion of ongoing electrical and physical effects and writing and reviewing of the article. Co-authors participated in analyses (fluorescence microscopy, Raman spectroscopy, phase contrast microscopy), ASC culture preparation and dilution, FEM simulation, writing parts of the text depending on the analysis performed and reviewing the article.

4.5.3. The paper's contributions toward the progress of the field

The IDT sensor has been widely used in environmental sensing [146,147], biology [148,149] or water resources application [150]. Its versatility enables the usage as a conductivity sensor, capacitive sensor (impedance spectroscopy), or in a particular configuration of electrodes as an acoustic sensor generating surface acoustic wave (SAW). For the sake of clarity, this chapter serves as a state of the art comparison limited to label-free biosensor applications of IDT used as a sensor for impedance spectroscopy.

IDT sensors have been used in biology research as the platform for the detection of aminoacids, proteins, macromolecular compounds, cells and cell cultures [148,151], bacteria [152], and cervical cancer cells [153]. Its straightforward principle with variable coating and ease of use enabled the development of commercial measuring devices such as xCelligence®[148,154].

The xCelligence® system is used to determine the optimal point for further processing of the cells. During cultivation in the cultivation plate, all phases of cell settling and growth can be observed in cell index numbers [148]. This system works with gold

electrodes which show highly current density in their vicinity than gold electrodes coated with nanocrystalline diamond.

The design and fabrication of the biosensor with gold electrodes coated with nanocrystalline diamond enables the novel method of tuning wettability, which cell cultures react to [155]. Moreover, it brings new possibilities for functionalisation while preserving biocompatibility. According to my findings and simulations in COMSOL® [ARef:2], the diamond coating lowers the influence of the currents during measurement on cell growth. The comparative study performed in this article [ARef:2] led to the finding that the commercially available system is more sensitive after cells settle to the confluent layer. The system proposed is more sensitive in the early stages of cell growth and enables further functionalisation of the surface.

4.5.4. Compliance with the objectives of the thesis

The NCD-based IDT sensors were successfully fabricated on 15 x 15 x 1 mm^3 Corning Eagle XG® substrate to preserve optical transparency for monitoring purposes. Human adipose tissue-derived stem cells (ASCs) were isolated from lipoaspirate obtained by liposuction. Dulbecco's Modified Eagle's Culture Medium® (DMEM) with the 10 % addition of fetal bovine serum and human recombinant fibroblast growth factor-2 (FGF-2, 10 $ng{\cdot}ml^{-1}$) culture solutions with adipose-derived stem cells were prepared. Long-term measurements with cells and control long-term measurements determining the stability of the sensor under culture medium were performed for validation of measured results. The goal of fabricating NCD thin film in high quality was achieved as the sensors showed good stability and biocompatibility “in vitro”. The new sensor was developed with NCD thin-film overcoating the IDT electrodes, and its surface was superficially modified with hydrogen. The sensor was successfully used with adipose-derived stem cells (ASC), and the results were published in peer-reviewed journals.

This work dealt with the enhancement of the properties of the commonly used solution by a nanocrystalline diamond as a platform for monitoring adhering cells and their viability. The results contributed to better resolution during real-time monitoring of the early stages of cell culture growth. At the same time, it opened new possibilities for surface functionalisation, coating and patterning of the surface.

4.6. Detection of proteins by quartz crystal microbalance sensor coated with a nanocrystalline diamond thin film

Based on: Detection of globular and fibrillar proteins by quartz crystal microbalance sensor coated with a functionalised diamond thin film, published in Applied Surface Science
DOI: http://dx.doi.org/10.1016/j.apsusc.2022.153017

Václav Procházka[1,2], Pavel Kulha[2], Tibor Izsák[1,4], Egor Ukrainstev[1,2], Marián Varga[1,4], Vít Jirásek[1,5], Alexander Kromka[1,3]

[1]Institute of Physics, Czech Academy of Sciences, Cukrovarnicka 10, 162 00 Prague, Czech Republic
[2]Faculty of Electrical Engineering, Czech Technical University in Prague, Technicka 2, 166 27 Prague, Czech Republic
[3]Faculty of Civil Engineering, Czech Technical University in Prague, Thakurova 7, 166 29 Prague, Czech Republic
[4]Institute of Electrical Engineering, Slovak Academy of Sciences, Dúbravská cesta 9, 841 04 Bratislava, Slovak Republic
[5]Institute of Plasma Physics, Czech Academy of Sciences, Za Slovankou 1782/3, 182 00 Prague, Czech Republic

4.6.1. Summary

In this work, the NCD thin film was deposited on the QCM sensor surface (NCD-QCM). The deposition of NCD on temperature-sensitive quartz was a technological challenge due to possible delamination and disruption of piezoelectric properties. The NCD was superficially treated in hydrogen and oxygen plasma to achieve hydrophobic and hydrophilic properties.

Two protein solutions were tested: bovine serum albumin (BSA) and fibronectin (FN). Reference measurements were performed using serial resonant frequency (SRF) of clean QCMs without protein and loaded with protein and compared with SRF shifts of NCD coated QCMs without proteins and loaded with proteins. We compared masses estimated from the Sauerbrey equation to characterise the adhesive properties of the studied proteins. Comparing bare QCM and NCD-QCM, we discovered that nanocrystalline diamond thin film enhances the sensing performance of proteins. At the same time, it saturates quickly with phosphate buffer saline used as a diluent solution for proteins. Results showed a significant increase in protein adhesion confirmed by the increase of the mass for both oxygen and hydrogen-terminated NCD-QCMs. Moreover, a different time-dependent behaviour (i.e., different adsorption rate, degrees of physisorption and preference of the diamond surface functionalisation) of the O-NCD and H-NCD QCMs was observed for BSA and FN proteins. A study with FN and BSA was performed as a representant of fibrillar and globular proteins with adhesive capabilities (See Figure 4.10).

By this, the proof of concept has been made for a future variety of surface functionalisation with excellent stability and biocompatibility.

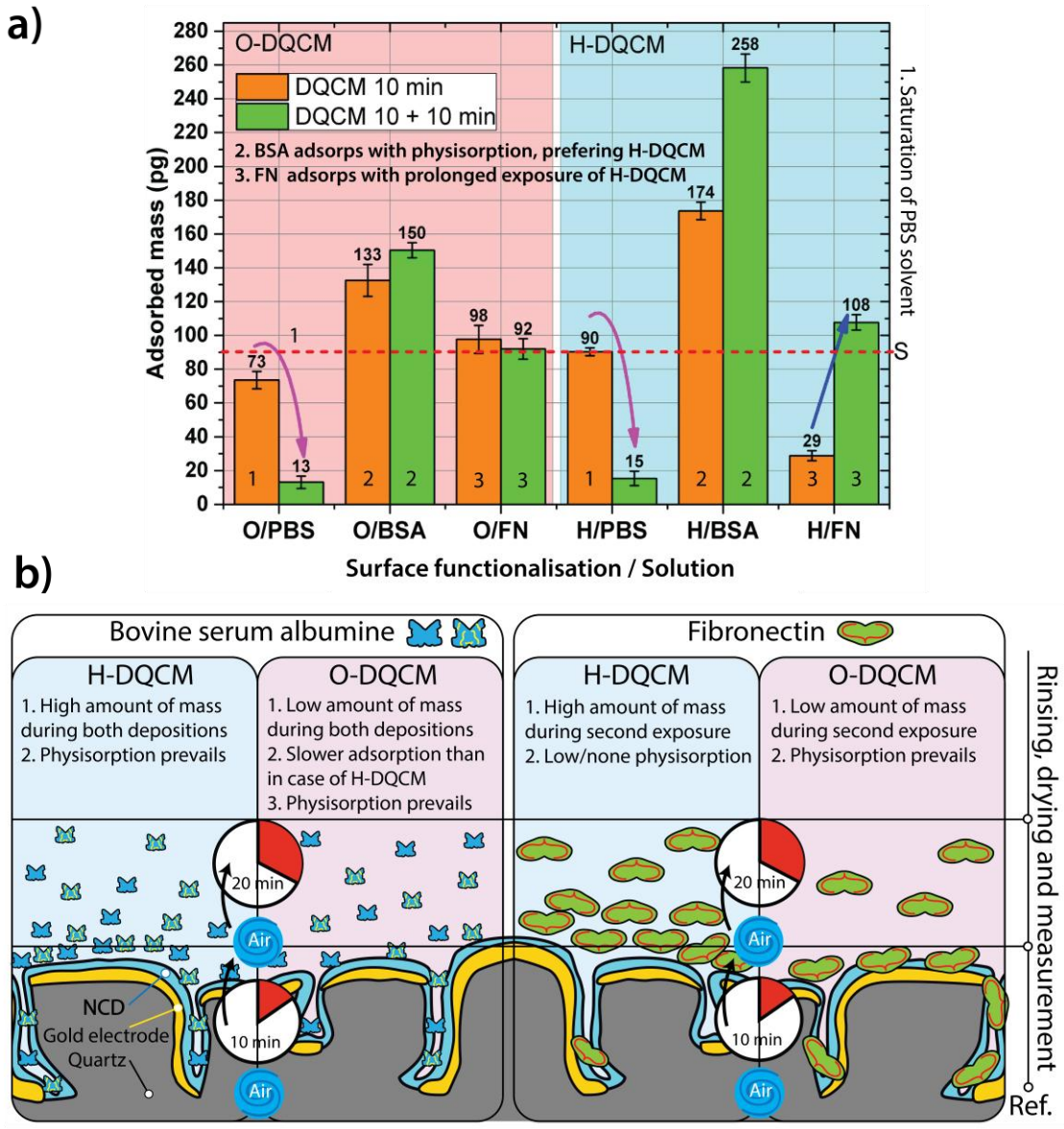

Figure 4.10 a) The results of adsorption compared for short and prolonged exposure time with standard deviation. b) The model of the ongoing effects during protein adhesion on the NCD-QCM sensor's surface

4.6.2. Author's contribution

I participated in this research with the design of the experiment, preparation of the samples, wettability modification (plasma treatment), measurement of the impedance response to different solutions, and evaluation of the data, followed by discussion and composing and reviewing of the article. Co-authors participated in the simulation, conceptualising the initial experiment and the deposition of diamond, writing parts of the text depending on the analysis performed and reviewing the article.

4.6.3. The paper's contributions toward the progress of the field

The latest knowledge focusing on the control of protein adsorption has shown many possible combinations of coatings with subsequential analysis using QCM methods. In the [156] study, the bases focused on creating a polyelectrolyte control multi-layer coating for minimizing non-specific adsorption. Using this, they have successfully minimized the adsorption of albumin, fibrinogen, and other seral proteins.

The QCM method is very often used in experiments concerning aptamer functionalisation [157], the formation of biofilm [158], the adsorption of surfactants [159] and tissue engineering [160] and immunoassays [161]. The generic goal of immunoassay coatings is to detect very low concentrations of analyte in the solution while preserving selectivity. Slightly different methods label-free methods of detection are used for the research of surface interaction. It utilises as a coating a layer which is mimicking the investigated surface, and it detects the mass preferentially binding to the surface, as described in the study focused on viral interactions with the host cell surface [162].

Other studies utilising the QCM sensor for the detection of serum proteins showed that there is a difference in adhesion depending on the surface charge of the protein. In [119], the adhered mass of diamond nanoparticles covered by bovine serum albumin and lysine was measured and cross-compared with ATR-FTIR analysis of their surface. This method was chosen because of the limitations of CVD deposition of NCD onto QCMs surface due to temperature. This issue has been overgone in [163], although the QCM sensor has been used for gas sensing applications. Until this article came to light, QCM was never coated with the diamond before.

In article [ARef:4], NCD coated QCMs were used for the first time in label-free detection of globular and fibrillar adhesive proteins. The nanocrystalline coating on QCM enables much easier, broader, and more stable functionalisation. On top of that, the morphology of the surface can be modified by tuning the deposition parameters. To validate the nondisruptive properties of the NCD on QCM gold electrode, the COMSOL® simulations were created, showing there is a dampening only in the form of a mass of the diamond layer, which agreed with the experiments.

4.6.4. Compliance with the objectives of the thesis

The goal has been to fabricate the QCM sensor with nanocrystalline diamond coating using the low-temperature deposition (< 350 °C) overwent the known problem of low Currie point of quartz. The simulation in the COMSOL® environment has been done to evaluate the influence of the diamond/Au/quartz interface on the sensing properties of the sensor. The simulations were performed to investigate the disruptive impact of diamond thin film on sensor piezoelectric properties. Following the preparation of the sensors, an experiment was performed with adhesive proteins (globular and fibrillar)

and different types of surface functionalisation with the accent on a different multitude of adhesion on a hydrophobic or hydrophobic solution. The QCM sensor showed a significant response, which differs depending on the surface modification. This finding contributes to understanding the ongoing effects on the interface of protein / nanocrystalline diamond. The results were discussed, and a simplified model was proposed as shown in Figure 4.10. The presented article has been published in Applied Surface Science Journal (IF=6.7, 2022).

5. Conclusion

Nowadays, diamond layers are widely used for experimental evaluations to outperform previous results and find new biosensors and cell detection applications. This fact leads to rapid improvements in fabrication technology and procedures. Researchers are each year closer to achieving the desired purity and homogeneity of the material for multiple uses in the electronic industry. New methods are developed, and new types of machinery are built, whether for industrial use or in the interests of science. In this thesis, diamond is used primarily as a material for sensing the application of living organisms, like non-adherent, non-polar yeast cells, adult stem cells, and their growth, activity, and adhesion. In the frame of this work, three types of diamond-based sensors were developed and realised. The results were summarised and published in peer-reviewed impacted journals and presented at international conferences based on experiments fully described in the attached publications.

The first developed device was a diamond-based SGFET sensor, which was used to characterise the cell/sensor interface using non-excitable nonpolar yeast cells. During the fabrication, one major problem occurred with the quality of the diamond channel in a few cases. The NCD channel is very sensitive to temperature changes and applied solutions. The sensors were damaged by temperature during reservoir settling several times. Another possible complication was the cracking of the diamond layer during the cooling down of the substrate. Both problems were identified and have been solved by different placement of the functional structures and by restriction of the temperature changes. Experiments were performed to characterise the cell / sensor interface. Based on measured results, the simplified model has been proposed. The results were published in Applied Surface Science (IF = 3.1, in 2017), and the reference can be found in [ARef:1] and in Appendix 8.1.

The second type of sensor presented in this thesis is the interdigitated transducer impedance sensor. This sensor detects the change of permittivity of the dielectric (cells) between contacts and, in the case of golden contacts without a diamond layer on the top, as well as the change of solutions conductivity. Such change occurs when the cell appears in the close vicinity or between the contacts. Few realised configurations are shown in Figure 3.11. These sensors were fabricated by standard optical lithography procedure. Sensors were used with adult stem cells to characterise the sensitivity of the sensor on cell growth. The results showed good sensitivity to cell activity, especially in the early stages of growth. The research was published in Colloids & Surfaces B Biointerfaces (IF = 4.1, in 2019), and the reference can be found in [ARef:2] and in Appendix 8.2.

The third type of sensor realised in this research was a quartz crystal microbalance sensor coated with the diamond thin film. Its working principle was based on the piezoelectric effect, the deformation of the crystal lattice in an electric field.

The impedance characteristics of sensors were measured at different times after the application of specific proteins, and shifts in serial resonant frequency peak positions were evaluated. These shifts were dependent on the amount of protein adhered to the surface. This amount differs if hydrogen or oxygen termination was used because of its wettability. Results were presented at international conferences and published in Applied Surface Science (IF = 6.7, in 2022) [ARef:4] and in Appendix 8.3.

5.1. Scientific contribution

My contribution to the presented research activities relies on the implementation of novel and unique approaches in the field of diamond-based biosensors. With the use of well-known sensing electrical and electro-mechanical principles enhanced by extraordinary properties of the nanocrystalline thin films, living organisms and cell cultures are monitored real-time, label-free and “in vitro” without disturbing their metabolic state.

The first sensor, the SGFET, was unique with its sensitivity and the novelty lies in its use with nonadherent yeast cells and parts of the HIV genome. The shifts in transfer characteristics were dependent on the ionic strength of the solution, and a significant shift was observed with the use of non-adherent yeast cells. By this technique, I monitored the viability of the cell culture electrically. With the knowledge from the fabrication and measurement of used SGFET sensors, I created a new design of the sensor to increase reliability, conductivity, and sensitivity and to lower the “faulty from fabrication” rate.

Inspired by results accumulated during the use of the SGFET sensor and understanding factors disrupting the SGFETs measuring capability (i.e., with the adhesive molecules), the examination of protein adhesion on the nanocrystalline diamond came to my attention.

This brings us to the second type of sensor, the QCM sensor used for the first time coated by NCD as a biosensor for label-free protein detection, which showed sensitivity to the mass of adhered proteins. By this method, I further characterised the mechanism of the protein adhesion on the hydrophobic and hydrophilic substrates. The SRF shifts revealed that the D-QCM sensor functionalised with oxygen is less sensitive to both FN and BSA with a faster saturation rate than the sensor functionalised with hydrogen. On the other hand, the sensor functionalised by hydrogen is susceptible to promoting FN’s adhesion. I performed the measurement in triplets to minimize the outlying results' influence and provide standard deviations.

The third sensor principle I dealt with is the IDT sensor covered by nanocrystalline diamond. Such sensors were used for label-free impedance measurement of living cultures to characterise their viability in real-time. The novelty of this research is ensured by a coating of gold IDT electrodes with nanocrystalline diamond

and using such a system with a living culture. In addition, the presence of high-quality nanocrystalline diamond enabled further modification of the surface, thus tuning the sensors' sensitivity and selectivity. Biocompatible structures were created, and with the cooperation of the Biotechnology and biomedicine centre in Vestec, the IDT sensors were characterised in working conditions under the influence of ASC cell culture. The research confirmed that the diamond IDT sensors have remarkable sensitivity in an early stage of cell growth, higher than commercially used Au/SiO_2 X-Celligence® sensors.

It can be concluded that within the scope of this thesis, the diamond-based biosensors were designed, fabricated, and validated with the experiment in a novel way while following the current directions in the field of diamond-based biosensors. The models were proposed based on experimental results, describing the interaction of nanocrystalline diamond with proteins, aptamers, and living cells. The obtained knowledge contributed to the field of label-free diamond biosensors.

5.2. Prospects

During my Ph.D. study, I found several new possibilities for how to use each sensor, which have not been fully explored in this work. In the case of SGFET, I would like to use it with bacteria and develop a method to differentiate between several species based on their surface properties. Another possible improvement would be to use a new design of the SGFET sensor and structure its conductive channel with etching to create a 3D diamond structure and observe the response of such sensor. In the future, monitoring of different cell cultures with specifically tailored surface properties (modifying surface functionalisation) is planned.

In the case of mass and impedance sensors (i.e., QCM and IDT), I am currently experimenting with the possibility of combining them into one sensor. Such a sensor could serve as the detector QCM sensor and IDT sensor and can combine both measurement procedures into one, not to mention the IDT electrodes can be used for stimulation or excitation of the living material on its surface. In the future, I would like to use gained knowledge to employ more sensing principles and perhaps develop a combined sensor, which could be used for multisensory measurement

The abovementioned sensors utilise intrinsic, i.e., non-doped nanocrystalline diamond. A wide variety of surface functionalisation and morphology changes combined with doped conductive diamond offers new possibilities for future research.

6. References

[1] P. Strobel, M. Riedel, J. Ristein, L. Ley, O. Boltalina, Surface transfer doping of diamond by fullerene, Diam. Relat. Mater. 14 (2005) 451–458. https://doi.org/10.1016/j.diamond.2004.12.051.

[2] A. Rahim Ruslinda, K. Tanabe, S. Ibori, X. Wang, H. Kawarada, Effects of diamond-FET-based RNA aptamer sensing for detection of real sample of HIV-1 Tat protein, Biosens. Bioelectron. 40 (2013) 277–282. https://doi.org/10.1016/j.bios.2012.07.048.

[3] J.W. Morgan, E. Anderst, Chemical composition, 77 (1980) 6973–6977.

[4] S.K. Tiwari, V. Kumar, A. Huczko, R. Oraon, A. De Adhikari, G.C. Nayak, Magical Allotropes of Carbon: Prospects and Applications, Crit. Rev. Solid State Mater. Sci. 41 (2016) 257–317. https://doi.org/10.1080/10408436.2015.1127206.

[5] Z. Zhuo, X. Wu, J. Yang, Me-graphene: a graphene allotrope with near zero Poisson's ratio, sizeable band gap, and high carrier mobility, Nanoscale. 12 (2020) 19359–19366. https://doi.org/10.1039/D0NR03869E.

[6] V. Georgakilas, J.A. Perman, J. Tucek, R. Zboril, Broad Family of Carbon Nanoallotropes: Classification, Chemistry, and Applications of Fullerenes, Carbon Dots, Nanotubes, Graphene, Nanodiamonds, and Combined Superstructures, Chem. Rev. 115 (2015) 4744–4822. https://doi.org/10.1021/cr500304f.

[7] J.M. Zazula, On Graphite Transformations at High Temperature and Pressure Induced by Absorption of the LHC Beam, Cern. (1997) 15.

[8] A. Krueger, Carbon Materials and Nanotechnology, Wiley, 2010. https://doi.org/10.1002/9783527629602.

[9] O.A. Shenderova, V. V. Zhirnov, D.W. Brenner, Carbon Nanostructures, Crit. Rev. Solid State Mater. Sci. 27 (2002) 227–356. https://doi.org/10.1080/10408430208500497.

[10] P. Atkins, Physical Chemistry, 2021. https://doi.org/10.1007/s00897010493a.

[11] S.F. Mitura, S. Mitura, K. Mitura, P. Niedzielski, P. Louda, V. Danilenko, Analysis of the relationship between the spectrum of optical measurement signal and blood parameters View project Grant supp. by Minister of Science and Higher Education of Poland No NN205144833 View project, (2007). https://www.researchgate.net/publication/40804793 (accessed February 14, 2022).

[12] C. FRONDEL, U.B. MARVIN, Lonsdaleite, a Hexagonal Polymorph of Diamond, Nature. 214 (1967) 587–589. https://doi.org/10.1038/214587a0.

[13] D. Demarchi, A. Tagliaferro, Carbon for sensing devices, Springer International Publishing, Cham, 2015. https://doi.org/10.1007/978-3-319-08648-4.

[14] P.A. Nistor, P.W. May, Diamond thin films: Giving biomedical applications a new shine, J. R. Soc. Interface. 14 (2017) 20170382. https://doi.org/10.1098/rsif.2017.0382.

[15] H. Liu, D.S. Dandy, Diamond chemical vapor deposition: nucleation and early growth stages, Elsevier, 1996.

[16] A.M. Zaitsev, N.M. Kazuchits, V.N. Kazuchits, K.S. Moe, M.S. Rusetsky, O.V. Korolik, K. Kitajima, J.E. Butler, W. Wang, Nitrogen-doped CVD diamond: Nitrogen concentration, color and internal stress, Diam. Relat. Mater. 105 (2020) 107794. https://doi.org/10.1016/j.diamond.2020.107794.

[17] R. Kalish, C. Uzan-Saguy, B. Philosoph, V. Richter, J.P. Lagrange, E. Gheeraert, A. Deneuville, A.T. Collins, Nitrogen doping of diamond by ion implantation, Diam. Relat. Mater. 6 (1997) 516–520. https://doi.org/10.1016/S0925-9635(96)00657-7.

[18] S. Szunerits, C.E. Nebel, R.J. Hamers, Surface functionalization and biological applications of CVD diamond, MRS Bull. 39 (2014) 517–524. https://doi.org/10.1557/mrs.2014.99.

[19] K. Mizuuchi, K. Inoue, Y. Agari, Y. Morisada, M. Sugioka, M. Tanaka, T. Takeuchi, J. Tani, M. Kawahara, Y. Makino, Processing of diamond particle dispersed aluminum matrix composites in continuous solid–liquid co-existent state by SPS and their thermal properties, Compos. Part B Eng. 42 (2011) 825–831. https://doi.org/10.1016/j.compositesb.2011.01.012.

[20] H. Luo, K.M. Ajmal, W. Liu, K. Yamamura, H. Deng, Polishing and planarization of single crystal diamonds: State-of-the-art and perspectives, Int. J. Extrem. Manuf. 3 (2021). https://doi.org/10.1088/2631-7990/abe915.

[21] O.A. Williams, Nanocrystalline diamond, Diam. Relat. Mater. 20 (2011) 621–640. https://doi.org/10.1016/j.diamond.2011.02.015.

[22] W. Gajewski, P. Achatz, O.A. Williams, K. Haenen, E. Bustarret, M. Stutzmann, J.A. Garrido, Electronic and optical properties of boron-doped nanocrystalline diamond films, Phys. Rev. B - Condens. Matter Mater. Phys. 79 (2009) 045206.

https://doi.org/10.1103/PHYSREVB.79.045206/FIGURES/14/MEDIUM.

[23] F. Neugart, A. Zappe, F. Jelezko, C. Tietz, J.P. Boudou, A. Krueger, J. 1rg Wrachtrup, Dynamics of Diamond Nanoparticles in Solution and Cells, (2007). https://doi.org/10.1021/nl0716303.

[24] N. Kossovsky, A. Gelman, H.J. Hnatyszyn, S. Rajguru, R.L. Garrell, S. Torbati, S.S.S.F. Freitas, G.M. Chow, Surface-Modified Diamond Nanoparticles as Antigen Delivery Vehicles, Bioconjug. Chem. 6 (2002) 507–511. https://doi.org/10.1021/BC00035A001.

[25] H.B. Man, D. Ho, Nanodiamonds as platforms for biology and medicine, J. Lab. Autom. 18 (2013) 12–18. https://doi.org/10.1177/2211068212456198.

[26] W. Jakubowski, G. Bartosz, P. Niedzielski, W. Szymanski, B. Walkowiak, Nanocrystalline diamond surface is resistant to bacterial colonization, Diam. Relat. Mater. 13 (2004) 1761–1763. https://doi.org/10.1016/J.DIAMOND.2004.03.003.

[27] W. Okrój, M. Kamińska, L. Klimek, W. Szymański, B. Walkowiak, Blood platelets in contact with nanocrystalline diamond surfaces, Diam. Relat. Mater. 15 (2006) 1535–1539. https://doi.org/10.1016/J.DIAMOND.2005.12.033.

[28] R.J. Narayan, W. Wei, C. Jin, M. Andara, A. Agarwal, R.A. Gerhardt, C.C. Shih, C.M. Shih, S.J. Lin, Y.Y. Su, R. Ramamurti, R.N. Singh, Microstructural and biological properties of nanocrystalline diamond coatings, Diam. Relat. Mater. 15 (2006) 1935–1940. https://doi.org/10.1016/J.DIAMOND.2006.08.024.

[29] O. Auciello, P. Gurman, M.B. Guglielmotti, D.G. Olmedo, A. Berra, M.J. Saravia, Biocompatible ultrananocrystalline diamond coatings for implantable medical devices, MRS Bull. 39 (2014) 621–629. https://doi.org/10.1557/MRS.2014.134.

[30] E.M.A. Fuentes-Fernandez, J.J. Alcantar-Peña, G. Lee, A. Boulom, H. Phan, B. Smith, T. Nguyen, S. Sahoo, F. Ruiz-Zepeda, M.J. Arellano-Jimenez, P. Gurman, C.A. Martinez-Perez, M.J. Yacaman, R.S. Katiyar, O. Auciello, Synthesis and characterization of microcrystalline diamond to ultrananocrystalline diamond films via Hot Filament Chemical Vapor Deposition for scaling to large area applications, Thin Solid Films. 603 (2016) 62–68. https://doi.org/10.1016/j.tsf.2015.11.088.

[31] O.A. Williams, M. Nesladek, M. Daenen, S. Michaelson, A. Hoffman, E. Osawa, K. Haenen, R.B. Jackman, Growth, electronic properties and applications of nanodiamond, Diam. Relat. Mater. 17 (2008) 1080–1088. https://doi.org/10.1016/j.diamond.2008.01.103.

[32] G.M. Klemencic, J.M. Fellows, J.M. Werrell, S. Mandal, S.R. Giblin, R.A. Smith, O.A. Williams, Fluctuation spectroscopy as a probe of granular superconducting diamond films, Phys. Rev. Mater. 1 (2017) 044801. https://doi.org/10.1103/PhysRevMaterials.1.044801.

[33] M. Mertens, M. Mohr, N. Wiora, K. Brühne, H.J. Fecht, N-type conductive ultrananocrystalline diamond films grown by hot filament CVD, J. Nanomater. 2015 (2015). https://doi.org/10.1155/2015/527025.

[34] H.O. Pierson, Handbook of carbon, graphite, diamonds and fullerenes: processing, properties and applications, William Andrew, 2012.

[35] P.W. May, Diamond thin films: a 21st-century material, Philos. Trans. R. Soc. London. Ser. A Math. Phys. Eng. Sci. 358 (2000) 473–495. https://doi.org/10.1098/rsta.2000.0542.

[36] K. Tsugawa, M. Ishihara, J. Kim, M. Hasegawa, Y. Koga, Large-area and low-temperature nanodiamond coating by microwave plasma chemical vapor deposition, 2006. https://www.researchgate.net/publication/236737100 (accessed January 23, 2020).

[37] M. Kamo, Y. Sato, S. Matsumoto, N. Setaka, Diamond synthesis from gas phase in microwave plasma, J. Cryst. Growth. 62 (1983) 642–644. https://doi.org/10.1016/0022-0248(83)90411-6.

[38] A. Kromka, O. Babchenko, T. Izak, K. Hruska, B. Rezek, Linear antenna microwave plasma CVD deposition of diamond films over large areas, Vacuum. 86 (2012) 776–779. https://doi.org/10.1016/j.vacuum.2011.07.008.

[39] S. Prawer, R.J. Nemanich, Raman spectroscopy of diamond and doped diamond, Philos. Trans. R. Soc. London. Ser. A Math. Phys. Eng. Sci. 362 (2004) 2537–2565. https://doi.org/10.1098/rsta.2004.1451.

[40] M. Varga, A. Laposa, P. Kulha, J. Kroutil, M. Husak, A. Kromka, Quartz crystal microbalance gas sensor with nanocrystalline diamond sensitive layer, Phys. Status Solidi Basic Res. 252 (2015) 2591–2597. https://doi.org/10.1002/pssb.201552229.

[41] O. Babchenko, Z. Remes, T. Izak, B. Rezek, A. Kromka, Deposition of nanocrystalline diamond films on temperature sensitive substrates for infrared reflectance spectroscopy, Phys. Status Solidi Basic Res. 248 (2011) 2736–2739. https://doi.org/10.1002/pssb.201100119.

[42] J.H. Yang, M. Degawa, K.S. Song, C. Wang, H. Kawarada, Fabrication of calcium ion sensitive

diamond field effect transistors (FETs) based on immobilized calmodulin, Mater. Lett. 64 (2010) 2321–2324. https://doi.org/10.1016/j.matlet.2010.02.057.

[43] R. Müller, A. Denisenko, M. Adamschik, E. Kohn, On the ion-sensitivity of H-terminated surface channel devices on diamond, Diam. Relat. Mater. 11 (2002) 651–656. https://doi.org/10.1016/S0925-9635(01)00704-X.

[44] M. Panizza, G. Cerisola, Application of diamond electrodes to electrochemical processes, Electrochim. Acta. 51 (2005) 191–199. https://doi.org/10.1016/j.electacta.2005.04.023.

[45] J. V. Macpherson, The Use of Conducting Diamond in Electrochemistry, in: 2015: pp. 163–210. https://doi.org/10.1002/9783527697489.ch5.

[46] F. Gao, C.E. Nebel, Micro- and Nano-structured Diamond in Electrochemistry, in: Nanocarbons Electroanal., John Wiley & Sons, Ltd, Chichester, UK, 2017: pp. 197–226. https://doi.org/10.1002/9781119243915.ch8.

[47] A. Fujishima, Y. Einaga, T.N. Rao, D.A. Tryk, Diamond Electrochemistry., (2005) 609.

[48] D.R. Wur, J.L. Davidson, W.P. Kang, D.L. Kinser, Polycrystalline diamond pressure sensor, J. Microelectromechanical Syst. 4 (1995) 34–41. https://doi.org/10.1109/84.365368.

[49] M. Werner, O. Dorsch, E. Obermeier, High-temperature pressure sensor using p-type diamond piezoresistors, Diam. Relat. Mater. 4 (1995) 873–876. https://doi.org/10.1016/0925-9635(94)05231-X.

[50] A. Yamamoto, N. Nawachi, T. Tsutsumoto, A. Terayama, Pressure sensor using p-type polycrystalline diamond piezoresistors, Diam. Relat. Mater. 14 (2005) 657–660. https://doi.org/10.1016/J.DIAMOND.2004.09.001.

[51] M.S.J. Barson, P. Peddibhotla, P. Ovartchaiyapong, K. Ganesan, R.L. Taylor, M. Gebert, Z. Mielens, B. Koslowski, D.A. Simpson, L.P. McGuinness, J. McCallum, S. Prawer, S. Onoda, T. Ohshima, A.C. Bleszynski Jayich, F. Jelezko, N.B. Manson, M.W. Doherty, Nanomechanical Sensing Using Spins in Diamond, Nano Lett. 17 (2017) 1496–1503. https://doi.org/10.1021/acs.nanolett.6b04544.

[52] M. Gulka, D. Wirtitsch, V. Ivády, J. Vodnik, J. Hruby, G. Magchiels, E. Bourgeois, A. Gali, M. Trupke, M. Nesladek, Room-temperature control and electrical readout of individual nitrogen-vacancy nuclear spins, Nat. Commun. 2021 121. 12 (2021) 1–8. https://doi.org/10.1038/s41467-021-24494-x.

[53] Y. Sekiguchi, Y. Yasui, K. Tsurumoto, Y. Koga, R. Reyes, H. Kosaka, Geometric entanglement of a photon and spin qubits in diamond, Commun. Phys. 4 (2021) 264. https://doi.org/10.1038/S42005-021-00767-1.

[54] N. Savage, Quantum diamond sensors, Nature. 591 (2021) S37. https://doi.org/10.1038/D41586-021-00742-4.

[55] Y. Gurbuz, W.P. Kang, J.L. Davidson, D.L. Kinser, D. V. Kerns, Diamond microelectronic gas sensors, Sensors Actuators, B Chem. 33 (1996) 100–104. https://doi.org/10.1016/0925-4005(96)01839-4.

[56] A. Kromka, M. Davydova, B. Rezek, M. Vanecek, M. Stuchlik, P. Exnar, M. Kalbac, Gas sensing properties of nanocrystalline diamond films, Diam. Relat. Mater. 19 (2010) 196–200. https://doi.org/10.1016/j.diamond.2009.10.006.

[57] C.S. Lee, S. Kyu Kim, M. Kim, Ion-sensitive field-effect transistor for biological sensing, Sensors. 9 (2009) 7111–7131. https://doi.org/10.3390/s90907111.

[58] M. Davydova, P. Kulha, A. Laposa, K. Hruska, P. Demo, A. Kromka, Gas sensing properties of nanocrystalline diamond at room temperature, Beilstein J. Nanotechnol. 5243. 5 (2014) 2339–2345. https://doi.org/10.3762/BJNANO.5.243.

[59] A. Helwig, G. Müller, J.A. Garrido, M. Eickhoff, Gas sensing properties of hydrogen-terminated diamond, Sensors Actuators B Chem. 133 (2008) 156–165. https://doi.org/10.1016/J.SNB.2008.02.007.

[60] A. Hikavyy, P. Clauws, K. Vanbesien, P. De Visschere, O.A. Williams, M. Daenen, K. Haenen, J.E. Butler, T. Feygelson, Atomic layer deposition of ZnO thin films on boron-doped nanocrystalline diamond, Diam. Relat. Mater. 16 (2007) 983–986. https://doi.org/10.1016/J.DIAMOND.2006.11.035.

[61] F.A. Almeida, M. Belmonte, A.J.S. Fernandes, F.J. Oliveira, R.F. Silva, MPCVD diamond coating of Si3N4-TiN electroconductive composite substrates, Diam. Relat. Mater. 16 (2007) 978–982. https://doi.org/10.1016/j.diamond.2006.11.021.

[62] A. Saravanan, B.R. Huang, D. Kathiravan, Surface and interface properties of monolayer graphene on hydrophobic and hydrophilic ultrananocrystalline diamond structures for hydrogen sensing applications, Int. J. Hydrogen Energy. 47 (2022) 4959–4969.

https://doi.org/10.1016/J.IJHYDENE.2021.11.067.
[63] H. Kawarada, A.R. Ruslinda, Diamond electrolyte solution gate FETs for DNA and protein sensors using DNA/RNA aptamers, Phys. Status Solidi Appl. Mater. Sci. 208 (2011) 2005–2016. https://doi.org/10.1002/pssa.201100503.
[64] A. Härtl, B. Baur, M. Stutzmann, J.A. Garrido, Enzyme-modified field effect transistors based on surface-conductive single-crystalline diamond, Langmuir. 24 (2008) 9898–9906. https://doi.org/10.1021/la8014139.
[65] A. Härtl, E. Schmich, J.A. Garrido, J. Hernando, S.C.R. Catharino, S. Walter, P. Feulner, A. Kromka, D. Steinmüller, M. Stutzmann, Protein-modified nanocrystalline diamond thin films for biosensor applications, Nat. Mater. 3 (2004) 736–742. https://doi.org/10.1038/nmat1204.
[66] C.E. Nebel, B. Rezek, D. Shin, H. Watanabe, Surface electronic properties of H-terminated diamond in contact with adsorbates and electrolytes, Phys. Status Solidi Appl. Mater. Sci. 203 (2006) 3273–3298. https://doi.org/10.1002/pssa.200671401.
[67] D. Zemmyo, S. Miyata, Evaluation of Lipid Accumulation Using Electrical Impedance Measurement under Three-Dimensional Culture Condition., Micromachines. 10 (2019). https://doi.org/10.3390/mi10070455.
[68] H.S. Jun, L.T.M. Dao, J.C. Pyun, S. Cho, Effect of cell senescence on the impedance measurement of adipose tissue-derived stem cells, Enzyme Microb. Technol. 53 (2013) 302–306. https://doi.org/10.1016/J.ENZMICTEC.2013.07.001.
[69] C.M. Lopez, H.S. Chun, S. Wang, L. Berti, J. Putzeys, C. Van Den Bulcke, J.W. Weijers, A. Firrincieli, V. Reumers, D. Braeken, N. Van Helleputte, A multimodal CMOS MEA for high-throughput intracellular action potential measurements and impedance spectroscopy in drug-screening applications, IEEE J. Solid-State Circuits. 53 (2018) 3076–3086. https://doi.org/10.1109/JSSC.2018.2863952.
[70] C. Sprössler, D. Richter, M. Denyer, A. Offenhäusser, Long-term recording system based on field-effect transistor arrays for monitoring electrogenic cells in culture, Biosens. Bioelectron. 13 (1998) 613–618. https://doi.org/10.1016/S0956-5663(98)00016-5.
[71] P.O. Bagnaninchi, N. Drummond, Real-time label-free monitoring of adipose-derived stem cell differentiation with electric cell-substrate impedance sensing, Proc. Natl. Acad. Sci. U. S. A. 108 (2011) 6462–6467. https://doi.org/10.1073/pnas.1018260108.
[72] V. Procházka, M. Cifra, P. Kulha, T. Ižák, B. Rezek, A. Kromka, Influence of non-adherent yeast cells on electrical characteristics of diamond-based field-effect transistors, Appl. Surf. Sci. 395 (2017) 214–219. https://doi.org/10.1016/j.apsusc.2016.05.003.
[73] V. Procházka, R. Matějka, T. Ižák, O. Szabó, J. Štěpanovská, E. Filová, L. Bačáková, V. Jirásek, A. Kromka, Nanocrystalline diamond-based impedance sensors for real-time monitoring of adipose tissue-derived stem cells, Colloids Surfaces B Biointerfaces. 177 (2019) 130–136. https://doi.org/10.1016/j.colsurfb.2019.01.048.
[74] E. van Vliet, L. Stoppini, M. Balestrino, C. Eskes, C. Griesinger, T. Sobanski, M. Whelan, T. Hartung, S. Coecke, Electrophysiological recording of re-aggregating brain cell cultures on multi-electrode arrays to detect acute neurotoxic effects, Neurotoxicology. 28 (2007) 1136–1146. https://doi.org/10.1016/j.neuro.2007.06.004.
[75] M. Ohara, M. Kameyama, K. Yazawa, M. Kaibara, An Improved Method for Isolating Cardiac Myocytes Useful for Patch-Clamp Studies, Jpn. J. Physiol. 40 (1990) 157–163. https://doi.org/10.2170/jjphysiol.40.157.
[76] C.E. Nebel, D. Shin, B. Rezek, N. Tokuda, H. Uetsuka, H. Watanabe, Diamond and biology, J. R. Soc. Interface. 4 (2007) 439–461. https://doi.org/10.1098/rsif.2006.0196.
[77] M. Krátká, A. Kromka, B. Rezek, A. Brož, M. Kalbáčová, Characteristics of Nanocrystalline Diamond SGFETs Under Cell Culture Conditions, WDS'11 Proc. Contrib. Pap. 5 (2011) 160–165.
[78] A. Thalhammer, R.J. Edgington, L.A. Cingolani, R. Schoepfer, R.B. Jackman, The use of nanodiamond monolayer coatings to promote the formation of functional neuronal networks, Biomaterials. 31 (2010) 2097–2104. https://doi.org/10.1016/j.biomaterials.2009.11.109.
[79] R. Narayan, Diamond-based materials for biomedical applications, Elsevier, 2013.
[80] M. Verdanova, B. Rezek, A. Broz, E. Ukraintsev, O. Babchenko, A. Artemenko, T. Izak, A. Kromka, M. Kalbac, M. Hubalek Kalbacova, Nanocarbon Allotropes - Graphene and Nanocrystalline Diamond - Promote Cell Proliferation, Small. 12 (2016) 2499–2509. https://doi.org/10.1002/smll.201503749.
[81] B. Rezek, E. Ukraintsev, L. Michalíková, A. Kromka, J. Zemek, M. Kalbacova, Adsorption of fetal

bovine serum on H/O-terminated diamond studied by atomic force microscopy, Diam. Relat. Mater. 18 (2009) 918–922. https://doi.org/10.1016/j.diamond.2009.02.009.

[82] M.R. Blatt, C.L. Slayman, KCl leakage from microelectrodes and its impact on the membrane parameters of a nonexcitable cell, J. Membr. Biol. 72 (1983) 223–234. https://doi.org/10.1007/BF01870589.

[83] M. Dankerl, S. Eick, B. Hofmann, M.H.S. Ingebrandt, A. Offenhäusser, M. Stutzmann, J.A. Garrido, Diamond transistor array for extracellular recording from electrogenic cells, Adv. Funct. Mater. 19 (2009) 2915–2923. https://doi.org/10.1002/adfm.200900590.

[84] A. Ahnood, H. Meffin, D.J. Garrett, K. Fox, K. Ganesan, A. Stacey, N. V. Apollo, Y.T. Wong, S.G. Lichter, W. Kentler, O. Kavehei, U. Greferath, K.A. Vessey, M.R. Ibbotson, E.L. Fletcher, A.N. Burkitt, S. Prawer, Diamond Devices for High Acuity Prosthetic Vision, Adv. Biosyst. 2 (2018) 1800043. https://doi.org/10.1002/adbi.201800043.

[85] V. Maybeck, R. Edgington, A. Bongrain, J.O. Welch, E. Scorsone, P. Bergonzo, R.B. Jackman, A. Offenhäusser, Boron-doped nanocrystalline diamond microelectrode arrays monitor cardiac action potentials, Adv. Healthc. Mater. 3 (2014) 283–289. https://doi.org/10.1002/adhm.201300062.

[86] M. Thein, F. Asphahani, A. Cheng, R. Buckmaster, M. Zhang, J. Xu, Response characteristics of single-cell impedance sensors employed with surface-modified microelectrodes, Biosens. Bioelectron. 25 (2010) 1963–1969. https://doi.org/10.1016/j.bios.2010.01.023.

[87] H.L. Gomes, R.B. Leite, R. Afonso, P. Stallinga, M.L. Cancela, A microelectrode impedance method to measure interaction of cells, Proc. IEEE Sensors, 2004. (2004) 1011–1013. https://doi.org/10.1109/ICSENS.2004.1426344.

[88] P. Bergonzo, A. Bongrain, E. Scorsone, A. Bendali, L. Rousseau, G. Lissorgues, P. Mailley, Y. Li, T. Kauffmann, F. Goy, B. Yvert, J.A. Sahel, S. Picaud, 3D shaped mechanically flexible diamond microelectrode arrays for eye implant applications: The MEDINAS project, Irbm. 32 (2011) 91–94. https://doi.org/10.1016/j.irbm.2011.01.032.

[89] T. Ižák, K. Novotná, I. Kopová, L. Bačáková, B. Rezek, A. Kromka, H-terminated diamond as optically transparent impedance sensor for real-time monitoring of cell growth, Phys. Status Solidi Basic Res. 250 (2013) 2741–2746. https://doi.org/10.1002/pssb.201300098.

[90] M. Krátká, A. Kromka, E. Ukraintsev, M. Ledinský, A. Brož, M. Kalbacova, B. Rezek, Function of thin film nanocrystalline diamond-protein SGFET independent of grain size, Sensors Actuators, B Chem. 166–167 (2012) 239–245. https://doi.org/10.1016/j.snb.2012.02.049.

[91] B. Rezek, D. Shin, H. Watanabe, C.E. Nebel, Intrinsic hydrogen-terminated diamond as ion-sensitive field effect transistor, Sensors Actuators, B Chem. 122 (2007) 596–599. https://doi.org/10.1016/j.snb.2006.07.004.

[92] B. Rezek, E. Ukraintsev, A. Kromka, M. Ledinský, A. Brož, L. Nosková, H. Hartmannová, M. Kalbacova, Assembly of osteoblastic cell micro-arrays on diamond guided by protein pre-adsorption, Diam. Relat. Mater. 19 (2010) 153–157. https://doi.org/10.1016/j.diamond.2009.09.016.

[93] P.K. Ang, K.P. Loh, T. Wohland, M. Nesladek, E. Van Hove, Supported lipid bilayer on nanocrystalline diamond: Dual optical and field-effect sensor for membrane disruption, Adv. Funct. Mater. 19 (2009) 109–116. https://doi.org/10.1002/adfm.200800770.

[94] D. Havelka, O. Kučera, M.A. Deriu, M. Cifra, Electro-acoustic behavior of the mitotic spindle: A semi-classical coarse-grained model, PLoS One. 9 (2014) e86501. https://doi.org/10.1371/journal.pone.0086501.

[95] O. Kučera, D. Havelka, M. Cifra, Vibrations of microtubules: Physics that has not met biology yet, Wave Motion. 72 (2017) 13–22. https://doi.org/10.1016/j.wavemoti.2016.12.006.

[96] O. Kučera, M. Cifra, J. Pokorný, Technical aspects of measurement of cellular electromagnetic activity, Eur. Biophys. J. 39 (2010) 1465–1470. https://doi.org/10.1007/s00249-010-0597-8.

[97] A. Bendali, C. Agnès, S. Meffert, V. Forster, A. Bongrain, J.C. Arnault, J.A. Sahel, A. Offenhäusser, P. Bergonzo, S. Picaud, Distinctive glial and neuronal interfacing on nanocrystalline diamond, PLoS One. 9 (2014) e92562. https://doi.org/10.1371/journal.pone.0092562.

[98] A.E. Hadjinicolaou, R.T. Leung, D.J. Garrett, K. Ganesan, K. Fox, D.A.X. Nayagam, M.N. Shivdasani, H. Meffin, M.R. Ibbotson, S. Prawer, B.J. O'Brien, Electrical stimulation of retinal ganglion cells with diamond and the development of an all diamond retinal prosthesis, Biomaterials. 33 (2012) 5812–5820. https://doi.org/10.1016/j.biomaterials.2012.04.063.

[99] P.T. Mitrikeski, Yeast competence for exogenous DNA uptake: Towards understanding its genetic

component, Antonie van Leeuwenhoek, Int. J. Gen. Mol. Microbiol. 103 (2013) 1181–1207. https://doi.org/10.1007/s10482-013-9905-5.

[100] D.E. Amory, P.G. Rouxhet, J.P. Dufour, Flocculence of Brewery Yeasts and Their Surface Properties: Chemical Composition, Electrostatic Charge and Hydrophobicity, J. Inst. Brew. 94 (1988) 79–84. https://doi.org/10.1002/j.2050-0416.1988.tb04561.x.

[101] D.J. Fisher, Flocculation—Some Observations on the Surface Charges of Yeast Cells, J. Inst. Brew. 81 (1975) 107–110. https://doi.org/10.1002/j.2050-0416.1975.tb03670.x.

[102] K.J. Verstrepen, F.M. Klis, Flocculation, adhesion and biofilm formation in yeasts, Mol. Microbiol. 60 (2006) 5–15. https://doi.org/10.1111/j.1365-2958.2006.05072.x.

[103] H.D. Mortensen, K. Dupont, L. Jespersen, W.G.T. Willats, N. Arneborg, Identification of amino acids involved in the Flo11p-mediated adhesion of Saccharomyces cerevisiae to a polystyrene surface using phage display with competitive elution, J. Appl. Microbiol. 103 (2007) 1041–1047. https://doi.org/10.1111/j.1365-2672.2007.03325.x.

[104] S. Koyama, T. Tsubouchi, K. Usui, K. Uematsu, A. Tame, Y. Nogi, Y. Ohta, Y. Hatada, C. Kato, T. Miwa, T. Toyofuku, T. Nagahama, M. Konishi, Y. Nagano, F. Abe, Involvement of flocculin in negative potential-applied ITO electrode adhesion of yeast cells, FEMS Yeast Res. 15 (2015) fov064. https://doi.org/10.1093/femsyr/fov064.

[105] S.E. Van Mulders, E. Christianen, S.M.G. Saerens, L. Daenen, P.J. Verbelen, R. Willaert, K.J. Verstrepen, F.R. Delvaux, Phenotypic diversity of Flo protein family-mediated adhesion in Saccharomyces cerevisiae, FEMS Yeast Res. 9 (2009) 178–190. https://doi.org/10.1111/j.1567-1364.2008.00462.x.

[106] Y. Fang, Label-Free Biosensors for Cell Biology, Int. J. Electrochem. 2011 (2011) 1–16. https://doi.org/10.4061/2011/460850.

[107] Y. Xu, X. Xie, Y. Duan, L. Wang, Z. Cheng, J. Cheng, A review of impedance measurements of whole cells, Biosens. Bioelectron. 77 (2016) 824–836. https://doi.org/10.1016/j.bios.2015.10.027.

[108] H.K. Hunt, A.M. Armani, Label-free biological and chemical sensors, (n.d.). https://doi.org/10.1039/c0nr00201a.

[109] C.E. Nebel, B. Rezek, D. Shin, H. Uetsuka, N. Yang, Diamond for bio-sensor applications, J. Phys. D. Appl. Phys. 40 (2007) 6443–6466. https://doi.org/10.1088/0022-3727/40/20/S21.

[110] M. Davydova, M. Stuchlik, B. Rezek, K. Larsson, A. Kromka, Sensing of phosgene by a porous-like nanocrystalline diamond layer with buried metallic electrodes, Sensors Actuators, B Chem. 188 (2013) 675–680. https://doi.org/10.1016/j.snb.2013.07.079.

[111] L. Ley, J. Ristein, F. Meier, M. Riedel, P. Strobel, Surface conductivity of the diamond: A novel transfer doping mechanism, Phys. B Condens. Matter. 376–377 (2006) 262–267. https://doi.org/10.1016/j.physb.2005.12.068.

[112] T. Izak, M. Krátká, A. Kromka, B. Rezek, Osteoblastic cells trigger gate currents on nanocrystalline diamond transistor, Colloids Surfaces B Biointerfaces. 129 (2015) 95–99. https://doi.org/10.1016/j.colsurfb.2015.03.035.

[113] P.A. Zuk, The adipose-derived stem cell: Looking back and looking ahead, Mol. Biol. Cell. 21 (2010) 1783–1787. https://doi.org/10.1091/mbc.E09-07-0589.

[114] D. Johannsmann, The Quartz Crystal Microbalance in Soft Matter Research, Springer International Publishing, Cham, 2015. https://doi.org/10.1007/978-3-319-07836-6.

[115] R.D. Vaughan, C.K. O'Sullivan, G.G. Guilbault, Development of a quartz crystal microbalance (QCM) immunosensor for the detection of Listeria monocytogenes, Enzyme Microb. Technol. 29 (2001) 635–638. https://doi.org/10.1016/S0141-0229(01)00449-5.

[116] Y. Zhihua, Z. Liang, S. Kaixin, H. Weiwei, Characterization of quartz crystal microbalance sensors coated with graphene films, Procedia Eng. 29 (2012) 2448–2452. https://doi.org/10.1016/j.proeng.2012.01.330.

[117] M.Z. Atashbar, B. Bejcek, A. Vijh, S. Singamaneni, QCM biosensor with ultra thin polymer film, Sensors Actuators, B Chem. 107 (2005) 945–951. https://doi.org/10.1016/j.snb.2004.12.047.

[118] U. Latif, S. Can, O. Hayden, P. Grillberger, F.L. Dickert, Sauerbrey and anti-Sauerbrey behavioral studies in QCM sensors-Detection of bioanalytes, Sensors Actuators, B Chem. 176 (2013) 825–830. https://doi.org/10.1016/j.snb.2012.09.064.

[119] M. Aramesh, O. Shimoni, K. Ostrikov, S. Prawer, J. Cervenka, Surface charge effects in protein adsorption on nanodiamonds, Nanoscale. 7 (2015) 5726–5736. https://doi.org/10.1039/C5NR00250H.

[120] L. Tedeschi, L. Citti, C. Domenici, An integrated approach for the design and synthesis of

oligonucleotide probes and their interfacing to a QCM-based RNA biosensor, Biosens. Bioelectron. 20 (2005) 2376–2385. https://doi.org/10.1016/j.bios.2004.12.013.

[121] N. Lassalle, P. Mailley, E. Vieil, T. Livache, A. Roget, J.P. Correia, L.M. Abrantes, Electronically conductive polymer grafted with oligonucleotides as electrosensors of DNA: Preliminary study of real time monitoring by in situ techniques, J. Electroanal. Chem. 509 (2001) 48–57. https://doi.org/10.1016/S0022-0728(01)00537-X.

[122] I. Ben-Dov, I. Willner, E. Zisman, Piezoelectric Immunosensors for Urine Specimens of *Chlamydia trachomatis* Employing Quartz Crystal Microbalance Microgravimetric Analyses, Anal. Chem. 69 (1997) 3506–3512. https://doi.org/10.1021/ac970216s.

[123] X. Mao, L. Yang, X.L. Su, Y. Li, A nanoparticle amplification based quartz crystal microbalance DNA sensor for detection of Escherichia coli O157:H7, Biosens. Bioelectron. 21 (2006) 1178–1185. https://doi.org/10.1016/j.bios.2005.04.021.

[124] J. Rickert, T. Weiss, W. Kraas, G. Jung, W. Göpel, A new affinity biosensor: Self-assembled thiols as selective monolayer coatings of quartz crystal microbalances, Biosens. Bioelectron. 11 (1996) 591–598. https://doi.org/10.1016/0956-5663(96)83294-5.

[125] M. Kaspar, H. Stadler, T. Weiß, C. Ziegler, Thickness shear mode resonators ("mass-sensitive devices") in bioanalysis, Fresenius. J. Anal. Chem. 366 (2000) 602–610. https://doi.org/10.1007/s002160051555.

[126] J. Strauss, Y. Liu, T.A. Camesano, Bacterial adhesion to protein-coated surfaces: An AFM and QCM-D study, Jom. 61 (2009) 71–74. https://doi.org/10.1007/s11837-009-0138-z.

[127] V.C.H. Wu, S.H. Chen, C.S. Lin, Real-time detection of Escherichia coli O157:H7 sequences using a circulating-flow system of quartz crystal microbalance, Biosens. Bioelectron. 22 (2007) 2967–2975. https://doi.org/10.1016/j.bios.2006.12.016.

[128] Y. Zhang, S. Asahina, S. Yoshihara, T. Shirakashi, Fabrication and characterization of diamond quartz crystal microbalance electrode, J. Electrochem. Soc. 149 (2002). https://doi.org/10.1149/1.1514649.

[129] O.A. Williams, V. Mortet, M. Daenen, K. Haenen, Nanocrystalline diamond enhanced thickness shear mode resonator, Appl. Phys. Lett. 90 (2007) 1–4. https://doi.org/10.1063/1.2471649.

[130] P. Krempl, G. Schleinzer, W. Wallnöfer, Gallium phosphate, gapo4: A new piezoelectric crystal material for high-temperature sensorics, Sensors Actuators, A Phys. 61 (1997) 361–363. https://doi.org/10.1016/S0924-4247(97)80289-0.

[131] Š. Potocký, O. Babchenko, K. Hruška, A. Kromka, Linear antenna microwave plasma CVD diamond deposition at the edge of no-growth region of C-H-O ternary diagram, Phys. Status Solidi Basic Res. 249 (2012) 2612–2615. https://doi.org/10.1002/pssb.201200124.

[132] T. Izak, O. Babchenko, M. Varga, S. Potocky, A. Kromka, Low temperature diamond growth by linear antenna plasma CVD over large area, Phys. Status Solidi Basic Res. 249 (2012) 2600–2603. https://doi.org/10.1002/pssb.201200103.

[133] P. Kulha, J. Kroutil, A. Laposa, V. Procházka, M. Husák, Quartz Crystal Micro-Balance Gas Sensor with Ink-Jet Printed Nano-Diamond Sensitive Layer, J. Electr. Eng. 67 (2016) 61–64. https://doi.org/10.1515/jee-2016-0009.

[134] A.I.N. Electronic, P. Technologies, 8 th International Conference on ADVANCES IN ELECTRONIC AND, in: J. D. Jandura, P. Maniaková, I. Lettrichová, J. Kováč (Ed.), 8 Th Int. Conf. Adv. Electron., University of Zilina in EDIS-Publishing Centre of UZ, Podbanské, 2020: p. 261. https://doi.org/ISBN 978-80-554-1806-3.

[135] I. Kopova, B. Rezek, S. Stehlik, E. Ukraintsev, N. Slepickova Kasalkova, P. Slepicka, S. Potocky, L. Bacakova, Growth of Primary Human Osteoblasts on Plasma-Treated and Nanodiamond-Coated PTFE Polymer Foils, Phys. Status Solidi Basic Res. 255 (2018) 1700595. https://doi.org/10.1002/pssb.201700595.

[136] N.A. Ahmad, R.A. Rahim, B. Rezek, A. Kromka, N.S. Ismail, S.C.B. Gopinath, T. Izak, V. Prochazka, F.N.M. Faudzi, A.S.Z. Abidin, N.N.M. Maidizn, Nanocrystalline diamond electrolyte-gates in field effect transistor for a prolific aptasensing HIV-1 tat on hydrogen-terminated surface, Int. J. Nanoelectron. Mater. 13 (2020) 295–306.

[137] M. Josowicz, J. Janata, K. Ashley, S. Pons, Electrochemical and Ultraviolet—Visible Spectroelectrochemical Investigation of Selectivity of Potentiometric Gas Sensors Based on Polypyrrole, Anal. Chem. 59 (1987) 253–258. https://doi.org/10.1021/AC00129A008/ASSET/AC00129A008.FP.PNG_V03.

[138] P.K. Ang, W. Chen, A.T.S. Wee, P.L. Kian, Solution-gated epitaxial graphene as pH sensor, J. Am.

Chem. Soc. 130 (2008) 14392–14393. https://doi.org/10.1021/ja805090z.
[139] Y. Sasaki, H. Kawarada, Low drift and small hysteresis characteristics of diamond electrolyte-solution-gate FET, J. Phys. D. Appl. Phys. 43 (2010) 374020. https://doi.org/10.1088/0022-3727/43/37/374020.
[140] H. Karimi, R. Yusof, R. Rahmani, H. Hosseinpour, M.T. Ahmadi, Development of solution-gated graphene transistor model for biosensors, Nanoscale Res. Lett. 9 (2014) 1–11. https://doi.org/10.1186/1556-276X-9-71.
[141] J.H. Yang, K.S. Song, S. Kuga, H. Kawarada, Characterization of direct immobilized probe DNA on partially functionalized diamond solution-gate field-effect transistors, Japanese J. Appl. Physics, Part 2 Lett. 45 (2006). https://doi.org/10.1143/JJAP.45.L1114.
[142] Y. Kim, Y. Inoue, H. Hasegawa, Y. Yoshida, T. Sakata, In Situ Electrical Monitoring of Methylated DNA Based on Its Conformational Change to G-Quadruplex Using a Solution-Gated Field-Effect Transistor, Anal. Chem. 93 (2021) 16709–16717. https://doi.org/10.1021/ACS.ANALCHEM.1C04466.
[143] D. Han, R. Chand, Y.S. Kim, Microscale loop-mediated isothermal amplification of viral DNA with real-time monitoring on solution-gated graphene FET microchip, Biosens. Bioelectron. 93 (2017) 220–225. https://doi.org/10.1016/J.BIOS.2016.08.115.
[144] M. Krátká, O. Babchenko, E. Ukraintsev, J. Vachelová, M. Davídková, M. Vandrovcová, A. Kromka, B. Rezek, Gamma radiation effects on hydrogen-terminated nanocrystalline diamond bio-transistors, Diam. Relat. Mater. 63 (2016) 186–191. https://doi.org/10.1016/j.diamond.2015.10.015.
[145] R. Garcia-Cortadella, E. Masvidal-Codina, J.M. De la Cruz, N. Schäfer, G. Schwesig, C. Jeschke, J. Martinez-Aguilar, M. V. Sanchez-Vives, R. Villa, X. Illa, A. Sirota, A. Guimerà, J.A. Garrido, Distortion-Free Sensing of Neural Activity Using Graphene Transistors, Small. 16 (2020). https://doi.org/10.1002/SMLL.201906640.
[146] A.H. Assen, O. Yassine, O. Shekhah, M. Eddaoudi, K.N. Salama, MOFs for the Sensitive Detection of Ammonia: Deployment of fcu-MOF Thin Films as Effective Chemical Capacitive Sensors, ACS Sensors. 2 (2017) 1294–1301. https://doi.org/10.1021/ACSSENSORS.7B00304.
[147] C. Wena, C. Zhuc, Y. Jua, H. Xua, Y. Qiua, A novel NO2 gas sensor using dual track SAW device, Sensors Actuators A Phys. 159 (2010) 168–173. https://doi.org/10.1016/J.SNA.2010.03.012.
[148] N. Ke, X. Wang, X. Xu, Y.A. Abassi, The xCELLigence System for Real-Time and Label-Free Monitoring of Cell Viability, Methods Mol. Biol. 740 (2011) 33–43. https://doi.org/10.1007/978-1-61779-108-6_6.
[149] P. Kenchetty, T. Miura, S. Uno, Computer simulation for electrochemical impedance of a living cell adhered on the inter-digitated electrode sensors, Jpn. J. Appl. Phys. 58 (2019). https://doi.org/10.7567/1347-4065/AB00F0.
[150] Q.M. Abdelal, M.A. Alsmadi, N.A. Jaber, Low cost monitoring systems for environmental and water resources applications, World Environ. Water Resour. Congr. 2019 Emerg. Innov. Technol. Int. Perspect. - Sel. Pap. from World Environ. Water Resour. Congr. 2019. (2019) 96–103. https://doi.org/10.1061/9780784482322.010.
[151] J. Park, K.S. Hwang, S. Cho, Dependence of impedance measurement sensitivity of cell growth on sensing area of circular interdigitated electrode, J. Nanosci. Nanotechnol. 15 (2015) 7886–7890. https://doi.org/10.1166/JNN.2015.11230.
[152] I. Tubía, J. Paredes, E. Pérez-Lorenzo, S. Arana, Antibody biosensors for spoilage yeast detection based on impedance spectroscopy, Biosens. Bioelectron. 102 (2018) 432–438. https://doi.org/10.1016/J.BIOS.2017.11.057.
[153] H. Wang, T. Lakshmipriya, Y. Chen, S.C.B. Gopinath, Squamous Cell Carcinoma Biomarker Sensing on a Strontium Oxide-Modified Interdigitated Electrode Surface for the Diagnosis of Cervical Cancer, Biomed Res. Int. 2019 (2019). https://doi.org/10.1155/2019/2807123.
[154] N. Guan, J. Deng, T. Li, X. Xu, J.T. Irelan, M.-W. Wang, Label-free monitoring of T cell activation by the impedance-based xCELLigence system, Mol. Biosyst. 9 (2013) 1035. https://doi.org/10.1039/c3mb25421f.
[155] J. Liskova, O. Babchenko, M. Varga, A. Kromka, D. Hadraba, Z. Svindrych, Z. Burdikova, L. Bacakova, Osteogenic cell differentiation on H-terminated and O-terminated nanocrystalline diamond films, Int. J. Nanomedicine. 10 (2015) 869–884. https://doi.org/10.2147/IJN.S73628.
[156] T. Kruk, M. Bzowska, A. Hinz, M. Szuwarzyński, K. Szczepanowicz, Control of specific/nonspecific protein adsorption: Functionalization of polyelectrolyte multilayer films as a potential coating for

biosensors, Materials (Basel). 14 (2021). https://doi.org/10.3390/MA14247629.

[157] G. Bayramoglu, M. Kilic, M. Yakup Arica, Selective isolation and sensitive detection of lysozyme using aptamer based magnetic adsorbent and a new quartz crystal microbalance system, Food Chem. 382 (2022). https://doi.org/10.1016/J.FOODCHEM.2022.132353.

[158] U. Ajdnik, L.F. Zemljič, O. Plohl, L. Pérez, J. Trček, M. Bračič, T. Mohan, Bioactive Functional Nanolayers of Chitosan-Lysine Surfactant with Single- And Mixed-Protein-Repellent and Antibiofilm Properties for Medical Implants, ACS Appl. Mater. Interfaces. 13 (2021) 23352–23368. https://doi.org/10.1021/ACSAMI.1C01993.

[159] L.X. Gan, C.L. Hao, X.M. Jiang, Controllable adsorption and desorption of a cationic surfactant at quartz directed by host-guest complex, Colloids Surfaces A Physicochem. Eng. Asp. 625 (2021). https://doi.org/10.1016/J.COLSURFA.2021.126880.

[160] R. Lu, X. Zhang, X. Cheng, X. Zan, W. Geng, Secondary Structure-Dominated Layer-by-Layer Growth Mode of Protein Coatings, Langmuir. 37 (2021) 13000–13011. https://doi.org/10.1021/ACS.LANGMUIR.1C02062.

[161] S.D. Carrigan, G. Scott, M. Tabrizian, Real-time QCM-D immunoassay through oriented antibody immobilization using cross-linked hydrogel biointerfaces, Langmuir. 21 (2005) 5966–5973. https://doi.org/10.1021/LA0503294/ASSET/IMAGES/MEDIUM/LA0503294N00001.GIF.

[162] M. Bally, S. Block, F. Höök, G. Larson, N. Parveen, G.E. Rydell, Physicochemical tools for studying virus interactions with targeted cell membranes in a molecular and spatiotemporally resolved context, Anal. Bioanal. Chem. 413 (2021) 7157–7178. https://doi.org/10.1007/S00216-021-03510-5.

[163] M. Varga, A. Laposa, P. Kulha, M. Davydova, J. Kroutil, M. Husak, A. Kromka, Fabrication of diamond based quartz crystal microbalance gas sensor, Key Eng. Mater. 605 (2014) 589–592. https://doi.org/10.4028/WWW.SCIENTIFIC.NET/KEM.605.589.

7. Authors Outputs and Informations

7.1. List of Author's Publications

Reference	Citation	Type of contribution	Year
[ARef:1]	**Procházka, V.**, Cifra, M., Kulha, P., Ižák, T., Rezek, B., & Kromka, A. (2017). Influence of non-adherent yeast cells on electrical characteristics of diamond-based field-effect transistors. Applied Surface Science, 395, 214–219. https://doi.org/10.1016/j.apsusc.2016.05.003	Article, IF 3.19 (2017), 5 citations	2017
[ARef:2]	**Procházka, V.**, Matějka, R., Ižák, T., Szabó, O., Štěpanovská, J., Filová, E., Bačáková, L., Jirásek, V., & Kromka, A. (2019). Nanocrystalline diamond-based impedance sensors for real-time monitoring of adipose tissue-derived stem cells. Colloids and Surfaces B: Biointerfaces, 177, 130–136. https://doi.org/10.1016/j.colsurfb.2019.01.048	Article, IF 4.1 (2019), 1 citation	2019
[ARef:3]	Ahmad, N. A., Rahim, R. A., Rezek, B., Kromka, A., Ismail, N. S., Gopinath, S. C. B., Izak, T., **Procházka, V.**, Faudzi, F. N. M., Abidin, A. S. Z., & Maidizn, N. N. M. (2020). Nanocrystalline diamond electrolyte-gates in field effect transistor for a prolific aptasensing HIV-1 tat on hydrogen-terminated surface. International Journal of Nanoelectronics and Materials, 13(2), 295–306.	Article, IF 1.1 (2020) 0 citations	2021
[ARef:4]	**Procházka, V.**, Kulha, P., Izsák, T., Ukraintsev, E., Varga, M., Jirásek, V., & Kromka, A. (2022). Detection of globular and fibrillar proteins by quartz crystal microbalance sensor coated with a functionalized diamond thin film. Applied Surface Science, 589, 153017. https://doi.org/10.1016/j.apsusc.2022.153017	Article, IF 6.7 (2022), 0 citations	2022
[ARef:5]	Kulha, P., Kroutil, J., Laposa, A., **Procházka, V.**, & Husák, M. (2016). Quartz Crystal Micro-Balance Gas Sensor with Ink-Jet Printed Nano-Diamond Sensitive Layer. Journal of Electrical Engineering, 67(1), 61–64. https://doi.org/10.1515/jee-2016-0009	Article, IF 0.5, (2016) 4 citations	2016
[ARef:6]	Ižák, T., **Procházka, V.**, Sakata T., Rezek B., Kromka A. - Real-Time Monitoring of Cell Activities by Diamond Solution-Gated Field Effect Transistor in Procedia Engineering, 30th Eurosensors Conference 2016, https://doi.org/10.1016/j.proeng.2016.11.130	Article in conference proceeding	2016

[ARef:7]	**Procházka, V.**, Ižák, T., & Kromka, A. (2017). Influence of Buffers and Culture Media on Diamond Solution-Gated Field Effect Transistors Regarding Stability and Memory Effect. In Proceedings (Vol. 1, Issue 4, p. 525). https://doi.org/10.3390/proceedings1040525	Article in conference proceeding	2017
[Aref:8]	**Procházka, V.**, Kulha, P., Ižák, T., Ukraintsev, E., Varga, M. - et al.: Diamond Coated Quartz Crystal Microbalance Sensor for Detection of Protein Adsorption. In XV. Workshop of Physical Chemists and Electrochemists. 2015, p. 142-145. ISBN 978-80-210-7857-4.	Abstract in conference proceeding	2015
[ARef:9]	Kulha, P., **Procházka, V.,** Bokůvka, L.: Quartz Crystal Microbalance Gas Sensor with Ink-Jet Printed Nanodiamond Sensitive Layer. In IMAPS Flash Conference. Brno: NOVPRESS, 2015, vol. 1, ISBN 978-80-214- 5270-1.	Abstract in conference proceeding	2015
[ARef:10]	**Procházka, V.,** Cifra, M, Kulha, P., Ižák, T., Rezek, B. - et al.: Influence of Non-adherent Yeast Cells on Electrical Characteristics of Diamond- based Field-effect Transistors. In Nanocon 2015, 7th International Conference. Ostrava: Tanger, 2015, p. 61. ISBN 978- 80-87294-59-8.	Abstract in conference proceeding	2015
[ARef:11]	**Procházka, V.,** Cifra, M., Kulha, P., Ižák, I., Rezek, B., Kromka, A.: Electrical monitoring of yeast cells by diamond SGFETs In Hasselt Diamond Workshop 2016	Abstract in conference proceeding	2016
[ARef:12]	**Procházka, V**., Kulha, P., Ižák, T., Ukraintsev, E., Varga, M. - et al., Detection of protein adsorption by quartz crystal microbalance sensor coated by functionalized diamond film at NANOSea 2018	Abstract in conference proceeding	2018
[ARef:13]	**Procházka, V.**, Krátká, M., Izsák, T., Rezek, B., Kromka, A., Diamond-Based Solution-Gated Transistors for Biosensor Use in Proceedings of The International Conference on Advances in Electronic and Photonic Technologies, ADEPT 2021, p. 1-4, ISBN 978-80-554-1806-3	Abstract in conference proceeding	2021
[ARef:14]	Matějka, R., **Procházka, V.**, Ižák, T., Štěpanovská, J., Kromka, A., Trávníčková, M., Bačáková, L. CZ Utility model No. 30691 (18.5.2017): "Kultivační komora pro in-vitro opticko-elektrické monitorování biologických kultur s impedančními opticky-transparentními diamantovými elektrodami"	Utility model	2017

7.2. Attendance at the conferences

Year of attendance	Conference name	Type of contribution
2014	"Setkání fyzikálních chemiků a elektrochemiků"	Poster presentation, Proceeding abstract
2015	"Nanocon"	Poster presentation, Proceeding abstract
2016	"Eurosensors"	Poster presentation, Proceeding abstract
2017	Hasselt Diamond Workshop	Poster presentation, Proceeding abstract
2017	Nano-Structures and Nanomaterials Self-Assembly ("NANOSea")	Poster presentation, Proceeding abstract
2021	Advances in Electronic and Photonic Technologies ("ADEPT")	Poster presentation, Proceeding abstract

7.3. Internships

Date of attendance	Institution	Project
1.6.2018–30.6.2018	Johannes Kepler University in Linz	MŠMT 8J18AT010 "Polymerní kompozity jako funkční materiály pro zabudované senzory a optické vlnovody"
1.5.2019–1.12.2019	University of Melbourne	"Mimoevropská bilaterální dohoda"

During my Ph.D. study, I participated in the bilateral mobility project with **Johannes Kepler University (JKU) in Linz**. In the Year 2018, I was on a **month-long internship** in the abovementioned institution. At JKU, I researched the new ways to employ screen-printing for diamond growth technology and designed a new 3D printed chamber for biosensor measurements. As a second internship, I spent **six months** at the **University of Melbourne (world QS rank at 2019 = 36th place) as a Study Abroad Research Student (SA-RES)**, where I participated in biosensor research in the group of prof. Steven Prawer (ORCID https://orcid.org/0000-0002-4959-0828), under the supervision of Dr. David Garret (ORCID https://orcid.org/0000-0002-4676-8387). During this internship, I worked on the problematics of laser machining of the quartz and designed a new type of combined sensor.

7.4. Funding and projects

Project	Grant Agency	Time period	Project Number
„Příprava, modifikace a charakterizace materiálů zářením“	Grant Agency of Czech Republic	2012–2018	P108/12/G108
Application of adipose tissue-derived stem cells obtained by liposuction in tissue engineering.	Ministry of Health	2015–2018	15-33018A
Development of diamond-based biosensors for life science.	Ministry of Education, Youth and Sports	2016–2021	LM2018110
„3D tištěné diamantové kompozitní komponenty pro účinnější energetiku“	Technology Agency of Czech Republic	2019–2023	TK02020094
Developing a nanocrystal diamond layers-based biosensor for measurement properties of living cells.	Czech Technical University	2015–2017	SGS15/159/ OHK3/2T/13 (2 years project)
Development of a diamond thin film-based biosensors.	Czech Technical University	2017–2019	SGS17/136/ OHK4/2T/13 (2 years project)
Use of superficially modified and 3D structured nanocrystalline diamond layers in sensors and biosensors.	Czech Technical University	2019–2020	SGS19/112/ OHK4/2T/13 (1 year project)

8. Appendix

8.1. Influence of non-adherent yeast cells on electrical characteristics of diamond-based field-effect transistors

Applied Surface Science 395 (2017) 214–219

Contents lists available at ScienceDirect

Applied Surface Science

journal homepage: www.elsevier.com/locate/apsusc

Influence of non-adherent yeast cells on electrical characteristics of diamond-based field-effect transistors

Václav Procházka[a,b,*], Michal Cifra[c], Pavel Kulha[a,b], Tibor Ižák[b], Bohuslav Rezek[a,b], Alexander Kromka[b,d]

[a] Faculty of Electrical Engineering, Czech Technical University in Prague, Technická 2, 16627 Prague, Czechia
[b] Institute of Physics, The Czech Academy of Sciences, Cukrovarnická 10/112, 162 00 Prague, Czechia
[c] Institute of Photonics and Electronics, The Czech Academy of Sciences, Chaberská 57, 182 51 Prague, Czechia
[d] Faculty of Civil Engineering, Czech Technical University in Prague, Thákurova 7, 16629 Prague, Czechia

ARTICLE INFO

Article history:
Received 27 January 2016
Received in revised form 30 April 2016
Accepted 1 May 2016
Available online 9 May 2016

Keywords:
Nanocrystalline diamond
Yeast cells
Field-effect transistor
Transfer characteristics
pH sensitivity

ABSTRACT

Diamond thin films provide unique features as substrates for cell cultures and as bio-electronic sensors. Here we employ solution-gated field effect transistors (SGFET) based on nanocrystalline diamond thin films with H-terminated surface which exhibits the sub-surface p-type conductive channel. We study an influence of yeast cells (*Saccharomyces cerevisiae*) on electrical characteristics of the diamond SGFETs. Two different cell culture solutions (sucrose and yeast peptone dextrose–YPD) are used, with and without the cells. We have found that transfer characteristics of the SGFETs exhibit a negative shift of the gate voltage by −26 mV and −42 mV for sucrose and YPD with cells in comparison to blank solutions without the cells. This effect is attributed to a local pH change in close vicinity of the H-terminated diamond surface due to metabolic processes of the yeast cells. The pH sensitivity of the diamond-based SGFETs, the role of cell and protein adhesion on the gate surface and the role of negative surface charge of yeast cells on the SGFETs electrical characteristics are discussed as well.

1. Introduction

Diamond is considered as a perspective material in cells and tissue oriented life sciences. In addition to unique mechanical, thermal, and electrical properties, diamond is also biocompatible and exhibits surface conductivity which is highly sensitive to changes in surrounding environment due to surface transfer doping mechanism [1,2]. Thanks to these properties diamond-based transistors do not need any gate dielectric layer.

There are many types of diamond-based bio-electronic devices of new generation. They differ in type of diamond (intrinsic or boron-doped polycrystalline diamond in form of thin films deposited on different substrates (mainly glass), or robust single-crystalline diamond substrates) as well as working principle. The working principle of devices for direct electrical measurement of cells activity and for study the cell-cell or cell-substrate interactions differs for individual device configuration and specific applications such as impedance measurements, field-effect transistor configuration, etc. For example, impedance measurement techniques employ microelectrode arrays (MEAs) [3,4]. MEAs found application in the study of immune system response efficiency [5], direct monitoring of cardiac action potentials of cells [4] or for action potential recording and stimulation of neural networks for both in vitro applications (rigid substrate) as well as for in vivo retinal prostheses (flexible biocompatible substrate) [6]. Interdigital electrodes based on hydrogen-terminated diamond on glass substrates were found prospective as optically transparent devices for real-time monitoring of cellular activity (incubation, cultivation, adhesion, etc.) [7].

In contrast to impedance-based devices, solution-gated field effect transistors (SGFETs) with hydrogen-terminated diamond surface allow study of a single cell. They have found use in research of solution/cell-surface interactions, living microorganisms and tissue cells as biocompatible sensors. The properties of diamond SGFETs, such as influence of the diamond film morphology [8], pH [9], protein adsorption [8] or membrane adsorption and disruption [10] on the electrical characteristics has been well described. In another study enzyme-modified field effect transistors were applied for detection of enzymatic reactions [11] or for measurement of surface potential of living cells [12]. Micro and nanoscopic field SGFETs have a potential for study of electrodynamic cellular

* Corresponding author at: Academy of Science Czech Republic, Institute of Physics, Cukrovarnická 10, Prague, Czech Republic.
E-mail addresses: prochazkav@fzu.cz, prochva4@fel.cvut.cz (V. Procházka).

http://dx.doi.org/10.1016/j.apsusc.2016.05.003
0169-4332/

Table 1
Average conductivity and pH of used solutions.

Measured at 18.9 °C	pH		Conductivity	
	before the addition of cells	30 min. after the addition of cells (measurement start)	Without cells (mS cm^{-1})	C_{CELLS} ~1.10^8 cells ml^{-1} (mS cm^{-1})
YPD	6.4	6.1	3.21 ± 0.04	3.10 ± 0.04
Sucrose (2 wt%)	7.0	6.8	0.43 ± 0.02	0.41 ± 0.02

behavior, which is theoretically predicted [13] yet challenging to detect [14]. The functionalized diamond surface was used in several studies for pattern guided formation of glial and retinal neuron networks [15,16], and it was also demonstrated as perfect solution for photo-sensitive retinal prosthesis and neural interfacing device [17]. However, the studies were focused on the interactions of mammal adherent cells or excitable cells with strong surface potential. There is a lack of studies focused on the interactions of non-adherent, non-excitable cells.

Thus in presented work we focused on yeast cells (*Saccharomyces cerevisiae*), which are widely used as basic model of eukaryotic cells in molecular biology and genetics [18]. Yeast cells enable a wide variety of genetic engineering techniques and the strict functional analyzes of proteins. They are non-polar, non-excitable and non-adherent cells. Their inner and surface structures are well defined and understood. They have a stable negative surface charge with very weak pH dependency, which determines their behavior in the solution [19,20]. In general, yeast cells are known as non-adherent cells, although some yeasts such as *S. cerevisiae*, *Candida albicans* and *Candida glabrata* have the ability to adhere to plastic surfaces [21,22]. The yeast cell adhesion to plastic substrates is believed to depend on hydrophobic interaction [23]. Novel methods for attachment and cultivation of specifically positioned single yeast cells on a microelectrode surface employ a weak electrical potential (−0.2 and −0.4 V) [24]. It was reported that the yeast cells attached to the negative potential-applied ITO electrodes showed normal cell proliferation.

We study the influence of different solutions (sucrose and yeast peptone dextrose without or with yeast cells) on the H-diamond SGFET electrical characteristics. We discuss interactions of the yeast cells and cell culture solutions with H-terminated diamond surface on the transistor gate. We suggest that metabolic activity of yeast cells can be detected by the H-diamond SGFET.

2. Experimental

2.1. Fabrication of the sensor

Fused silica glass substrates (in size of 10 mm × 10 mm × 1 mm) were ultrasonically cleaned in isopropyl alcohol and deionized water (DI) and subsequently were immersed for 10 min into an ultrasonic bath with a colloidal suspension of diamond nanopowder with nominal particle size of ~5 nm. This process leads to the formation of a 5 ÷ 25 nm thin layer of diamond powder necessary to initiate the diamond growth in a thin film.

Nanocrystalline diamond (NCD) thin films were grown in a microwave ellipsoidal cavity reactor by chemical vapor deposition (CVD) process for 4.5 h, at following conditions: gas pressure 30 mbar, gas mixture 1% CH_4 in H_2 and microwave power 1000 W. The deposition temperature was in the range of 550 ÷ 600 °C. These deposition parameters led to the growth of ~450 nm thick diamond film with grain sizes ~250 nm [3]. Diamond films were further hydrogenated in the same microwave plasma reactor at 600 °C in hydrogen plasma for 10 min to induce the surface conductivity.

Photolithographic masks were applied on H-terminated NCD films using a positive MA-P1215 photoresist to define FET channels and contacts. The NCD films were treated in oxygen radio-frequency plasma (300 W, 3 min exposition time) to generate insulating O-terminated areas, which surround the H-terminated channels (5 μm wide and 60 μm long stripes) connecting source and drain contacts. The source and drain contacts were prepared by thermal evaporation (10 nm of Ti and ~50 nm of Au) followed by the lift-off technique. The samples were cleaned in acetone and photoresist stripper (mr-REM 660). The area between contacts was covered with a positive photoresist ma-P 1240 (thickness 4 μm). The final photolithographic step created openings of 60 μm × 60 μm to define the active gate area (Fig. 3) [25].

2.2. Experimental procedure

Yeast cells *Saccharomyces cerevisiae* (Euroscarf collection; genetic background BY4741, *MAT*a) were used in experiments. Sucrose medium was prepared by dissolving it in DI water to achieve 2% weight concentration. YPD medium was autoclave-sterilized contained: 1%(w/v) yeast extract (Chemos CZ, s.r.o.), 2%(w/v) peptone (Chemos CZ, s.r.o), 2%(w/v) D-glucose (Penta, s.r.o.) in DI water. Glucose was filtration sterilized (200 nm diameter filter pores) and added to medium after sterilization. Cells for experiments were cultivated as follows. Glass Erlenmeyer flask (100 ml) was filled with autoclave sterilized 10 ml of YPD medium. The medium was inoculated with yeast cells from YPD agar plate and the culture was cultivated at 30 °C on an orbital shaker at 180 rpm for 16 h. Then, the cell culture was centrifuged at 3000 RPM for 5 min, supernatant discarded and cells transferred to either sucrose or YPD medium to achieve final cells concentration C_{Cells} = 108cells ml^{-1}. Blank media (without cells) were used as references. Electrical conductivities of the employed media were measured by the conductivity meter calibrated after each measurement with 10 repetitions for accuracy. The resulting values are shown in Table 1.

For electrical measurements, two high precision source-meter units were used (Keithley 327). The first unit was connected between the channel electrodes of the sensor (i.e. source and drain), the second between the AgCl electrode and source electrode. The AgCl electrode was immersed into a drop of solution on the sensor gate area. Image of the setup is shown in Fig. 1. The drain and source electrodes are completely commutable due to sensor symmetry, thus there is no physical difference between them. For measurements of transistor transfer characteristics the U_{DS} was kept constant (U_{DS} = −0.6 V). First set of measurements was done with blank solutions (sucrose or YPD) by covering of the SGFETs active opening area with a 10 μl droplet. After each measurement, the SGFETs were rinsed by ethanol followed by deionized water. Second set of measurements was performed with cells contained in the medium (sucrose or YPD). The cells were let to sediment on the surface for 10 min prior to the measurements.

3. Results and discussion

Functionality and properties of diamond-based transistors were at first characterized by electrical measurements in standard phosphate buffer saline solutions (PBS) at different pH. Fig. 2a shows the gate voltage dependence of the diamond-based SGFET measured at constant current I_{DS} = 5 nA for pH varied from 9 to 4

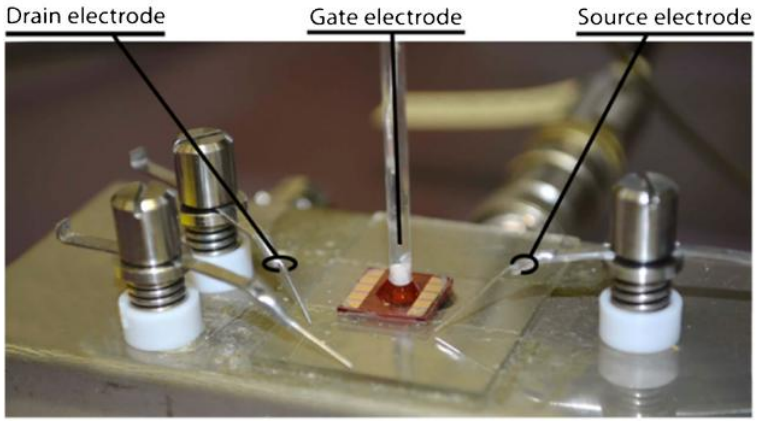

Fig. 1. Photo of the sensor setup for electrical measurements.

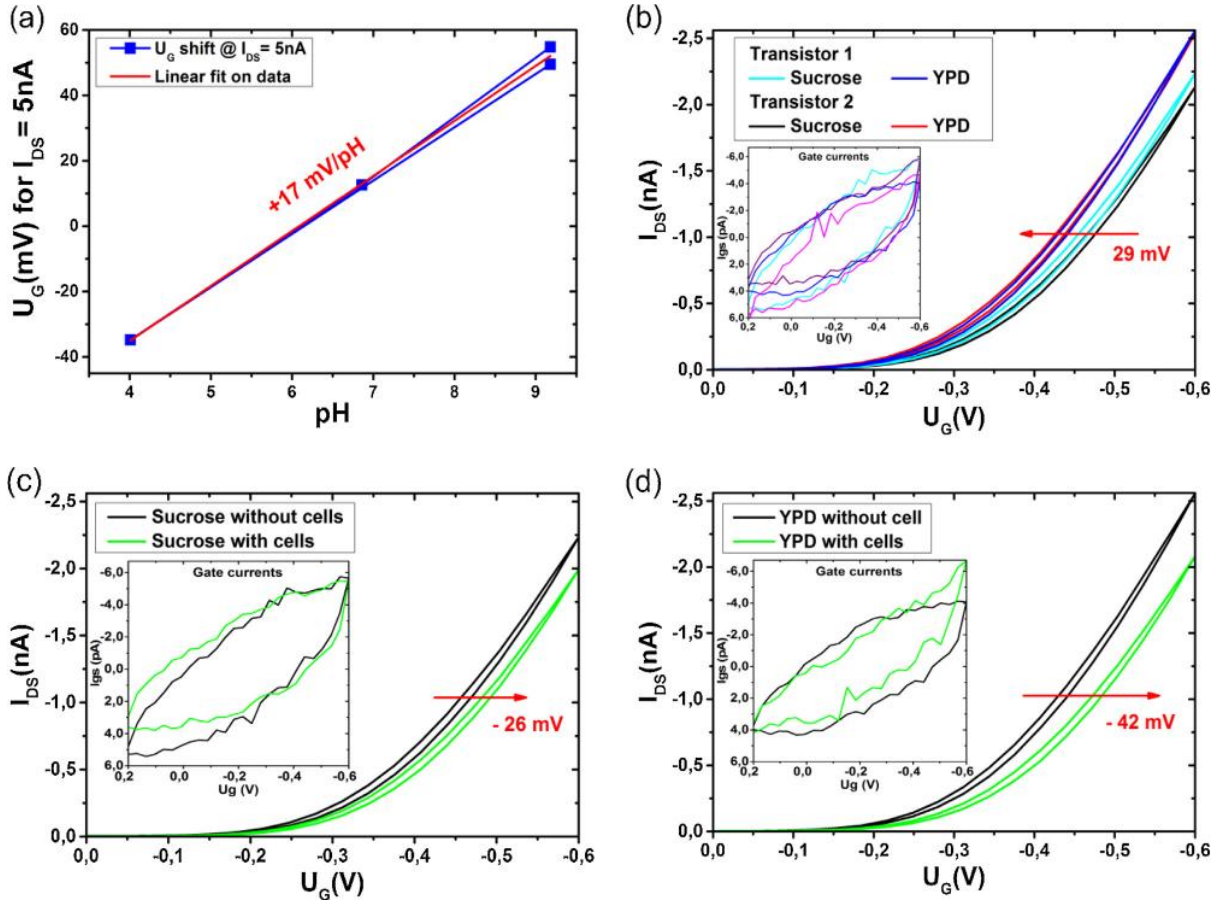

Fig. 2. a) Gate voltage dependence of the diamond-based SGFET measured in phosphate buffer saline with different pH. b) Comparison of the transfer characteristics of two transistors for sucrose and YPD solutions. c, d) Negative shift in transfer characteristics of SGFET "after addition of yeast cells into solution" for sucrose (c) and YPD (d) solution.

and back and using Ag/AgCl electrode. The pH sensitivity shown approx. +17 mV pH^{-1} linear dependence of the gate voltage shift, which is comparable with previously published values (approx. +15 mV pH^{-1} in such configuration) [9,12,26].

Transfer characteristics of SGFETs in sucrose and YPD solutions without cells are shown in Fig. 2b. For reliable determination of the transistor stability and the behavior in solutions the characteristics are shown for two different transistors prepared on the same substrate (i.e. the same chip and thus the same diamond film morphology). Transfer characteristics showed consistently a significant gate voltage shifts between the two used solution: +29 mV and +18 mV (compared at $I_{DS} = -1$ nA) for transistor nos. 1 and 2, respectively. The gate voltages shift differences between the transistor 1 and 2 are most likely caused by inhomogeneities of diamond

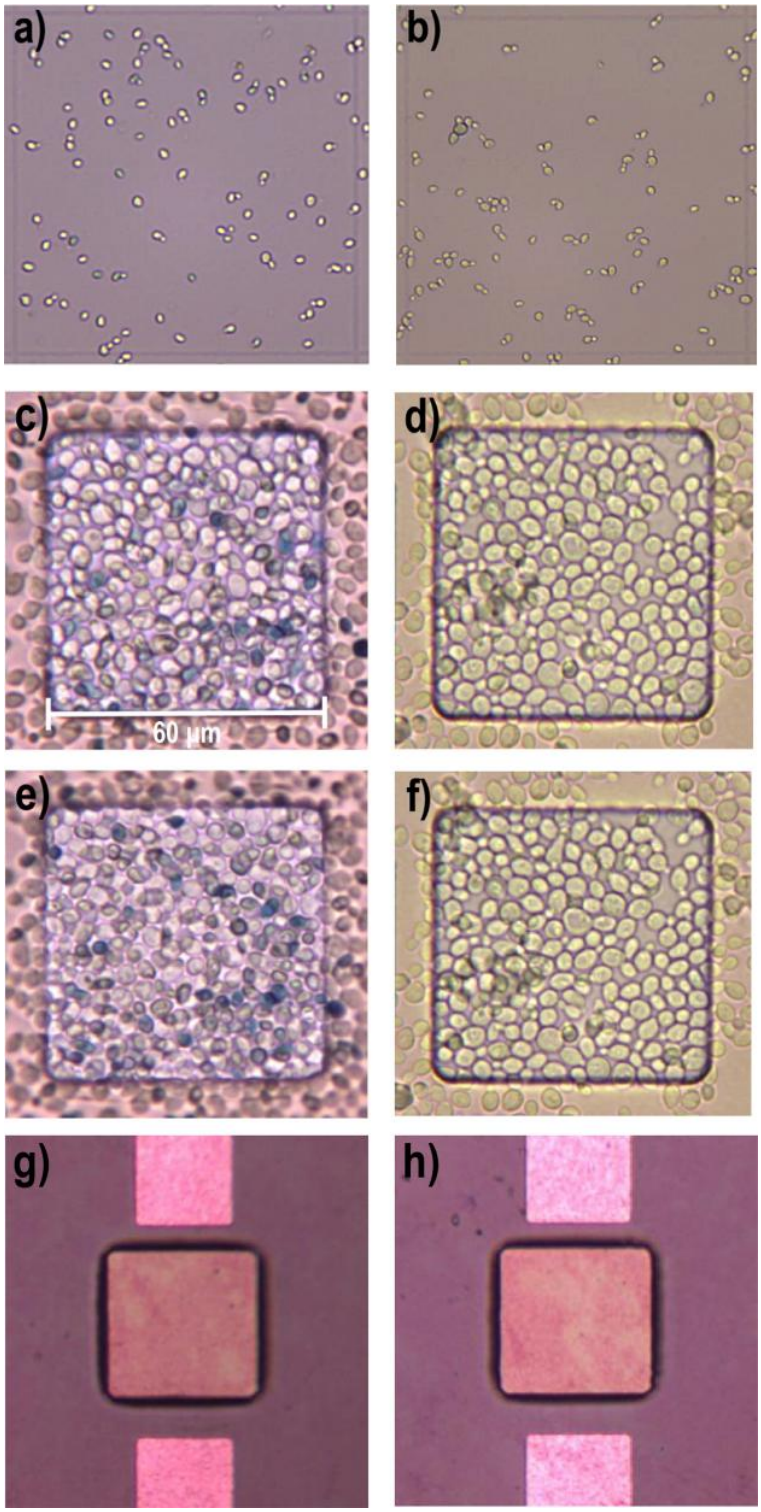

Fig. 3. Optical microscope images of sensor active area with cells in YPD and sucrose solution: cells suspended in sucrose (a) or YPD medium (b) counted in Burker chamber for determination of viability (m. 20×); cells suspended in sucrose (c) or YPD medium (d) before measurement (m. 50×); cells suspended in sucrose (e) or YPD medium (f) after measurement (m. 50×). Optical image of washed and rinsed sensor active area after measurement of g) sucrose with cells and h) YPD medium with cells solutions (m. 20×) (*Note*: the sensor opening area is $60 \times 60\ \mu m^2$).

layer (i.e. mainly the H-conductive channel area). The transistor no. 1 with the higher channel conductivity was used for further experiments.

Transfer characteristics of SGFET with blank YPD solution were shifted to more positive gate voltage values (+29 mV), with respect to transfer characteristics of SGFET with blank sucrose. Difference

Table 2
Comparison of cell viability after their transfer to the medium, before measurement (30 min after cell transfer) and after measurement (40 min after cell transfer).

	After transfer of cells to the medium (%)	Before measurement (%)	After measurement (%)
Sucrose 2 wt%	91.3	85.71	83.33
YPD	98.7	93.95	92.65

in pH between sucrose solution and YPD solution is −0.6 pH (see Table 1). This would correspond to a negative shift in transfer characteristics equal to −10 mV (based on Fig. 2a). Thus, the positive shift from sucrose to YPD cannot be attributed to pH change. Another factor behind the shift could be adsorption of molecules from YPD solution on the gate, such as in the case of protein FETs [27]. However, the measured shift was also in negative direction in that case. Thus, the only remaining reason of the positive shift is different conductivity of sucrose and YPD solution. Wetted area on the sensor was the same for both solutions in all measurements. The sensor opening was fully flooded. YPD solution has a higher conductivity by an order of magnitude (see Table 1). Different conductivities change the potential drop across the solution and thereby actual potential applied on the transistor gate surface. The actual voltage on the channel surface will be higher, hence conductivity of the channel increases.

Fig. 2c and d shows transfer characteristics of SGFET after addition of yeast cells into sucrose or YPD solutions. Both SGFET transfer characteristics exhibit a negative shift of the gate voltage by −26 mV for sucrose and −42 mV for YPD, with respect to characteristics of blank solutions without cells.

Considering negative charge of the yeast cell membrane the gate voltage shift should be expected oriented oppositely (to more positive values), if the membranes are on the diamond surface. Thus the shift of characteristics does not correspond to the field-effect of the negatively charged cells, i.e. with the increased holes concentration in the p-type channel.

Assuming that as the yeast cells form a layer over the conductive channel (Fig. 3), additional gate resistance will arise in dc measurements. In this configuration, the voltage drops across the diamond interface and then the channel conductivity will decrease. Consequently, the voltage drop will contribute to the shift of transfer characteristics in the negative direction. However, the formation of such electrically resistive layer was not confirmed by significant change in gate currents (see Fig. 2c, d), which was observed for instance with adsorbed protein layers [8]. Note also that the yeast cells are non-adherent cells, i.e. they donít adhere to the gate surface. In conformity with that, we did not observe any increase of leakage gate currents during cell cultivation, unlike in the case of adherent cells. For instance when adherent SAOS-2 cells adhered on the H-terminated diamond channel the gate current increased up to 100× [28]. Transistor gate currents recovered to original values, when the cells were washed away (Fig. 3g, 3h). Cells morphology appears to be unchanged (see Fig. 3c, e for sucrose, Fig. 3d, f for YPD). Monitoring the cell culture viability at the end of measurement in comparison with initial viability (counted in Burker chamber), no significant change has been found. Viability was tested in every phase of the experiment and was monitored by cell staining (standard 0.4% trypan blue solution) (see Table 2). It is important to note that staining with trypan blue is slightly toxic for cells and therefore cell death can be caused just by staining [29].

The last factor to consider is a metabolic activity of cells. The yeast cells produce CO_2 to surroundings. It causes acidification in the cells vicinity: $CO_2 + H_2O \rightarrow HCO_3^- + H_3O^+$ [30,31]. According to the pH sensitivity in Fig. 2a, this leads to negative gate voltage shift on the H-diamond SGFET. The shift by −26 mV or −42 mV would correspond to pH change by −2 pH to −3 pH. This may seem relatively large. However it is related to a local near-surface effect and does not represent the change of bulk pH in the whole cell medium. The value is comparable to FET sensors of embryonic cells where respiration activity of a single embryo caused about −0.7 pH change [32]. Thus the metabolic activity of the yeast cells is the most likely explanation of the observed gate potential shifts in our case. This conclusion is also corroborated by the fact that when the cells are in a nutrient rich YPD medium, which enables more intensive metabolism than sucrose medium, their effect on SGFET gate voltage is higher than for cells in sucrose media.

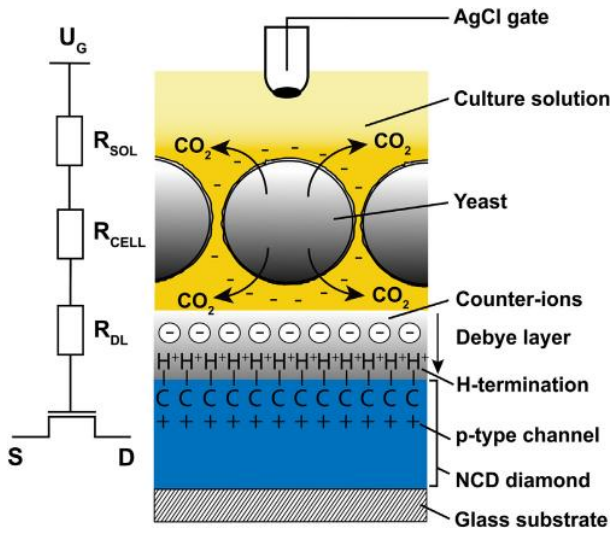

Fig. 4. A schematic view of SGFET channel part in the cell solution (cross-section view) and equivalent electrical circuit.

The above analysis is summarized in a model in Fig. 4. It shows a schematic cross-section of the SGFET sensor including equivalent electrical circuit along the left side. Note that the circuit representation does not completely reflect reality as the model includes only real component of the resistance and omits serial and parallel capacitive components (cells, Debyeís layer, etc.). Impedance elements in this case are neglected, since the transfer characteristics of the transistor are measured in the DC regime with a long time interval (20 ms) for the stabilization on each of the measured voltage level.

4. Conclusion

We showed that the performance of solution-gated field effect transistor (SGFET) based on nanocrystalline diamond thin films with H-terminated surface is sensitive to non-adherent yeast cells. SGFET transfer characteristics exhibited a positive shift of the gate voltage for a change from sucrose to YPD medium without cells. This effect was attributed to a different potential drop across the solutions due to their order of magnitude different conductivity. After addition of cells, the transfer characteristics showed a negative shift of the gate voltage with respect to blank solutions without cells. Several effects were considered to explain these shifts such as a negative surface charge of yeast cells, the influence of electrical field on the cells, and the cell adhesion to the active surface of the transistor. The most likely cause of the observed effect is the change of pH in a close vicinity of the H-terminated diamond surface due to metabolic activity of the yeast cells. This is corroborated by the fact that the effect is enhanced in the YPD medium which provides more nutrients for the yeast cells. A global change of pH due to yeast activity plays only a minor role in this response. We proposed

an overall model describing the electronic interaction of the yeast cells with the H-terminated diamond surface. The H-terminated diamond seems to be promising for an electronic monitoring of metabolic activity of non-adherent cells.

Acknowledgements

The work was supported by Czech Science Foundation (GA CR) grant no. P108/12/G108 and Czech Technical University grant no. SGS15/159/OHK3/2T/13. The work occurred in the frame of LNSM infrastructure.

References

[1] P. Strobel, M. Riedel, J. Ristein, L. Ley, O. Boltalina, Surface transfer doping of diamond, Diam. Relat. Mater. 14 (2005) 451–458, http://dx.doi.org/10.1016/j.diamond.2004.12.051.
[2] C.E. Nebel, H. Kato, B. Rezek, D. Shin, D. Takeuchi, H. Watanabe, T. Yamamoto, Electrochemical properties of undoped hydrogen terminated CVD diamond, Diam. Relat. Mater. 15 (2006) 264–268, http://dx.doi.org/10.1016/j.diamond.2005.08.012.
[3] M. Thein, F. Asphahani, A. Cheng, R. Buckmaster, M. Zhang, J. Xu, Response characteristics of single-cell impedance sensors employed with surface-modified microelectrodes, Biosens. Bioelectron. 25 (2010) 1963–1969, http://dx.doi.org/10.1016/j.bios.2010.01.023.
[4] V. Maybeck, R. Edgington, A. Bongrain, J.O. Welch, E. Scorsone, P. Bergonzo, R.B. Jackman, A. Offenhäusser, Boron-doped nanocrystalline diamond microelectrode arrays monitor cardiac action potentials, Adv. Healthc. Mater. 3 (2014) 283–289, http://dx.doi.org/10.1002/adhm.201300062.
[5] H.L. Gomes, R.B. Leite, R. Afonso, P. Stallinga, M.L. Cancela, A microelectrode impedance method to measure interaction of cells, Proc. IEEE Sens. 2004 (2004) 1011–1013, http://dx.doi.org/10.1109/ICSENS.2004.1426344.
[6] P. Bergonzo, A. Bongrain, E. Scorsone, A. Bendali, L. Rousseau, G. Lissorgues, P. Mailley, Y. Li, T. Kauffmann, F. Goy, B. Yvert, J.A. Sahel, S. Picaud, 3D shaped mechanically flexible diamond microelectrode arrays for eye implant applications: the MEDINAS project, IRBM 32 (2011) 91–94, http://dx.doi.org/10.1016/j.irbm.2011.01.032.
[7] T. Ižák, K. Novotná, I. Kopová, L. Bačáková, B. Rezek, A. Kromka, H-terminated diamond as optically transparent impedance sensor for real-time monitoring of cell growth, Phys. Status Solidi B Basic Res. 250 (2013) 2741–2746, http://dx.doi.org/10.1002/pssb.201300098.
[8] M. Krátká, A. Kromka, E. Ukraintsev, M. Ledinský, A. Brož, M. Kalbacova, B. Rezek, Function of thin film nanocrystalline diamond-protein SGFET independent of grain size, Sens. Actuators B Chem. 166–167 (2012) 239–245, http://dx.doi.org/10.1016/j.snb.2012.02.049.
[9] B. Rezek, D. Shin, H. Watanabe, C.E. Nebel, Intrinsic hydrogen-terminated diamond as ion-sensitive field effect transistor, Sens. Actuators B Chem. 122 (2007) 596–599, http://dx.doi.org/10.1016/j.snb.2006.07.004.
[10] P.K. Ang, K.P. Loh, T. Wohland, M. Nesladek, E. Van Hove, Supported lipid bilayer on nanocrystalline diamond: dual optical and field-effect sensor for membrane disruption, Adv. Funct. Mater. 19 (2009) 109–116, http://dx.doi.org/10.1002/adfm.200800770.
[11] A. Härtl, B. Baur, M. Stutzmann, J.A. Garrido, Enzyme-modified field effect transistors based on surface-conductive single-crystalline diamond, Langmuir ACS J. Surf. Colloids 24 (2008) 9898–9906, http://dx.doi.org/10.1021/la8014139.
[12] M. Dankerl, S. Eick, B. Hofmann, M.H.S. Ingebrandt, A. Offenhäusser, M. Stutzmann, J.A. Garrido, Diamond transistor array for extracellular recording from electrogenic cells, Adv. Funct. Mater. 19 (2009) 2915–2923, http://dx.doi.org/10.1002/adfm.200900590.
[13] D. Havelka, O. Kučera, M.A. Deriu, M. Cifra, Electro-acoustic behavior of the mitotic spindle: a semi-classical coarse-grained model, PLoS One 9 (2014) e86501, http://dx.doi.org/10.1371/journal.pone.0086501.
[14] O. Kučera, M. Cifra, J. Pokorný, Technical aspects of measurement of cellular electromagnetic activity, Eur. Biophys. J. 39 (2010) 1465–1470, http://dx.doi.org/10.1007/s00249-010-0597-8.
[15] A. Bendali, C. Agnès, S. Meffert, V. Forster, A. Bongrain, J.-C. Arnault, J.-A. Sahel, A. Offenhäusser, P. Bergonzo, S. Picaud, Distinctive glial and neuronal interfacing on nanocrystalline diamond, PLoS One 9 (2014) e92562, http://dx.doi.org/10.1371/journal.pone.0092562.
[16] A. Thalhammer, R.J. Edgington, L.A. Cingolani, R. Schoepfer, R.B. Jackman, The use of nanodiamond monolayer coatings to promote the formation of functional neuronal networks, Biomaterials 31 (2010) 2097–2104, http://dx.doi.org/10.1016/j.biomaterials.2009.11.109.
[17] A.E. Hadjinicolaou, R.T. Leung, D.J. Garrett, K. Ganesan, K. Fox, D.A.X. Nayagam, M.N. Shivdasani, H. Meffin, M.R. Ibbotson, S. Prawer, B.J. O'Brien, Electrical stimulation of retinal ganglion cells with diamond and the development of an all diamond retinal prosthesis, Biomaterials 33 (2012) 5812–5820, http://dx.doi.org/10.1016/j.biomaterials.2012.04.063.
[18] H. Feldmann, Yeast: Molecular and Cell Biology, Wiley-Blackwell n.d., 2016, http://dx.doi.org/10.1002/9783527659180.
[19] D.E. Amory, P.G. Rouxhet, J.P. Dufour, Flocculence of brewery yeasts and their surface properties: chemical composition, electrostatic charge and hydrophobicity, J. Inst. Brew. 94 (1988) 79–84, http://dx.doi.org/10.1002/j.2050-0416.1988.tb04561.x.
[20] D.J. Fisher, Flocculation-some observations on the surface charges of yeast cells, J. Inst. Brew. 81 (1975) 107–110, http://dx.doi.org/10.1002/j.2050-0416.1975.tb03670.x.
[21] K.J. Verstrepen, F.M. Klis, Flocculation, adhesion and biofilm formation in yeasts, Mol. Microbiol. 60 (2006) 5–15, http://dx.doi.org/10.1111/j.1365-2958.2006.05072.x.
[22] H.d. Mortensen, K. Dupont, L. Jespersen, W.g.t. Willats, N. Arneborg, Identification of amino acids involved in the Flo11p-mediated adhesion of Saccharomyces cerevisiae to a polystyrene surface using phage display with competitive elution, J. Appl. Microbiol. 103 (2007) 1041–1047, http://dx.doi.org/10.1111/j.1365-2672.2007.03325.x.
[23] S.E. Van< Mulders, E. Christianen, S.M.G. Saerens, L. Daenen, P.J. Verbelen, R. Willaert, K.J. Verstrepen, F.R. Delvaux, Phenotypic diversity of Flo protein family-mediated adhesion in Saccharomyces cerevisiae, FEMS Yeast Res. 9 (2009) 178–190, http://dx.doi.org/10.1111/j.1567-1364.2008.00462.x.
[24] S. Koyama, T. Tsubouchi, K. Usui, K. Uematsu, A. Tame, Y. Nogi, Y. Ohta, Y. Hatada, C. Kato, T. Miwa, T. Toyofuku, T. Nagahama, M. Konishi, Y. Nagano, F. Abe, Involvement of flocculin in negative potential-applied ITO electrode adhesion of yeast cells, FEMS Yeast Res. 15 (2015), http://dx.doi.org/10.1093/femsyr/fov064 (fov064–fov064).
[25] A. Kromka, O. Babchenko, T. Izak, S. Potocky, M. Davydova, N. Neykova, H. Kozak, Z. Remes, K. Hruska, B. Rezek, Pulsed linear antenna microwave plasma –a step ahead in large area material depositions and surface functionalization, Carbon Nanotub. (2011).
[26] Y. Sasaki, H. Kawarada, Low drift and small hysteresis characteristics of diamond electrolyte-solution-gate FET, J. Phys. Appl. Phys. 43 (2010), http://dx.doi.org/10.1088/0022-3727/43/37/374020, 374020–374020.
[27] E. Ukraintsev, B. Rezek, A. Kromka, A. Broz, M. Kalbacova, Long-term adsorption of fetal bovine serum on H/O-terminated diamond studied in situ by atomic force microscopy, Phys. Status Solidi B 246 (2009) 2832–2835, http://dx.doi.org/10.1002/pssb.200982257.
[28] T. Izak, M. Krátk, A. Kromka, B. Rezek, Osteoblastic cells trigger gate currents on nanocrystalline diamond transistor, Colloids Surf. B Biointerfaces 129 (2015) 95–99, http://dx.doi.org/10.1016/j.colsurfb.2015.03.035.
[29] J. Kucsera, K. Yarita, K. Takeo, Simple detection method for distinguishing dead and living yeast colonies, J. Microbiol. Methods 41 (2000) 19–21, http://dx.doi.org/10.1016/S0167-7012(00)00136-6.
[30] K. Otterstedt, C. Larsson, R.M. Bill, A. Ståhlberg, E. Boles, S. Hohmann, L. Gustafsson, Switching the mode of metabolism in the yeast Saccharomyces cerevisiae, EMBO Rep. 5 (2004) 532–537, http://dx.doi.org/10.1038/sj.embor.7400132.
[31] B.P. Tu, R.E. Mohler, J.C. Liu, K.M. Dombek, E.T. Young, R.E. Synovec, S.L. McKnight, Cyclic changes in metabolic state during the life of a yeast cell, Proc. Natl. Acad. Sci. U.S.A. 104 (2007) 16886–16891, http://dx.doi.org/10.1073/pnas.0708365104.
[32] T. Sakata, A. Saito, J. Mizuno, H. Sugimoto, K. Noguchi, E. Kikuchi, H. Inui, Single embryo-coupled gate field effect transistor for elective single embryo transfer, Anal. Chem. 85 (2013) 6633–6638, http://dx.doi.org/10.1021/ac4001018.

8.2. Nanocrystalline diamond-based impedance sensors for real-time monitoring of adipose tissue-derived stem cells

Colloids and Surfaces B: Biointerfaces 177 (2019) 130–136

Contents lists available at ScienceDirect

Colloids and Surfaces B: Biointerfaces

journal homepage: www.elsevier.com/locate/colsurfb

Nanocrystalline diamond-based impedance sensors for real-time monitoring of adipose tissue-derived stem cells

Václav Procházka[a,b], Roman Matějka[c,d], Tibor Ižák[a,b,*], Ondrej Szabó[a], Jana Štěpanovská[a,d], Elena Filová[c], Lucie Bačáková[c], Vít Jirásek[a], Alexander Kromka[a,b]

[a] Institute of Physics, Czech Academy of Sciences v.v.i., Cukrovarnická 10, 162 00, Prague 6, Czech Republic
[b] Faculty of Electrical Engineering, Czech Technical University in Prague, Technická 2, 166 27, Prague, Czech Republic
[c] Institute of Physiology, Czech Academy of Sciences v.v.i., Videnska 1083, 14220, Prague 4, Czech Republic
[d] Faculty of Biomedical Engineering, Czech Technical University in Prague, nám. Sítná 3105, 272 01, Kladno, Czech Republic

ARTICLE INFO

Keywords:
Diamond film
Biosensor
Stem cells
Impedance spectroscopy

ABSTRACT

Cell-based impedance spectroscopy is a promising label-free method for electrical monitoring of cell activity. Here we present a diamond-based impedance sensor with built-in gold interdigitated electrodes (IDT) as a promising platform for simultaneous electrical and optical monitoring of adipose tissue-derived stem cells (ASCs). The impedance spectra were collected in a wide frequency range (from 100 Hz to 50 kHz) for 90 h of cell cultivation in chambers designed for static cultivation. Absolute impedance spectra were analyzed in terms of measured frequencies and cell properties monitored by a high-resolution digital camera. The control commercially-available impedance system, based on gold electrodes exposed to the cultivation media, and also our specially developed sensor with gold electrodes built into a diamond thin film detected three phases of cell growth, namely the phase of cell attachment and spreading, the phase of cell proliferation, and the stationary phase without significant changes in cell number. These results were confirmed by simultaneous live cell imaging. The design of the sensing electrode is discussed, pointing out its enhanced sensitivity for a certain case. The diamond-based sensor appeared to be more sensitive for detecting the cell-substrate interaction in the first phase of cell growth, while the control system was more sensitive in the second phase of cell growth.

1. Introduction

Bioelectrical sensors are of high interest as non-invasive label-free techniques for in vitro monitoring of biological events, due to their simplicity and fast response in real time. At the present time, there are two analytic approaches which employ either optical or electronic signal processing [1]. These two approaches have reached the state-of-the-art in a transducer type which converts a stimulus-induced cellular response into a quantifiable signal (i.e. a biosensor signal). Among the broad family of electronic systems, impedance measurement seems to be one of the simplest and most powerful methods for monitoring cellular signals during cell cultivation [2]. The main reason for its wide application is that the monitored impedance signal is sensitive not only to ionic currents but also to cell growth stages, i.e. cell attachment, spreading, shape, proliferation, differentiation and communication [3].

Diamond has been proposed as a promising material for life science and regenerative medicine due to its biocompatibility, chemical stability and favorable combination of optical, mechanical and electrical properties [4]. In addition, its surface can be covalently terminated by specific atoms or molecules which control cell occupation, adhesion, proliferation and cell differentiation [5]. In our previous studies, we have already introduced a surface-conductive diamond thin film as a functional layer in impedance sensors for biological studies [6,7] and for recognizing gas and chemical molecules [8,9]. It has been proven that intrinsic diamond thin film can be used as biocompatible biosensor for in-situ electronic (label-free) monitoring of cell behavior in cultures [6]. In that approach, the sensing principle of the diamond-based impedance sensor was based on impedance measurements, employing conductive hydrogen-terminated surface regions as in-plane electrodes that were separated by resistive oxidized surface regions. The thin diamond film was deposited on a glass substrate. This made it fully transparent in the visible range, including a low fluorescence background. Moreover, any possible and unwanted geometrical effects of metal electrodes (e.g. step edges) were avoided, and purely surface atom modifications defined and induced the p-type diamond surface conductivity [6]. Surface-conductive H-terminated diamond channels

* Corresponding author at: Institute of Physics, Czech Academy of Sciences v.v.i., Cukrovarnická 10, 162 00, Prague 6, Czech Republic.
E-mail address: izak@fzu.cz (T. Ižák).

https://doi.org/10.1016/j.colsurfb.2019.01.048
Received 8 November 2018; Received in revised form 22 January 2019; Accepted 23 January 2019
Available online 28 January 2019

were also applied in the case of solution-gated field effect transistors to study the interactions of human osteoblast-like SAOS-2 cells with a diamond surface [10].

In our present study, an impedance sensor with a functional diamond layer deposited on gold interdigitated electrodes is employed to monitor electrically and optically the growth activity of adipose tissue-derived stem cells (ASCs). ASCs were chosen because, together with human bone marrow mesenchymal stem cells, they had become the most popular adult stem cells used in tissue engineering, cell therapy and studies on cell differentiation towards various phenotypes [11]. For example, differentiation of ASCs towards adipocytes and osteoblasts was successfully quantitatively monitored in real time by impedance sensing [12]. Generally, cell differentiation is preceded by cell adhesion, spreading and proliferation, and these cell functions are also used for expanding the ASCs into desirable quantities for the purposes of further studies on various properties of these cells, and for their biomedical applications. In our study, we therefore focus on an investigation of cell adhesion, spreading and proliferation by impedance sensing with diamond-based impedance sensors. The results are compared with impedance measurements provided using a commercially-available gold interdigitated electrodes array (xCELLigence RTCA system, Roche Applied Science).

2. Experimental part

2.1. Preparation of sensors and measurement setup

The transducer of the sensor is formed by metal composite interdigitated electrodes (IDTs, 10 nm Ti and 80 nm Au) deposited on a quartz substrate (Corning XG, 15 × 15 mm^2 in size) (see Fig. S1a and S1b in the supplementary files). The width/gap of electrode periodicity was set to 100 µm. Samples with IDTs were coated with a diamond layer approx. 100 nm in thickness, using a linear antenna pulsed microwave plasma chemical vapor deposition system [13]. The deposition conditions were as follows: microwave power 2 × 1700 W, pressure 0.1 mbar, gas mixture 200/5/20 sccm of $H_2/CH_4/CO_2$, temperature 400 °C and process time 50 h. After deposition, the active sensor area was homogenously covered with a fully closed nanocrystalline diamond (NCD) film (Fig. S1c). The diamond character of the deposited film was confirmed by Raman spectroscopy [14].

Two types of sensors were used for the impedance measurements: gold IDT electrodes on glass (i) with a nanocrystalline diamond film, further labelled as “NCD sensor”, and (ii) without a nanocrystalline diamond film, further labelled as “Au sensor”. Before the experiments, the surface of the NCD sensors was oxygen-terminated using radio-frequency plasma. This step made the diamond surface hydrophilic and electrically insulating. To note, the surface of as grown diamond film is generally hydrogen-terminated due to high hydrogen content (> 88%) in the gas mixture used during deposition process. Hydrogen-terminated surface could lead to p-type surface conductivity. Therefore, to avoid any surface shortcuts and make the diamond surface well defined for cell cultivation, its oxygen-termination is needed.

The cells were cultivated in custom-built chambers designed for static cultivation (see Fig. S2b-S2d in supplementary files) in a 500 µl reservoir (made from polycarbonate) with a cultivation area of 7 × 10 mm^2. All materials that were used are biocompatible (nontoxic) to cells and are compatible with the autoclave sterilization process. The structure of the chambers is also optimized for real time microscopic imaging of the cells during their cultivation (Fig. S2a). During the experiments, the whole system was placed in an incubation chamber, where the temperature (37 °C) and the atmosphere (5% CO_2 and > 90% relative humidity) were kept constant. The impedance sensors were interconnected with a measuring device using gold spring connectors (Mill-Max Mfg. Corp., NY, USA). A custom multiplexer unit (MUX) was built to measure 8 parallel chambers during one experiment. Low-resistance reed relays were used (Littelfuse, Inc, IL, USA). The printed

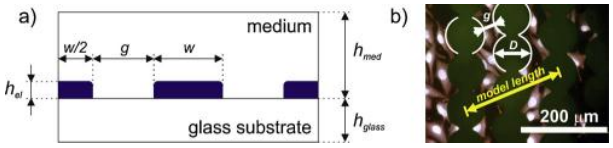

Fig. 1. a) Schematic draw of the computational domain used for FEM simulation. b) Representative fluorescence image of cells on xCELLigence sensor with highlighted dimensions of electrodes [6] (Note: the diameter (*D*) of circular-shape electrodes is ˜85 µm, and the gap (*g*) between electrodes with opposite polarity is ˜25 µm).

circuit board for MUX was optimized for equal length of traces for each channel to achieve similar impedance parameters.

The impedance parameters were measured using a Bode 100 (OMICRON electronics GmbH, Germany) vector analyser with custom built software for automated measurements of multiple channels. The impedance spectra were collected in a frequency range from 100 Hz to 50 kHz for 90 h cultivation. In this paper, we focus on impedance data measured at 1 kHz frequency.

Simultaneously with these experiments, reference measurements with the same cultivation conditions were performed using the xCELLigence RTCA system (Roche Applied Science) [3,15]. This system uses circular-shape Au IDT electrodes (Fig. 1b) and provides the time evolution of the so-called cell index, defined as $(Z_i\text{-}Z_0)/const$, where Z_i is the absolute impedance measured at time i and Z_0 is the starting impedance at time t = 0 s. Here, the measurement frequencies are limited to three discrete frequencies: 10 kHz, 25 kHz and 50 kHz.

2.2. Cell cultivation

Prior to cell cultivation, all parts of the cultivation chambers and impedance sensors were cleaned using 70% ethyl alcohol and were thoroughly rinsed with deionized water. Then the impedance sensor was installed in the cultivation chamber, and they were assembled all together (Fig. S2d). Finally, the assembly was sterilized using an autoclave (15 min at 121 °C) and was dried at 80 °C.

Human adipose tissue-derived stem cells (ASCs) were isolated from lipoaspirate obtained by liposuction [16]. The isolation was conducted in compliance with the tenets of the Declaration of Helsinki for experiments involving human tissues and under ethical approval issued by the Ethics Committee at the Bulovka Hospital in Prague (August 28, 2014). Written informed consent was obtained from the patient before the liposuction procedure. The cells in passage 2 were seeded on the impedance sensors and on the controls. The set contained eight cultivation chambers with 4x Au sensors and 4x NCD sensors. Here, 3 sensors from both the Au sensors and the NCD sensors were seeded with cells, while 1 sensor was left as the control (i.e. without cells), in order to investigate the influence of the culture medium, e.g. its evaporation and degradation over time. Pure and NCD-covered microscopic glass coverslips (both seeded with cells) were used as other control samples for a study of how the material of the sensor or the measurement itself affects the behavior of the cells.

The initial seeding density of ASCs was set according to refs. [17,18], and was adapted to the area of our designed culture chamber (0.7 cm^2) and the xCELLigence RTCA System (0.2 cm^2) (used for the reference measurements). The recommended density for RTCA is 3 000 cells/well (approx. 15 300 cells/cm^2), giving 11 000 cells/well for our home-made cultivation chamber. The cells were cultivated in standard high glucose Dulbecco's Modified Eagle's culture medium (DMEM) with the addition of 10% fetal bovine serum and human recombinant fibroblast growth factor-2 (FGF-2, 10 ng/ml). A 200 µl volume of the medium per well was applied in RTCA, and 650 µl per well was applied for our home-made cultivation chamber. After the cells had been seeded, the cultivation chambers equipped with sensors were connected to the MUX unit (Fig. S2), and time-lapse measurements began (i.e.

both electrical and optical monitoring). The measuring step period was set to 4 min.

After the impedance measurements, the cells were fixed using 4% paraformaldehyde and were fluorescence stained, using DAPI and phalloidin conjugated with tetramethylrhodamine (TRITC). The images of the fluorescently-stained ASCs on the impedance sensors and on controls were measured using a Leica DMi-8 microscope with a 10x objective and a Chroma multiband fluorescence filter.

2.3. FEM simulation

Finite element method (FEM) simulation using Comsol Multiphysics software was employed to study the distribution of the current density and the electric field for both the Au sensor and commercial xCELLigence RTCA system. For simplicity, in the first approach, the nanocrystalline diamond film was not taken into account, only the gold interdigitated electrodes with different width/gap periodicities deposited on glass substrates, and in the presence of a cell medium, were used for modelling in 2D geometry (see Fig. 1a). In the case of the xCELLigence system (circular electrodes), a perpendicular vertical cut along the centers of the circles was used as a computational domain (see "model length" in Fig. 1b). The other parameters were the same for both sensors, i.e. the height of the electrodes (h_{el}) 90 nm, the height of the glass substrate (h_{glass}) 100 μm, and the height of the cell medium (h_{med}) 200 μm. The height of the cell medium was chosen on the basis of the results of our first preliminary simulations, where we observed that higher values of h_{med} (≥200 μm) do not significantly affect the simulation results.

The conductivity of the cell culture medium (18.55 mS/cm) and the permittivity of water (80) were put as material properties in the finite element method model, as recommended in [19]. The specific electrical conductivity of gold was set to $\kappa = 49 \times 10^6$ S/m) [20]. For the glass substrate, conductivity 1×10^{-12} S/m and relative permittivity 4.2 were used.

In the FEM model, the time-harmonic equation of current continuity for the given AC frequency (1 kHz) was investigated, i.e. the investigated parameters are the amplitudes of the harmonic current and voltage forms. The voltage amplitude was set to 0.5 V. At the middle electrode the voltage was set to $U = U0*sin(\omega t)$, while at the edge electrodes $U = 0$ V.

3. Results and discussion

3.1. A comparison between the NCD sensor and the Au sensor

Fig. 2 summarizes the absolute and relative impedances measured by the pristine Au and NCD sensors (in the graphs labelled as 'Au' and 'NCD'), while the ASCs were being cultivated. The impedances are plotted for 1 kHz frequency. The as-measured absolute impedances for three NCD sensors and two Au sensors are plotted in Fig. 2a. Employing several sensors in a single experiment minimizes systematic errors and gives additional information about reliability and reproducibility of the sensors. For example, as can be seen in Fig. 2a, the absolute impedance values for the NCD sensors are approx. 2 times lower (˜300 Ω) than for the pristine Au sensors (˜600 Ω). This difference could be attributed to the character of the diamond layer. Generally, diamond is characterized as an insulating material. However, in the case of nanocrystalline diamond (NCD), the diamond film consist of small grains featured by the sp^3 carbon bonds (attributed to diamond) and the sp^2 carbon bonds (attributed to amorphous carbon) which are present at the grain boundaries. In the NCD films, sp^2 bonds dominate, making the diamond film less resistive [21]. In addition, the surface of a diamond film can exhibit p-type surface conductivity when it is finished by hydrogen atoms [6,22]. However, in our case we eliminated (minimized) this contribution while the surface was terminated by oxygen atoms using RF plasma, which is known as an insulating surface.

Further, we investigated the time evolution of the relative impedances as a function of sensor type (Fig. 2b). The relative impedances were calculated by subtracting the as-measured absolute impedances with Z_0 (i.e. Z_i-Z_0, where Z_0 is the impedance measured at time $t = 0$ s and Z_i is the impedance at time t_i). In Fig. 2b, the relative impedances measured for the medium with cells (Z_{cell}, solid lines) and without cells (Z_{medium}, dashed lines) for NCD sensors and Au sensors are plotted. Both Z_{medium} curves increased almost linearly, which could be attributed e.g. to the adsorption of proteins in the culture medium to the sensor surface. It has been reported that the adsorption of albumin, a major protein component of the serum supplement of the culture medium, can modulate the impedance, the electrical current and the potential of peptide-modified Au surfaces [23].

When Z_{medium} (the impedance measured for the medium without cells) is subtracted from Z_{cell} (the impedance measured for the medium with cells), we obtain in the first approximation of the impedance, which involves only the influence of cell cultivation. Side effects related to the ageing of the medium should be minimized [2] (see "baseline-corrected impedances" in Fig. 2c for one selected NCD sensor and for one Au sensor). These impedances are discussed below.

As can be seen in Fig. 2d, the time-dependent data of the baseline-corrected relative impedances can be divided into three main regions. At the beginning (up to 4 ÷ 6 h), there is a sharp increase of Z (region I). From 10 ÷ 12 h up to ˜60 ÷ 70 h (region II), the increase of Z is much slighter (the slope for this region is 10 ÷ 15 times lower than for region I). Finally, in region III at the end of the experiments (> 70 h), Z is almost constant or decreases slightly. Between these three main regions, we have defined two short intermediate regions. As was mentioned above, these data are plotted for 1 kHz frequency. However, the same behavior was also observed for impedance data measured at other frequencies. For example, Fig. S3a shows baseline-corrected impedances (i.e. Z_{cell}-Z_{medium}) for frequencies varying from 500 Hz to 20 kHz. As expected, the impedance decreases with increasing frequency. However, their time-dependent trends are almost the same (see the normalized impedance spectra in Fig. S3b). We therefore focus further on the impedance data interpretation measured at 1 kHz (Fig. 2d), especially on the explanation for the possible origins (causes) of regions I, II and III, also on the basis of the time-lapse optical images of the cells taken simultaneously during the experiments (Fig. 3).

The rapid increase in Z at the beginning (region I) seems to form a temporary period during which the cells were added to the cultivation medium, fell down onto the sensor active area, and started to adhere and spread on the substrate. Here, the shape of the cells was circular-like or ellipsoidal (see optical images in Fig. 3 (or in Fig. S4) from 0.5 h up to 3 h). From ˜4 h of the experiment, the first intermediate region began, in which the cells started to change their shape (Fig. 3). Most of the cells gained a spindle-like or polygonal morphology and formed numerous lamellipodia and filopodia. If the initial cell population density is enough low, i.e. if there is still reaming space between them on the sensor area, the cells proliferate quickly, causing a steep increase in Z (*cf.* Figs. 2d and 3 ; time from 6 h up to 15 h after cell seeding). Region II is characterized by a slighter increase in Z, which marks the formation of a confluent cell layer, accompanied by a slowdown of cell proliferation (*cf.* Figs. 2d and 3 ; from 17 h up to ˜65 h). Finally, region III (separated from region II with the second intermediated region) corresponds to cell confluence, i.e. full coverage of the active sensor area with cells. The cells stop their proliferation and their number is constant, or can even decrease slightly, due to their delamination from the surface, particularly from the Au surface (*cf.* Figs. 2d and 3 ; up to 90 h). Similar cell behavior was detected in NIH-3T3 fibroblasts cultured in a digital microfluidic system capable of impedance sensing [24], and also in mutant Chinese hamster V79 cells by an RT-CES system based on gold electrodes on silicon substrate [25], and operating on a similar principle similar to that of the xCELLigence system used in our present study.

In summary, the cell growth dynamics detected by our sensor

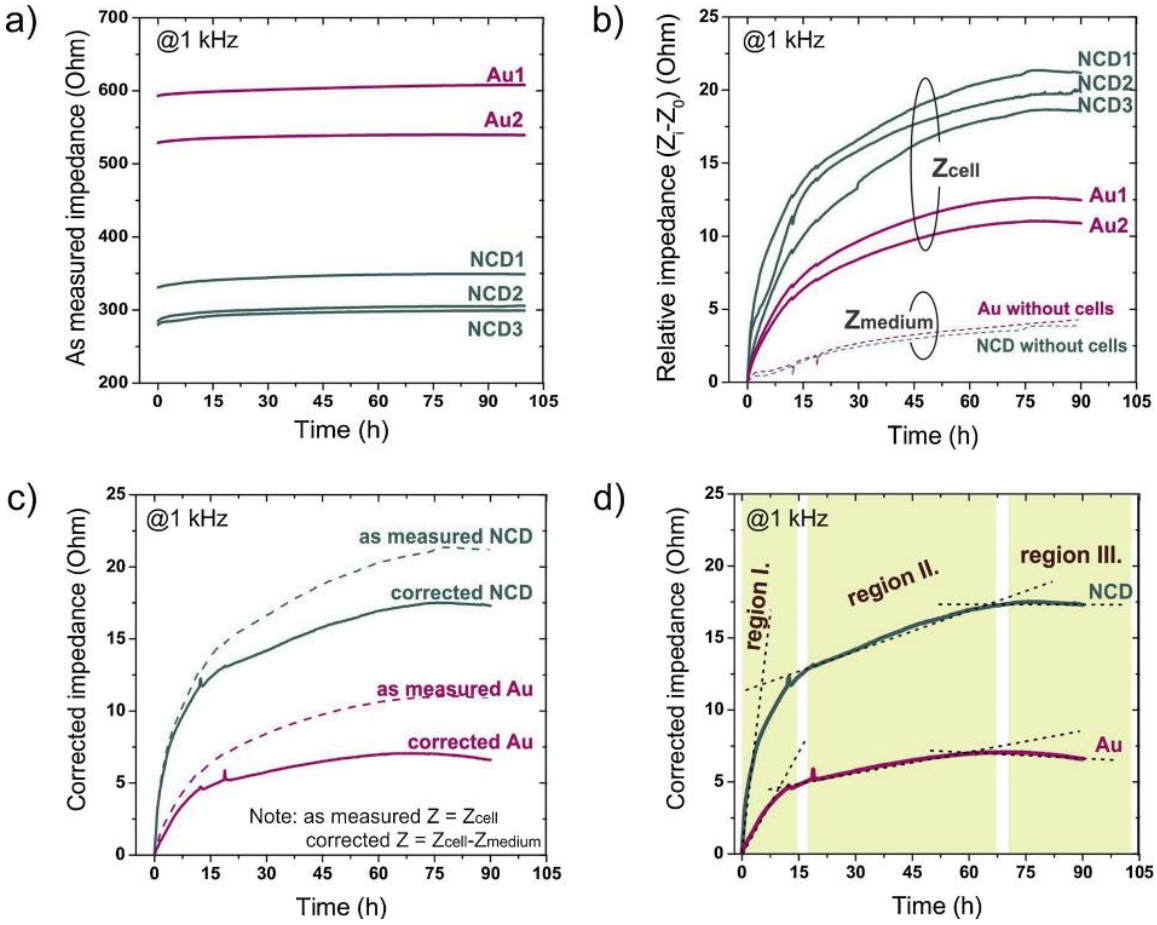

Fig. 2. a) As-measured absolute impedance, b) relative impedance and c),d) baseline-corrected impedance of adipose tissue-derived stem cells during the cultivation experiment, measured at frequency of 1 kHz for 4 days with diamond-coated and pristine Au IDT sensors (labelled as 'NCD' and 'Au', respectively). Notes: relative impedances represent shifted as-measured absolute impedances by Z_0 (impedance at time $t = 0$ s, i.e. Z_i-Z_0); baseline-corrected impedances are relative impedances subtracted by the impedances measured for medium without cells (i.e. Z_{cell}-Z_{medium}).

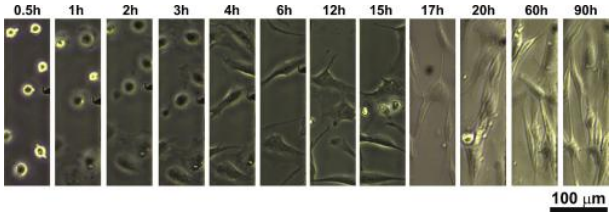

Fig. 3. Time-lapse optical images of cells on the NCD sensor surface during the cultivation and simultaneous electrical measurement.

resemble the classical "growth curves", which are widely used for evaluating the growth of cell populations. These growth curves consist of the following three major phases: the lag phase, in which the cells attach and spread on the cultivation substrate; the exponential phase, in which the cells proliferate; and the stationary phase, in which the cells reach confluence. Their numbers either do not change significantly or even decrease usually due to cell death and detachment [25–27]. The cell dynamics was also verified by direct cell counting in transparent regions of live cell-imaging pictures for the NCD sensor. The calculated time-dependent cell density on the NCD sensor is shown in Fig. S5a in the supplementary data. The resulting growth curve has standard cell growth behavior, consisting of three major phases: the lag phase, cell proliferation, and the stagnation phase. The cell growth curve, as will be discussed further, copies the cell index data of the xCELLigence sensor well (Fig. S5b). Note that the cell density data was obtained from time-lapse optical images of the cells on the surface of the NCD sensor; in the case of the xCELLigence system, real-time optical monitoring was not possible due to its specific structure, and just this simultaneous optical and electrical monitoring is the main advantage of our NCD sensor in comparison with commercial systems.

3.2. A comparison between the NCD sensor and the xCELLigence sensor

As has been mentioned above, simultaneously with the measurements performed by NCD and Au sensors, reference measurements were carried out using the commercially available xCELLigence RTCA system (i.e. by a gold interdigitated electrode array). Fig. 4a shows cell indexes measured by four xCELLigence sensors for the medium with cells (CI_{cell}, 2 blue and 2 green solid lines) and for the medium without cells (CI_{medium}, two red dashed lines). As in the impedance measurements taken by the Au sensors and NCD sensors, the cell indexes of the medium without cells were subtracted from the cell indexes of the medium with cells (i.e. the baseline-corrected cell index was calculated as $CI_{cell} - CI_{medium}$), and was compared with the impedance data measured by the NCD sensor (Fig. 4b).

As is shown in Fig. 4b, both plots consist of the three main regions described above. However, there are differences in slope steepness. While in the first region the slope is steeper for NCD sensor, in the second region the xCELLigence system shows steeper slope. It seems

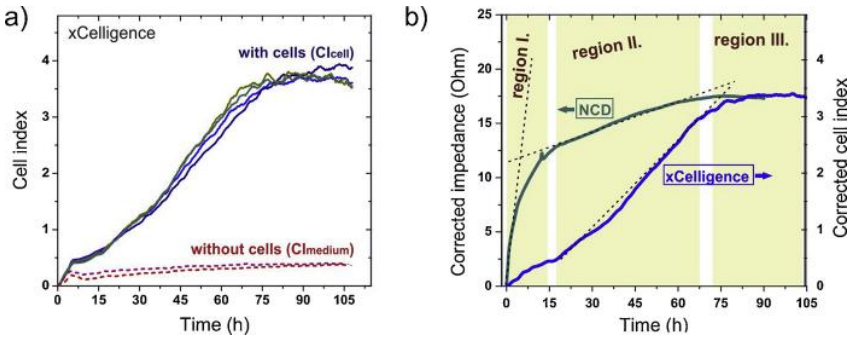

Fig. 4. a) Cell indexes measured by xCELLigence RTCA system for the medium with cells (CI_{cell}, blue solid lines) or without cells (CI_{medium}, red dashed lines). b) Comparison of baseline-corrected cell index (i.e. CI_{cell}-CI_{medium}, right y-axes) with baseline-corrected impedance (i.e. Z_{cell}-Z_{medium}, left y-axes) measured by xCELLigence RTCA system and NCD sensor, respectively (For interpretation of the references to colour in this figure legend, the reader is referred to the web version of this article).

that the NCD sensor is more sensitive that the xCELLigence system in the first region and less sensitive in the second region. Theoretically, the observed differences can be partially attributed to the different nature of diamond surface and gold/glass surfaces, and hence there are different cell adhesion properties in the early stage of cell cultivation, which could influence the impedance measurements. In our earlier studies and studies by other authors, NCD films have proved to be excellent substrates for cell adhesion [28,29], while Au is generally known to be rather bioinert. However, as shown in Fig. 2d, the NCD and Au sensors with the same IDT structures exhibit almost the same behaviors, so this explanation is not valid in our case. Another contribution is related to the different frequencies used during impedance measurements by the NCD sensor and by the xCELLigence system. However again, as shown in Fig. S3a and S3b (in the supplementary files), the frequency does not significantly influence the measurements for the NCD sensor.

Next, as shown in Fig. S5b, the cell growth curve, obtained from time-lapse optical images of cells on the NCD sensor surface, well copies the cell index data of the xCELLigence sensor. It is therefore supposed that the xCELLigence sensor should have similar cell growth curve. The difference in the impedance curves of NCD and xCELLigence sensors could be related to sizes of the IDTs. The NCD sensors and the xCELLigence RTCA system use different IDT structures. While for the NCD IDT sensor the width of the gap is the same as the electrode width (i.e. 100 µm, for example see Fig. S4), in the case of the xCELLigence IDT, the gap is much smaller than the electrode width. The width (or the diameter) of the circular-shape electrodes is 85 µm, and the gap between them is around 25 µm (Fig. 1b). This means that the ratio of the total electrode area to the gap area is 2:1 for the xCELLigence IDT and 1:1 for the NCD sensor.

The geometry of the IDT electrodes also influences the current density magnitude and its distribution over the sensor surface. Fig. 5 shows the distribution of the current density as simulated for two types of gold IDT electrodes on a glass substrate with 100/100 µm and 85/25 µm width/gap periodicity. The simulation predicts that for the xCELLigence sensor the maximum intensity of the current density is approx. twice as high as in the case of our Au IDT for the same AC voltage conditions.

The sensitivity distribution over the sensor surface is proportional to the relative current density. The regions of low current density will contribute less to the overall reduction in current (and therefore to the increase in impedance) when they are covered with cells. However, this will affect the sensitivity of the sensor by the same factor throughout the cell growth period.

Fig. 6 shows the current density distributions across the line between two electrodes at a Z-height of 1 µm. The current density peaks correspond to the electrode edges, with each peak having its half-width of half-maximum (HWHM) as indicated. Consequently, we can define the "sensitivity distribution ratio" (SDR) as

$$SDR = 4 \times HWHM \,/\, W_p \quad (1)$$

where W_p is the period width (the sum of the gap width and the electrode width). According to the simulation results, SDR is 0.052 for the Au IDT sensor and 0.073 for the xCELLigence system. In the first assumption the overall sensitivity of the two sensors is qualitatively comparable. However, differences in peak current density magnitudes may lead to different courses of Z_{medium}, as the electric properties of the medium are modified by the passage of the current. Indeed, as can be seen in the case of the xCELLigence sensor, Z_{medium} (CI) increases rapidly during the first 4 h, reaching 50% of its saturated value (see Fig. 4a). However, the increase in the Z_{medium} for the Au IDT sensor is much slower (compare with Fig. 2b). This may contribute to the steeper increase in the baseline-corrected impedance, as shown in Fig. 4b. However, the exact medium change mechanism is unknown in our case. More precise experimental measurement and simulation studies also need to be carried out in 3D geometry and taking into account the temporal and spatial change in the electrical properties of the medium + cells. However, this topic lies beyond the scope of present study.

Finally, 90 h after seeding, the cells reached confluence and were

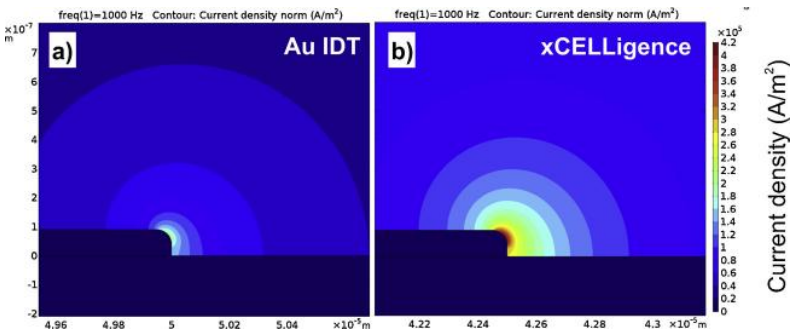

Fig. 5. Distribution of current density for Au IDT electrodes system (a) used for diamond deposition and for commercial xCELLigence sensor (b) plotted with the same scale bar.

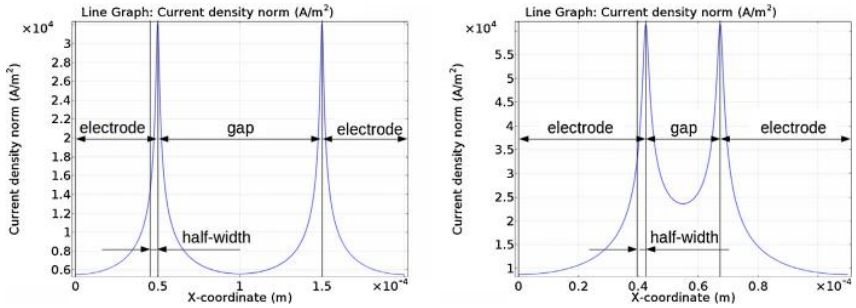

Fig. 6. Distribution of current density across the line located between electrodes of the Au IDT (left) and xCELLigence sensor (right) at 1 μm above the glass substrate.

homogenously distributed over the sensor area. Native pictures (Fig. S6 a–d in supplementary files) revealed that the cells were of spindle-shaped or polygonal morphology at the end of the experiments. Spindle-shaped morphology prevailed on the gold IDT sensor, while the polygonal morphology was more pronounced on the NCD-coated gold IDT sensor, and particularly on the NCD-coated and uncoated glass coverslips. The predominant spindle-shaped cell morphology could be a consequence of slightly delayed cell adhesion and spreading on the gold IDT sensor (Fig. 4b). It is generally known that gold surfaces are rather bioinert. For improved cell adhesion and growth, they should be further functionalized with chemical groups and/or biomolecules [30]. Nevertheless, the cells on all tested surfaces displayed a well-developed actin cytoskeleton (Fig. S6 e–h), as revealed by staining with TRITC-conjugated phalloidin, which binds filamentous (F) actin [31]. Generally, the microscopic observations of cell morphology proved that there were no significant differences between the gold IDT sensor, the NCD-coated gold IDT sensor and the control NCD-coated and uncoated glass surfaces. Also, the final cell population densities were similar on each tested surface (Fig. S6). These results are in good correlation with similar impedances and similar cell indexes detected by the gold IDT sensor and the NCD-coated gold IDT sensor in the interval of ˜75-90 h after cell seeding (Fig. 4b).

4. Conclusions

We have employed an impedance sensor type using a functional diamond layer deposited on metal interdigitated electrodes for monitoring the adhesion, growth and metabolic activity of adipose tissue-derived stem cells during cultivation. Wide frequency range measurements (100 Hz to 50 kHz) with time dependent impedance monitoring correlated with time-lapse optical microscopy enabled us to study the cell-cell and cell-substrate interactions and to investigate electrochemical processes at the electrode-electrolyte interface. The diamond-based sensor seems to be more sensitive during the early integration of cells with a diamond thin film (for cultivation time up to approx. 15 h after cell seeding), while the control commercially-available xCELLigence gold IDT system seems to be more sensitive in the later cell growth phase (for time interval from approx. 15 to 65 h after cell seeding). The simulated sensitivity distribution ratio rose more slowly for the Au IDT sensor than for the xCELLigence system, which is probably related to the steeper increase in its baseline-corrected impedance. However, the exact mechanism for these differences still needs further studies. We can conclude that the thin nanocrystalline diamond layer (100 nm) on the gold IDT provides a promising platform for future simultaneous electrical and optical monitoring of cell events on surfaces functionally terminated by various biomolecules.

Acknowledgments

This work was supported by the Ministry of Health of the Czech Republic (grant No. AZV 15-33018A), by CTU grant no. SGS17/136/OHK4/2T/13, and by Operational Programme Research, Development and Education financed by the European Structural and Investment Funds and the Czech Ministry of Education, Youth and Sports (Project No. SOLID21 - CZ.02.1.01/0.0/0.0/16_019/0000760). Mr. Robin Healey (Czech Technical University, Prague, Czech Republic) is gratefully acknowledged for his language revision of the manuscript.

Appendix A. Supplementary data

Supplementary material related to this article can be found, in the online version, at doi:https://doi.org/10.1016/j.colsurfb.2019.01.048.

References

[1] Y. Fang, Label-free biosensors for cell biology, Int. J. Electrochem. Sci. 2011 (2011) 1–16, https://doi.org/10.4061/2011/460850.
[2] Y. Xu, X. Xie, Y. Duan, L. Wang, Z. Cheng, J. Cheng, A review of impedance measurements of whole cells, Biosens. Bioelectron. 77 (2016) 824–836, https://doi.org/10.1016/j.bios.2015.10.027.
[3] N. Guan, J. Deng, T. Li, X. Xu, J.T. Irelan, M.-W. Wang, Label-free monitoring of T cell activation by the impedance-based xCELLigence system, Mol. Biosyst. 9 (2013) 1035, https://doi.org/10.1039/c3mb25421f.
[4] C.E. Nebel, B. Rezek, D. Shin, H. Uetsuka, N. Yang, Diamond for bio-sensor applications, J. Phys. Appl. Phys. 40 (2007) 6443–6466, https://doi.org/10.1088/0022-3727/40/20/S21.
[5] M. Verdanova, B. Rezek, A. Broz, E. Ukraintsev, O. Babchenko, A. Artemenko, T. Izak, A. Kromka, M. Kalbac, M. Hubalek Kalbacova, Nanocarbon allotropes-graphene and nanocrystalline diamond-promote cell proliferation, Small. 12 (2016) 2499–2509, https://doi.org/10.1002/smll.201503749.
[6] T. Ižák, K. Novotná, I. Kopová, L. Bačáková, B. Rezek, A. Kromka, H-terminated diamond as optically transparent impedance sensor for real-time monitoring of cell growth, Phys. Status Solidi B 250 (2013) 2741–2746, https://doi.org/10.1002/pssb.201300098.
[7] T. Izak, K. Novotná, I. Kopová, L. Bačáková, M. Varga, B. Rezek, A. Kromka, Hydrogen-terminated diamond sensors for electrical monitoring of cells, Key Eng. Mater. 605 (2014) 577–580, https://doi.org/10.4028/www.scientific.net/KEM.605.577.
[8] M. Davydova, M. Stuchlik, B. Rezek, K. Larsson, A. Kromka, Sensing of phosgene by a porous-like nanocrystalline diamond layer with buried metallic electrodes, Sens. Actuators B Chem. 188 (2013) 675–680, https://doi.org/10.1016/j.snb.2013.07.079.
[9] S. Stehlik, T. Izak, A. Kromka, B. Dolenský, M. Havlík, B. Rezek, Sensitivity of diamond-capped impedance transducer to tröger's base derivative, ACS Appl. Mater. Interfaces 4 (2012) 3860–3865, https://doi.org/10.1021/am3005829.
[10] T. Izak, M. Krátká, A. Kromka, B. Rezek, Osteoblastic cells trigger gate currents on nanocrystalline diamond transistor, Colloids Surf. B Biointerfaces 129 (2015) 95–99, https://doi.org/10.1016/j.colsurfb.2015.03.035.
[11] P.A. Zuk, The adipose-derived stem cell: looking back and looking ahead, Mol. Biol. Cell 21 (2010) 1783–1787, https://doi.org/10.1091/mbc.E09-07-0589.
[12] P.O. Bagnaninchi, N. Drummond, Real-time label-free monitoring of adipose-derived stem cell differentiation with electric cell-substrate impedance sensing, Proc. Natl. Acad. Sci. 108 (2011) 6462–6467, https://doi.org/10.1073/pnas.1018260108.
[13] Š. Potocký, M. Čada, O. Babchenko, T. Ižák, M. Davydova, A. Kromka, Perspectives of linear antenna microwave system for growth of various carbon nano-forms and its plasma study: perspectives of linear antenna microwave system, Phys. Status Solidi B 250 (2013) 2723–2726, https://doi.org/10.1002/pssb.201300085.
[14] V. Procházka, R. Matějka, T. Ižák, O. Szabó, J. Štěpanovská, L. Bačáková, A. Kromka, Real-time monitoring of stem cells by diamond-based impedance sensors, Proceedings 1 (2017) 515, https://doi.org/10.3390/proceedings1040515.
[15] F. Witzel, R. Fritsche-Guenther, N. Lehmann, A. Sieber, N. Blüthgen, Analysis of impedance-based cellular growth assays, Bioinformatics 31 (2015) 2705–2712, https://doi.org/10.1093/bioinformatics/btv216.

[16] M. Zhu, S. Heydarkhan-Hagvall, M. Hedrick, P. Benhaim, P. Zuk, Manual isolation of adipose-derived stem cells from human lipoaspirates, J. Vis. Exp. (2013), https://doi.org/10.3791/50585.
[17] K. Solly, X. Wang, X. Xu, B. Strulovici, W. Zheng, Application of real-time cell electronic sensing (RT-CES) technology to cell-based assays, Assay Drug Dev. Technol. 2 (2004) 363–372, https://doi.org/10.1089/adt.2004.2.363.
[18] J.Z. Xing, L. Zhu, J.A. Jackson, S. Gabos, X.-J. Sun, X. Wang, X. Xu, Dynamic monitoring of cytotoxicity on microelectronic sensors, Chem. Res. Toxicol. 18 (2005) 154–161, https://doi.org/10.1021/tx049721s.
[19] G. Blume, Electrical stimulation of NIH-3T3 cells with platinum-PEDOT-Electrodes integrated in a bioreactor, Open Biomed. Eng. J. 7 (2013) 125–132, https://doi.org/10.2174/1874120701307010125.
[20] E. Hering, K. Bressler, J. Gutekunst, Elektronik für Ingenieure und Naturwissenschaftler, Springer Berlin Heidelberg, Berlin, Heidelberg, 2014, https://doi.org/10.1007/978-3-642-05499-0.
[21] O.A. Williams, Nanocrystalline diamond, Diam. Relat. Mater. 20 (2011) 621–640, https://doi.org/10.1016/j.diamond.2011.02.015.
[22] A. Härtl, J.A. Garrido, S. Nowy, R. Zimmermann, C. Werner, D. Horinek, R. Netz, M. Stutzmann, The ion sensitivity of surface conductive single crystalline diamond, J. Am. Chem. Soc. 129 (2007) 1287–1292, https://doi.org/10.1021/ja066543b.
[23] H. Trzeciakiewicz, J. Esteves-Villanueva, R. Soudy, K. Kaur, S. Martic-Milne, Electrochemical characterization of protein adsorption onto YNGRT-Au and VLGXE-Au surfaces, Sensors 15 (2015) 19429–19442, https://doi.org/10.3390/s150819429.
[24] S.C.C. Shih, I. Barbulovic-Nad, X. Yang, R. Fobel, A.R. Wheeler, Digital microfluidics with impedance sensing for integrated cell culture andanalysis, Biosens. Bioelectron. 42 (2013) 314–320, https://doi.org/10.1016/j.bios.2012.10.035.
[25] J.Z. Xing, S. Gabos, B. Huang, T. Pan, M. Huang, J. Chen, High-throughput quantitative analysis with cell growth kinetic curves for low copy number mutant cells, Anal. Bioanal. Chem. 404 (2012) 2033–2041, https://doi.org/10.1007/s00216-012-6328-5.
[26] M. Toloudi, E. Ioannou, M. Chatziioannou, P. Apostolou, C. Kiritsis, S. Manta, D. Komiotis, I. Papasotiriou, Comparison of the growth curves of cancer cells and cancer stem cells, Curr. Stem Cell Res. Ther. 9 (2014) 112–116, https://doi.org/10.2174/1574888X0902140121163539.
[27] I. Kareva, G. Karev, From Experiment to Theory: What Can We Learn from Growth Curves? Bull. Math. Biol. 80 (2018) 151–174, https://doi.org/10.1007/s11538-017-0347-5.
[28] L. Grausova, L. Bacakova, A. Kromka, S. Potocky, M. Vanecek, M. Nesladek, V. Lisa, Nanodiamond as promising material for bone tissue engineering, J. Nanosci. Nanotechnol. 9 (2009) 3524–3534, https://doi.org/10.1166/jnn.2009.NS26.
[29] M. Amaral, A.G. Dias, P.S. Gomes, M.A. Lopes, R.F. Silva, J.D. Santos, M.H. Fernandes, Nanocrystalline diamond: *in vitro* biocompatibility assessment by MG63 and human bone marrow cells cultures, J. Biomed. Mater. Res. A 87A (2008) 91–99, https://doi.org/10.1002/jbm.a.31742.
[30] P.A. Santos, C.S. Rocha, M.S. Baptista, Adhesion and proliferation of HeLa and fibroblast cells on chemically-modified gold surfaces, Colloids Surf. B Biointerfaces 123 (2014) 429–438, https://doi.org/10.1016/j.colsurfb.2014.09.034.
[31] B. Chazotte, Labeling cytoskeletal F-Actin with rhodamine phalloidin or fluorescein phalloidin for imaging, Cold Spring Harb. Protoc. 2010 (2010), https://doi.org/10.1101/pdb.prot4947 pdb.prot4947-pdb.prot4947.

8.3. Detection of globular and fibrillar proteins by quartz crystal microbalance sensor coated with a functionalized diamond thin film

Applied Surface Science 589 (2022) 153017

Contents lists available at ScienceDirect

Applied Surface Science

journal homepage: www.elsevier.com/locate/apsusc

Full Length Article

Detection of globular and fibrillar proteins by quartz crystal microbalance sensor coated with a functionalized diamond thin film

V. Procházka [a,b,*], P. Kulha [b], T. Izsák [a,d], E. Ukraintsev [a,b], M. Varga [a,c,d], V. Jirásek [e], A. Kromka [a,c]

[a] Institute of Physics, Czech Academy of Sciences, Cukrovarnická 10, 162 00 Prague, Czech Republic
[b] Faculty of Electrical Engineering, Czech Technical University in Prague, Technická 2, 166 27 Prague, Czech Republic
[c] Institute of Electronics and Photonics, Faculty of Electrical Engineering and Information Technology, Slovak University of Technology, Ilkovičova 3, 812 19 Bratislava, Slovakia
[d] Institute of Electrical Engineering, Slovak Academy of Sciences, Dúbravská cesta 9, 841 04 Bratislava, Slovakia
[e] Institute of Plasma Physics, Czech Academy of Sciences, Za Slovankou 1782/3, 182 00 Prague, Czech Republic

ARTICLE INFO

Keywords:
NCD
Diamond
QCM
BSA
FN
Biosensors
Functionalization

ABSTRACT

This study presents a sensor based on quartz crystal microbalance (QCM) coated with nanocrystalline diamond (NCD) thin film, functionalization method and novel application of such sensor. Diamond-coated QCMs (DQCMs) were superficially terminated by hydrogen and oxygen (H-NCD and O-NCD) to control its surface dipole/potential. Two protein solutions were tested: bovine serum albumin (BSA) and fibronectin (FN). We performed reference measurements of serial resonant frequency (SRF) of clean QCMs loaded with protein and compared them with SRF shifts DQCMs loaded with proteins. In order to investigate the influence of the deposited NCD thin film on QCM measuring capabilities, additional FEM analysis was performed. The simulation results showed that QCM sensors maintain the sensing capabilities with a rigid thin film of NCD on its surface. The shift of SRF was demonstrably caused by the weight of protein adhered to the diamond film's surface. We compared masses estimated from the Sauerbrey equation to characterize the adhesive properties of the studied proteins. Comparing bare QCM and DQCM, we discovered diamonds enhance the sensing performance for proteins. At the same time, it saturates quickly with phosphate buffer saline used as a diluent solution for proteins. Results showed a significant increase in protein adhesion confirmed by the increase of the mass for both oxygen and hydrogen-terminated DQCMs. Moreover, a different time-dependent behaviour (i.e. different adsorption rate, degrees of physisorption and/or preference of the diamond surface functionalization) of the O-NCD and H-NCD QCMs was observed for BSA and FN proteins. In this meaning, we propose a schematic model which describes the detection principle of BSA and FN proteins on H- and O-terminated DQCM sensors. Finally, a simple proof of concept for using the functionalized diamond-coated sensors with current stimulation and EQCM (Electrochemical Quartz Crystal Microbalance) is also proposed.

1. Introduction

The quartz crystal microbalance (QCM) sensor is based on the piezoelectric effect. It is a high-resolution mass sensing technique with sensitivity at the picogram level and has been widely used in many fields such as surface chemistry, biochemistry and biomedical engineering [1]. Several works have shown that QCM is suitable for the detection of multiple types of substances, such as pollutant molecules in the air [2,3], antibodies, allergens [4,5], proteins [6], DNA sequence [7,8], bacteria [3,9,10] and cell culture layer [10]. Its certain advantages are low cost and relatively easy manipulation. However, bare QCMs (i.e. with Si0O2 or gold sensing surface) have low selectivity and are fragile in terms of mechanical properties. On the other hand, the sensitivity and selectivity can be improved by a wide range of surface modifications or functionalizations.

Generally, immunological detection methods are based on surface functionalization by specific antibodies which immobilize the detected substance to the surface of the sensor by direct binding via a functional group or Key-Lock system [11,12]. For example, for DNA detection, a complementary synthetic DNA sequence (oligonucleotide probe) is

* Corresponding author at: Institute of Physics, Czech Academy of Sciences, Cukrovarnická 10, 162 00 Prague, Czech Republic.
E-mail address: prochazkav@fzu.cz (V. Procházka).

https://doi.org/10.1016/j.apsusc.2022.153017
Received 14 April 2021; Received in revised form 2 March 2022; Accepted 3 March 2022
Available online 10 March 2022

usually used with a grafting point on the sensor surface. In the case of bacteria detection, common chemical compounds are applied, which are produced by the investigated organisms [13]. For example, the Escherichia coli detection was realized by using of O157:H7 sequence [14], and for the detection of Salmonella Enteritidis and Chlamydia trachomatis bacteria, thin layers of polyethyleneimine bound with glutaraldehyde and cystamine were applied, respectively [9].

Thus, it is evident that a proper and long-term stable surface functionalization of the QCM sensors is a vital issue for biosensor applications. As known, the basic configuration of the QCM device consists of circular-shaped quartz crystal, which is covered with a planar gold electrode on both sides. Thus, when the surface functionalization of the QCMs is mentioned, it primary means the surface functionalization of those gold electrodes. However, as it was already confirmed, the stability of (e.g.) gold–thiol functionalization strategies are questionable for long term monitoring of pathogens or other critical areas where a false negative signal could be a real risk in the evaluation of the measured data. In contrast to that, the stability of the diamond surface is unrivalled [15]. Diamond, due to its properties, provides the possibility to obtain stable surface termination using standard chemical-physical methods. Moreover, diamond exhibits low friction, high chemical stability, bio-inertness and tunable wettability to the nanoscale [16,17].

The idea of covering the QCM with a diamond film is not new, but unfortunately, the Curie point of quartz (573 °C) is lower than the deposition temperature of conventional diamond growth processes (600–1000 °C), and thus, the deposition of diamond on QCM was not widely utilized due to the loss of piezoelectric properties of the quartz. Nevertheless, some success has been already obtained by bonding a free-standing diamond to the QCM [18]; but these experiments resulted in a large reduction of quality factor Q, and this solution was not commercially viable due to the desired thickness of the free-standing diamond layer (>20 μm). One way how to overcome the problems with the low Curie point of quartz was the use of high melting point piezoelectric crystals such as langasite (no phase transition up to the melting point at 1500 °C) and gallium phosphate (950 °C) [19,20]. However, these materials are more expensive than quartz. In the last decade, there have been a lot of attempts to decrease the temperature of diamond film deposition [18]. This was successfully achieved by the development of surface wave plasma [21] or linear antenna microwave plasma deposition systems [22,23]. These methods allow the deposition of diamond films even at temperatures as low as 250 °C [24]. Linear antenna microwave plasma system was already successfully applied for deposition of a homogeneous diamond film on QCMs without loss of its piezoelectric properties [25]. These diamond-coated QCM sensors, developed by our group, were further successfully applied for a proof-of-concept study in gas sensor applications [25,26]. Here, in the present work, we further explore their applicability in the field of biosensors.

As known, QCM sensors have great applicability in biosensors. There are several studies on QCM sensors that dealt with the adhesion of living cells [27] or adhesion and metabolism of cancer cells [28]. However, in the detection of living cells, an important role plays the proteins, which mediate the living culture's adherence to the sensor surface and should strongly influence the sensor-cell interface. In addition, adsorption of the proteins onto various inorganic material surfaces is of significant importance also for medicine and pharmaceuticals, where a new generation of drugs might be designed to be transported on nanoparticles for specific drug delivery [29]. Therefore, our experiments related to the diamond-coated QCMs for biosensor applications were focused on protein adhesion studies. In the present study, two kinds of proteins were used: bovine serum albumin (BSA) and fibronectin (FN). These proteins were chosen because they are standard proteins serving in McCoy's medium for human cells cultivation. BSA is a flexible protein, and it is the most abundant plasma protein in the circulatory system with a negative surface charge at pH 7.0 [30]. FN is a ~450 kDa dimeric glycoprotein composed of two nearly identical polypeptide chains covalently linked by disulfide bridges near their carboxyl termini. FN is also the essential protein of the extracellular matrix, which indirectly mediate cell adhesion [31]. The adhesion of proteins was studied in terms of differently terminated diamond-coated QCMs (DQCM) surfaces, i.e. with hydrophilic (O-terminated) and/or hydrophobic (H-terminated) surface properties.

In general, highly hydrophilic surfaces prevent the adsorption of proteins, or these molecules are bound very weakly. However, on highly hydrophobic materials, proteins are adsorbed in rigid and denatured forms, hampering cell adhesion [32]. In the case of diamond films, it has been shown that FBS proteins assemble both on H-terminated (hydrophobic) and O-terminated (hydrophilic) surfaces in a 2–4 nm thin primary layer, although in different protein conformation [33]. Therefore, in this work, we demonstrate the successful fabrication of both hydrogen- and oxygen-terminated diamond-coated QCM devices, and we present the results of protein detection and adsorption studies of two standard proteins: bovine serum albumin (BSA) and fibronectin (FN).

2. Materials and methods

2.1. Fabrication and characterization of diamond-coated QCM sensors

We used AT-cut QCMs with 10 MHz serial resonance frequency (purchased from Krystaly, Hradec Králové, a.s., Czech Republic). The diameter of the circular-shaped piezoelectric QCM sensor was 14 mm with 6.5 mm circular gold electrodes (30 nm Cr, 100 nm of Au) at the centre sputtered on both sides of the sensor element (Fig. 1a). First, QCMs were seeded by applying ultrasonic agitation in a deionized water-based diamond powder suspension [34]. Samples were placed vertically into the chamber to ensure the diamond deposition on both sides of the QCM within one run (Fig. 1b). Nanocrystalline diamond (NCD) films were grown by pulsed linear antenna microwave plasma chemical vapour deposition system in $H_2/CH_4/CO_2$ gas mixture [22,23]. The parameters during the deposition process were as follows: 5% of CH_4 and 20% of CO_2 in a hydrogen atmosphere; a total gas pressure of 10 Pa; pulsed microwave power of 2 × 1.7 kW; and a substrate temperature was kept between 350 °C and 400 °C. After 34 h long deposition, a diamond film with a thickness of approx. 250 nm was achieved. The low growth rate (<10 nm × h^{-1}) is attributed to the low deposition temperature and low working pressure and/or low plasma density process conditions [35]. The Au contact pads were not covered by diamond (Fig. 1a). The diamond character of the deposited film was confirmed by Raman spectroscopy with an excitation wavelength of 442 nm (InVia Renishaw Raman spectrometer), and its morphology was evaluated with scanning electron microscopy (SEM, Maia3, Tescan).

After the diamond deposition, the surface of the diamond-coated QCMs was treated in hydrogen and oxygen plasma to obtain hydrophobic and hydrophilic properties, respectively. The functionalization by hydrogen was performed in a focused MW plasma CVD chamber (Aixtron P6 system, 1500 W, 30 mbar, 300 sccm of H_2, 10 min, 400 °C). These samples are further labelled as hydrogen-terminated diamond-coated quartz crystal microbalance (H-DQCM) sensors. The oxygen termination was achieved by exposure to capacitive radiofrequency plasma (FEMTO, Diener electronic GmbH, Germany, frequency 13.56 MHz, r.f. power 45 W, process pressure 50 Pa, time 1 min), and these samples are labelled as the oxygen-terminated diamond-coated quartz crystal microbalance (O-DQCM) sensors. These procedures were done in dedicated systems for such treatments to minimize unwanted memory effects in the deposition systems (i.e. chamber walls contamination with dopants, etc.). Chemical compositions of the differently terminated diamond surface have been evaluated by X-Ray photoelectron spectroscopy and published in our previous work [36].

Finally, the gold electrodes of the QCMs were connected to a socket using a silver nanoparticle conductive epoxy paste (Fig. 1c). The epoxy was cured for 5 h at 70 °C in the evacuated oven.

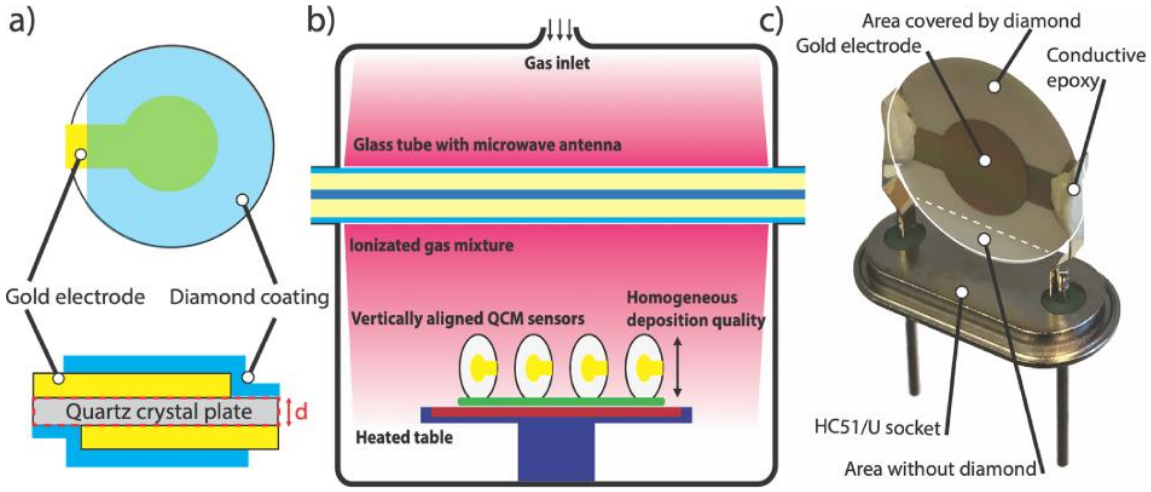

Fig. 1. (a) Schematic top and the cross-sectional view of the diamond-coated QCM. (b) Schematic drawing of the pulsed microwave plasma system with linear antenna arrangement with vertically positioned QCM sensors in the chamber. (c) Photo of the diamond-coated QCM sensor in the HC51/U socket. Note: one circular-shaped gold electrode is sputtered on the front side, and the second electrode is sputtered on the backside.

2.2. FEM simulation

In order to prove the function of the diamond-coated QCM sensor, FEM simulation was performed using COMSOL® environment to calculate the frequency spectrum of the loaded and unloaded sensor. The modelled element consisted of the 164.5 m thick and 13.9 mm in diameter quartz cylinder with the 100 nm thick and 6.5 mm in diameter cylindrical Au electrode fully covered (i.e. including the whole area of QCM) or uncovered with the diamond film of thickness approx. 250 nm. The diamond layer was considered homogenous, continuous (i.e. pinhole-free) and rigidly connected to the Au layer. The electrostatic equations were coupled with the elasticity equations via the coupling matrix related permittivity to the stress tensor. The diamond film was considered as a non-piezoelectric and elastic layer with a density of 3150 kg $\times$ m^{-3}, Young modulus 1140 GPa and Poisson ratio 0.069. These values were taken from the COMSOL® Multiphysics ver. 5.0 materials database, as well as all the properties of the AT-cut quartz and Au electrode. The added mass on the top of the diamond film was simulated as increased diamond thickness by a step 1 nm.

2.3. Protein adsorption measurements

The impedance spectroscopy was applied for the protein adsorption analysis on the diamond-coated QCMs. Impedance measurements were performed using an Omicron Bode 100 Vector Network and Impedance Analyzer system with a test fixture for connection of QCM sensors in HC51/U socket commonly used for oscillator packaging (Fig. 1c). To measure the serial (SRF) resonance frequency, multiple frequency sweep measurements with 2.4 Hz resolution (with a center frequency set to 10 MHz at first natural mode and frequency window of 40 kHz, measured at 16 501 points) were performed to ensure there is no temperature shift in SRF.

Bovine serum albumin (BSA) and fibronectin (FN) were used as representative examples of both globular and fibrillar proteins. Both compounds were dissolved in phosphate buffer saline (PBS; pH = 7) used as a transfer medium with a concentration of 1 wt%. Solutions in the volume of 150 µl were applied to the QCM (i.e. bare Au-QCM or DQCM) sensor active area by a drop-casting technique. First, the applied drop was kept on the QCM for 10 min, and then the QCM was rinsed with deionized water and dried by a nitrogen gas flow (step 1). After impedance measurement of the SRF shift, the second drop was applied to the same side of the sensor for an additional 10 min, and the whole procedure was repeated (step 2). This resulted in the deposition time of 20 min total (i.e. 10 + 10 min). These experiments were performed to study the influence of an additional protein layer on the SRF shift of the DQCM. As a reference, the clean diamond-coated QCM sensor (without applying any solutions) was used (step 0, see Tab. S1 in supplementary).

In summary, for impedance measurements of three applied solutions (PBS, BSA, FN), we used 36 QCM sensors, ie. three sets each of 12 sensors. One set consisted of following - the first half of the sensors was bare Au/QCM without diamond, where three of them were hydrogen-terminated (H-QCM), and three were oxygen-terminated (O-QCM). The second half of the sensors were diamond-coated QCM, and again, three were hydrogen-terminated (H-DQCM), and three were oxygen-terminated (O-DQCM) (see Tab. S2 in supplementary).

The shifts in SRF were measured (impedance characteristic shown in Supplementary material section in Fig. S1.) and converted to mass using the Sauerbrey equation (1):

$$\Delta f = -\frac{2f_0^2}{A\sqrt{\rho_q \mu_q}}\Delta m \tag{1}$$

where f_0 is the resonant frequency in *Hz*, Δm is the change of the mass in kg, Δf is the change of frequency with respect to the resonant frequency in *Hz*, A is the area of the electrode in m^2, ρ_q is the density of quartz (2684 kg $\times$ m^{-3}), μ_q is the shear modulus of AT-quartz in Pa (29.5 GPa). Because the SRF shift did not exceed 2%, the use of the Z-match method was not applied [37].

3. Results and discussion

3.1. Characterization of the diamond-coated QCM sensors

First, the diamond films were analysed by Raman spectroscopy on both sides of the DQCM sample, where the same diamond film quality was confirmed. The Raman spectrum reveals the typical character of the nanocrystalline diamond film: a sharp diamond-peak at ~1326 cm^{-1} attributed to sp^3 carbon bonds overlaying the broad D-band (~1350 cm^{-1}) observed in the presence of small crystallites, and a broad G-band at ~1580 cm^{-1} corresponding to sp^2 carbon bonds (Fig. 2) [38]. The redshift of the diamond peak (1332 cm^{-1}) is typically observed for ultrananocrystalline (UNCD) or nanocrystalline diamond (NCD) films with a small size of grains. The difference (approx. 3 cm^{-1}) in the diamond peak position for the diamond films grown on and outside the Au

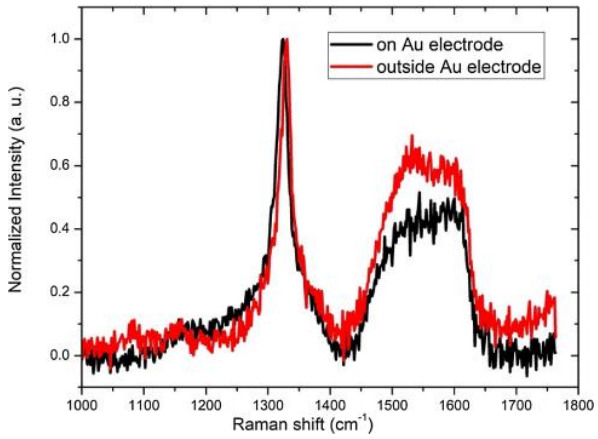

Fig. 2. Normalized Raman spectra of the diamond film grown on the QCM sensor measured on the gold electrode area and out of electrode area using laser with 442 nm excitation wavelength.

electrode area is caused by different morphology and induced stress at the substrate/diamond interface, and its value was evaluated to Δ 3 GPa [39].

Fig. 3a shows top and cross-sectional SEM images of the QCM sensors before (bare QCM) and after the diamond growth (DQCM). The SEM images were acquired in the centre of the QCM sensor, i.e. from the Au electrode area. It is clearly visible that the surface morphology of the bare QCM is characterized by deep scratches and significant roughness (approx. 250–500 nm). The diamond-coated QCM features a similar surface morphology because the deposited nanocrystalline diamond thin film well copies the initial morphology of the QCM. This means that bare and the diamond-coated QCMs can be well compared just in terms of their sensory behaviour, i.e. without any significant morphological impacts on the adhesiveness of protein solutions. On the other hand, the surface properties (hydrophilic vs hydrophobic) can be easily tailored by termination only in the case of the DQCM sensors, as shown in Fig. 3b. The surface termination by O- and H-atoms has no effect on bare QCM, i.e. its surface remains still hydrophilic.

3.2. FEM simulation

The FEM analysis was performed to evaluate the influence of the diamond film on the function of the QCM sensor. Fig. 4a shows the simulated serial resonant frequency (SRF) shifts compared to the calculated SRF values from the Sauerbrey equation as a function of added mass on the QCM surface. Here, the added mass represents the deposited diamond film (80–150 nm). As observed, there is an excellent agreement between the simulated and measured data, which proved that stiffness of the diamond did not alter the piezoelectric properties of the QCMs, and hence, the Sauerbrey equation for the diamond-coated QCMs remained valid. Therefore, the Sauerbrey equation can be used reliably to direct the conversion of the measured SRF data of the protein-coated DQCMs sensors to the adhered mass of proteins.

Fig. 4b shows the simulated displacement altitude of the loaded, bare quartz crystal (with thickness $d = 164.5$ μm) between two gold electrodes (see schematic drawing in Fig. 1a). It is apparent that the longitudinal wave has its maximum in the middle of the circular electrode (i.e. shear mode resonantor). The amplitude of the displacement decreases from the middle to the edge of the circular electrode and does not exceed 2 μm. In Fig. 4c, there is a comparison of the displacement for bare (i.e. uncoated) and diamond-coated QCM. It was observed that the difference in the displacement altitude is the largest at the surface of the QCM (see inset in Fig. 4c), but only approx. 2% lower for the diamond-coated QCM than in the case of the bare quartz resonator. Based on this simulation, we propose that the diamond film causes the same effect as a mass on the QCM surface, and thus, it does not disturb the sensor function in a non-linear way. According to our simulations, we confirm that the Sauerbrey

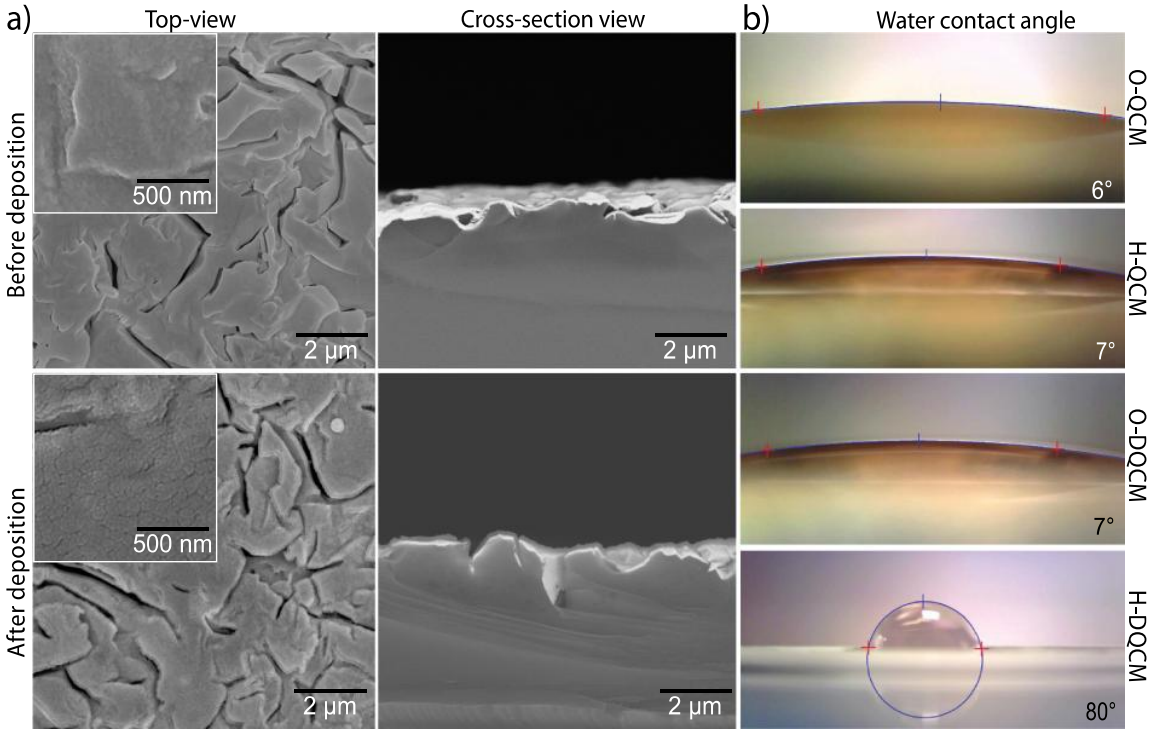

Fig. 3. (a) Top view (left column) and cross-section view in BSE mode (middle column) SEM images of the bare and diamond-coated QCM sensors. (b) Contact angle measurements on the bare and diamond-coated QCM sensors surface terminated by oxygen (O-QCM and O-DQCM) and hydrogen (H-QCM and H-DQCM) atoms.

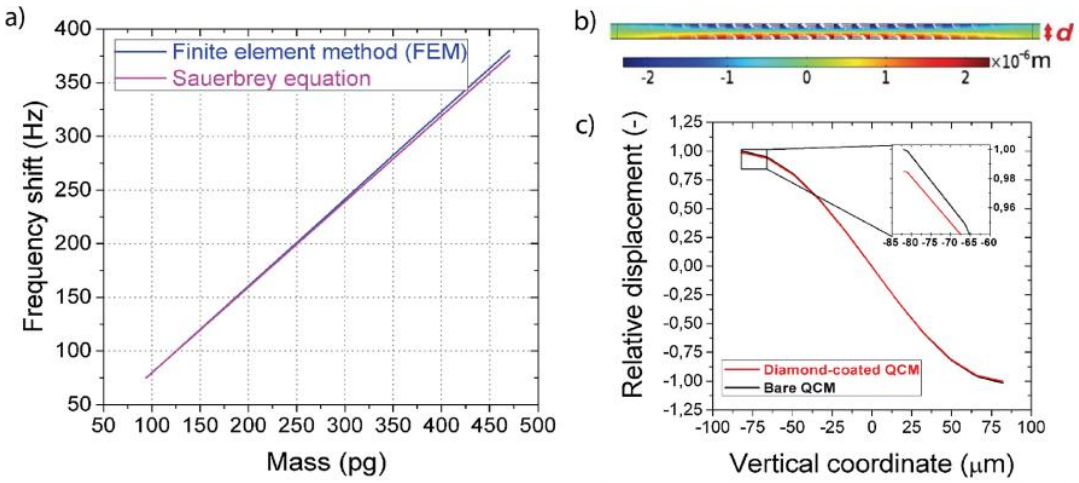

Fig. 4. (a) Serial resonant frequency (SRF) shift as a function of the added mass of the diamond-coated QCM sensor. The SRFs were calculated both from the Sauerbrey equation and evaluated from FEM simulations. The frequency of unloaded crystal was 9.975728 MHz. (b) The displacement amplitude of the loaded quartz crystal with thickness d = 164.5 μm (see schematic drawing in Fig. 1b) evaluated from FEM simulation at f = 9.975348 MHz frequency. (c) Comparison of the relative displacements of the diamond-coated and uncoated (i.e. bare) QCMs.

equation is valid also for DQCM sensors. Of course, compared with the bare QCM, there is an additional shift in SRF due to the deposited diamond film, but this shift is involved in the initial stage (i.e. reference background) of the diamond-coated QCMs prepared for the protein adsorption studies.

3.3. Protein adsorption on diamond-coated QCM sensors

AFM analysis of QCM samples after the BSA protein adhesion did not recognize any visible clusters of the proteins on the surface (see Fig. 5). The same result was also observed for the applied FN protein (not shown here). Although observation of protein is technologically challenging on a rough surface such as QCM, it is essential to confute the possibility of clusters, which can develop on the surface of the DQCM sensor. At the same time, from SRF shifts evaluated from impedance measurements, it is apparent that there is a mass of protein adhered on the surface. Based on our previous work [40], we supposed that one protein layer could have a thickness in the range of 2–4 nm. The surface roughness evaluated from AFM images is independent of the protein adhesion and is predominantly given by the macroscopic surface of the quartz crystal itself and slightly modulated by the diamond film nano-roughness.

On the other hand, impedance measurements revealed changes in SRF of the QCMs, indicating/confirming the protein adsorption. In our study, we focused on the analysis of the shift of the SRF, and because the SRF shift can be directly converted to the mass (see previous section 3.2.), in the further analysis, we use mass data calculated using the Sauerbrey equation.

Fig. 6 compares the adhered mass of two phosphate buffer based protein solutions and the clean reference PBS with pH = 7 (i.e. FN + PBS, BSA + PBS, PBS) on H- and O-terminated QCM and DQCM sensors for each step of the experiment. The measured data were analyzed regarding: i) protein adsorption on the QCMs, ii) effect of first (10 min) and additional-time (+10 min) protein adsorption and generally on iii) effect of protein type and surface termination. The experiment was conducted in three sets to ensure the repeatability of the sensor. Figs. 6 and 7 shows averaged mass adhered in three measurements and standard deviation for each measurement.

From Fig. 6a is apparent that more adsorbed proteins were observed on diamond-coated QCM than on the bare QCM for all the used solutions. The clearly highest mass value (BSA protein) was adsorbed on the hydrogen-terminated NCD surface, which is in accordance with the results obtained by Aramesh et al. [6], where the affinity of BSA was recorded as slightly higher to hydrogen-terminated nanodiamond (H-ND) particles. In spite of differences in the methodology of the measurement (meaning that in our study, we measured the mass of molecules directly bonded to the surface, oppositely of measuring the mass of superficially modified diamond nanoparticles with BSA adhered on them [6]), both studies revealed similar results.

Although the H-terminated diamond is hydrophobic, a significantly higher mass adsorption was observed than on hydrophilic oxygen-terminated diamond. This could be explained with the consideration of surface charge properties. In contrast to the O-terminated diamond surface, the H-terminated diamond surface is featured by C-H dipoles, which due to the transfer doping mechanism, makes the surface

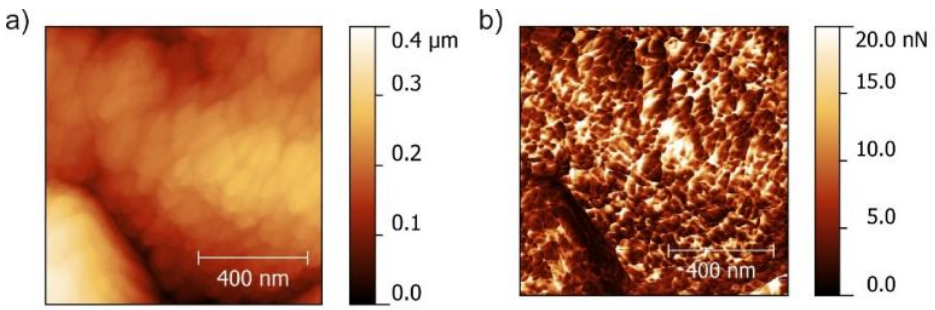

Fig. 5. (a) Representative AFM image of the diamond-coated QCM surface with applied BSA and (b) corresponding map of adhesion forces.

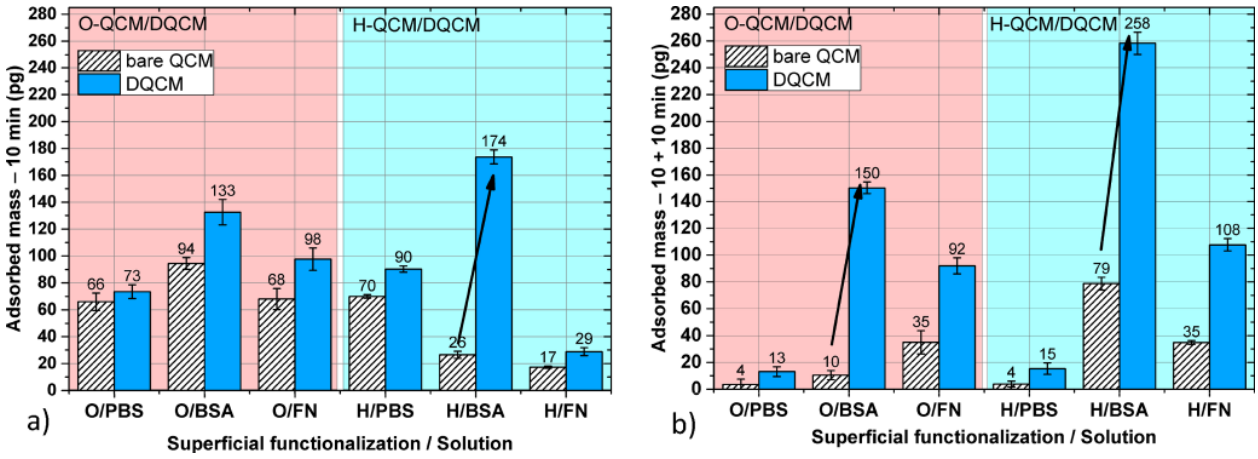

Fig. 6. Comparison of adsorbed mass on bare (white striped bars) and diamond-coated (blue bars) QCMs as a function of hydrogen and oxygen termination after (a) first (10 min) and (b) second exposure period (i.e. additional 10 min) for three different solutions (PBS, BSA and FN).

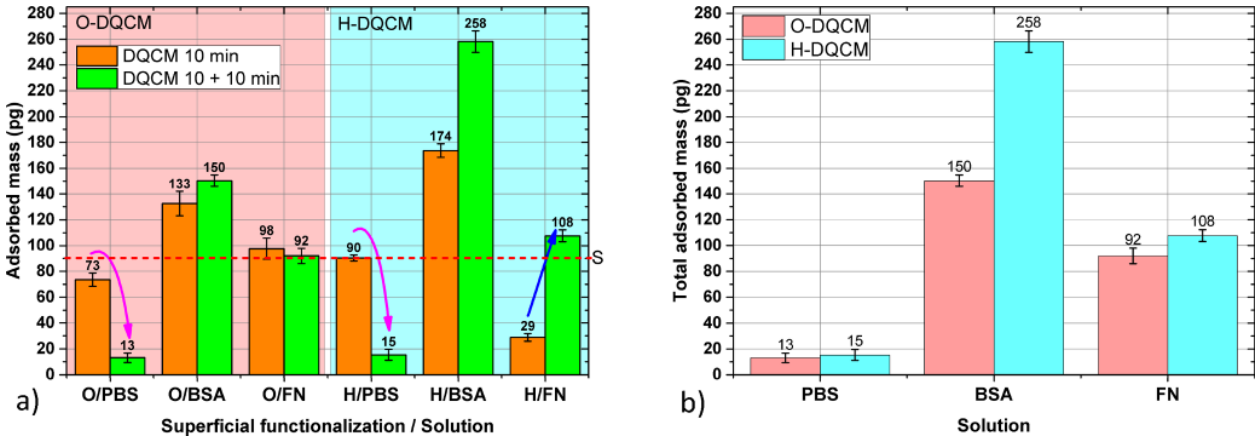

Fig. 7. (a) A comparison of adsorbed mass on DQCM during the additional time of deposition (orange bars) and adsorbed mass during the first 10 min long deposition (green bars). (b) Total adsorbed mass (after 20 min long exposure) with the use of oxygen (pink) and hydrogen (cyan) terminated diamond coating on QCM (to note, H-termination generally immobilized more matter on surfaced).

positively charged and leads to p-type surface conductivity [41,42]. It was shown that in electrolytes, this surface charge is mainly induced by the unsymmetrical adsorption of OH^- and H_3O^+ ions from the aqueous solution, resulting in a large interfacial charge [43,44]. This surface charge can have an important role in processes governed by the diamond/solution interface, such as electron transfer to charged redox molecules, ion sensitivity, or as in our case, in the adsorption of charged molecules and proteins. It is supposed that because the H-terminated surface is hydrophobic, the adsorbed proteins become denatured with their hydrophobic core sticking to the diamond surface and hydrophilic parts being solvated into the medium, such as in the case of FBS proteins [45]. Thus, different surface termination results in a changed conformation of proteins and leads to preferred adsorption on H-terminated diamond surfaces. In addition, NCD wettability can also be tailored by grafting other specific atoms and functional chemical groups (e.g. fluorine or amine groups) that influence the wettability and surface energy of NCD films in another way. To conclude, the diamond surface wettability, as well as its surface energy, can be widely modulated, thus can be made selective for specific compounds. Moreover, this property can be further utilized for specific use in immunoassays, where diamond could enable much better sensitivity and density of termination, than currently used solutions, without the need of changing the piezoelectric material because of its phase transition temperature [19].

Another benefit of DQCM is the fact that the presence of NCD enables much higher sensitivity of the sensor for macromolecular compounds in the additional re-deposited protein layer compared to bare QCMs, compare Fig. 6a and 6b. The adhered mass during re-deposition showed several times higher values for DQCMs (Fig. 6b, blue bars) in contrast to bare QCM (Fig. 6b, *white striped* bars).

We found out that not only FN (Fig. 7a, blue arrow) and BSA had shown higher adsorption to DQCM, with respect to bare QCM, it also preserved relatively low saturation level for PBS (Fig. 7a, magenta arrow) as did bare QCM without diamond. This convenient behaviour enables us to further distinguish between solvent and analyzed biomolecules, which significantly enhances the sensor's specificity. Investigation of superficial termination and preferential adsorption of macromolecules shown that for all three solutions, H-termination attracted a higher amount of molecules to the surface of DQCM than O-termination (see Fig. 7b). To note, in the case of FN on H-DQCM, there is a significant increase during second exposure to the solution. That can be caused by the prolonged conformation of FN on hydrophobic surfaces [46]. The abovementioned findings are schematically presented in Fig. 8.

The diamond film seems beneficial for multiple reasons; the first reason seems to be the generally higher sensitivity of the QCM sensor. It is attributed to a higher attraction of DQCM sensor, which enables

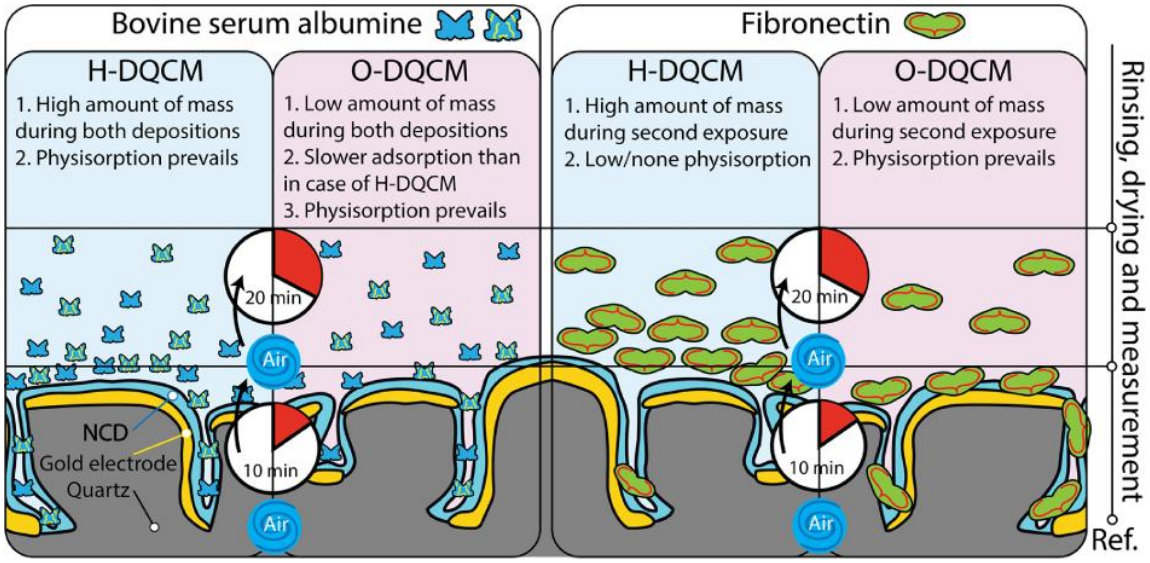

Fig. 8. A schematic diagram describing the detection/adsorption principle of BSA and FN proteins using H- and O-terminated diamond-coated QCM sensors.

physisorption much easier than bare Au/quartz surface. The second is the variability of sensor surface properties, and the third reason is the possibility of a simple modification of the morphology of the diamond (etching, growth parameters)

As the last trial, we performed measured conductivity (pico-amperemeter Keithley 6487) of Ag/AgCl → solution->NCD/Au channel to investigate the possibility of real-time electrical mobilization of the molecules/cells on the surface. We found out that there was slightly higher conductivity for H-DQCM than O-DQCM, i.e. 29 mS and 25 mS, respectively. Both measurements were performed on the samples with the same diamond deposition conditions. Thus, the modification of diamond thin film conductivity is possible next to changing the thin film morphology also by superficial treatment.

4. Conclusions

We have shown that surface wettability and functionality of nano-crystalline diamond-coated QCM can be simply controlled by hydrogen or oxygen termination. Both terminations were successfully tested for detection of phosphate buffer saline soluble proteins Bovine serum albumin and fibronectin and compared with clean phosphate saline buffer.

Both proteins exhibited enhanced adhesion on functionalized nano-crystalline diamond-coated QCM compared to bare gold QCM, resulting in higher serial resonance frequency shifts. We analyzed results regarding different adsorption rate, degrees of physisorption and/or preference of the diamond surface functionalization.

FN (single component) protein assay revealed a smaller amount of adhered mass than BSA, and the results implicate that the exposure time plays an essential role in its further adhesion. Variable interactions of FN with hydrophobic (H-NCD) and hydrophilic (O-NCD) diamond surfaces were attributed to a change in protein conformation. Furthermore, FN showed also additional adsorption during the second exposure only on the hydrophobic diamond surface. In contrast, BSA solution exhibited most of the adhered molecules during the first 10 min of exposure, unlike FN, which adhered most in the prolonged exposure period (20 min in total). Bovine serum albumin assay confirmed that BSA prefers H-NCD surface.

Overall, this study confirmed that D-QCM sensors are exceptionally promising due to the possibility of superficial and stable grafting of the carbon surface by many types of atomic groups and organic molecules. Combining such a sensor with chemical moieties offers a simple fabrication and enhanced sensitivity/selectivity, which has been proven by adjusting the wettability of the surface. Such a sensor will repeatably distinguish the adsorption of lighter molecules of solvent and heavier/bigger molecules in solution. Another potential lies in the detection of bacterial cultures, virulent particles and specific pathogens at very low concentrations.

Building on current research, we propose to combine QCM measurements with hydrogen-induced two-dimensional conductive diamond used to stimulate molecules/living cultures enabling simultaneous label-free monitoring and stimulation.

CRediT authorship contribution statement

V. Procházka: Investigation, Conceptualization, Visualization, Writing – original draft. **P. Kulha:** Conceptualization, Methodology. **T. Izsák:** Investigation, Writing – review & editing. **E. Ukraintsev:** Resources, Investigation. **M. Varga:** Methodology, Writing – review & editing. **V. Jirásek:** Formal analysis, Writing – review & editing. **A. Kromka:** Methodology, Funding acquisition, Supervision.

Declaration of Competing Interest

The authors declare that they have no known competing financial interests or personal relationships that could have appeared to influence the work reported in this paper.

Acknowledgements

The work has been supported by the Operational Programme Research, Development and Education financed by European Structural and Investment Funds and the Czech Ministry of Education, Youth and Sports (project no. SOLID21 - CZ.02.1.01/0.0/0.0/16_019/0000760) and by the CzechNanoLab Research Infrastructure (MEYS CR, project no. LM2018110). V. Procházka acknowledges the CTU grant no. SGS19/112/OHK4/2T/13. M. Varga and A. Kromka acknowledge project no.313011ASS8 supported under the Operational Program Integrated Infrastructure for the project: “Strategic research in the field of SMART monitoring, treatment and preventive protection against coronavirus (SARS-CoV-2)” co-financed by the European Regional Development Fund.

Appendix A. Supplementary data

Supplementary data to this article can be found online at https://doi.org/10.1016/j.apsusc.2022.153017.

References

[1] D. Johannsmann, The Quartz Crystal Microbalance in Soft Matter Research, Springer International Publishing, Cham, 2015. doi:10.1007/978-3-319-07836-6.
[2] R.D. Vaughan, C.K. O'Sullivan, G.G. Guilbault, Development of a quartz crystal microbalance (QCM) immunosensor for the detection of Listeria monocytogenes, Enzyme Microb. Technol. 29 (2001) 635–638, https://doi.org/10.1016/S0141-0229(01)00449-5.
[3] Y. Zhihua, Z. Liang, S. Kaixin, H. Weiwei, Characterization of quartz crystal microbalance sensors coated with graphene films, Procedia Eng. 29 (2012) 2448–2452, https://doi.org/10.1016/j.proeng.2012.01.330.
[4] M.Z. Atashbar, B. Bejcek, A. Vijh, S. Singamaneni, QCM biosensor with ultra thin polymer film, Sensors Actuators, B Chem. 107 (2005) 945–951, https://doi.org/10.1016/j.snb.2004.12.047.
[5] U. Latif, S. Can, O. Hayden, P. Grillberger, F.L. Dickert, Sauerbrey and anti-Sauerbrey behavioral studies in QCM sensors-Detection of bioanalytes, Sensors Actuators, B Chem. 176 (2013) 825–830, https://doi.org/10.1016/j.snb.2012.09.064.
[6] M. Aramesh, O. Shimoni, K. Ostrikov, S. Prawer, J. Cervenka, Surface charge effects in protein adsorption on nanodiamonds, Nanoscale 7 (2015) 5726–5736, https://doi.org/10.1039/C5NR00250H.
[7] L. Tedeschi, L. Citti, C. Domenici, An integrated approach for the design and synthesis of oligonucleotide probes and their interfacing to a QCM-based RNA biosensor, Biosens. Bioelectron. 20 (2005) 2376–2385, https://doi.org/10.1016/j.bios.2004.12.013.
[8] N. Lassalle, P. Mailley, E. Vieil, T. Livache, A. Roget, J.P. Correia, L.M. Abrantes, Electronically conductive polymer grafted with oligonucleotides as electrosensors of DNA: Preliminary study of real time monitoring by in situ techniques, J. Electroanal. Chem. 509 (2001) 48–57, https://doi.org/10.1016/S0022-0728(01)00537-X.
[9] I. Ben-Dov, I. Willner, E. Zisman, Piezoelectric Immunosensors for Urine Specimens of *Chlamydia trachomatis* Employing Quartz Crystal Microbalance Microgravimetric Analyses, Anal. Chem. 69 (1997) 3506–3512, https://doi.org/10.1021/ac970216s.
[10] X. Mao, L. Yang, X.-L. Su, Y. Li, A nanoparticle amplification based quartz crystal microbalance DNA sensor for detection of Escherichia coli O157:H7, Biosens. Bioelectron. 21 (2006) 1178–1185, https://doi.org/10.1016/j.bios.2005.04.021.
[11] J. Rickert, T. Weiss, W. Kraas, G. Jung, W. Göpel, A new affinity biosensor: Self-assembled thiols as selective monolayer coatings of quartz crystal microbalances, Biosens. Bioelectron. 11 (1996) 591–598, https://doi.org/10.1016/0956-5663(96)83294-5.
[12] M. Kaspar, H. Stadler, T. Weiß, C.h. Ziegler, Thickness shear mode resonators ('mass-sensitive devices') in bioanalysis, Fresenius, J. Anal. Chem. 366 (2000) 602–610, https://doi.org/10.1007/s002160051555.
[13] J. Strauss, Y. Liu, T.A. Camesano, Bacterial adhesion to protein-coated surfaces: An AFM and QCM-D study, Jom. 61 (2009) 71–74, https://doi.org/10.1007/s11837-009-0138-z.
[14] V.C.H. Wu, S.-H. Chen, C.-S. Lin, Real-time detection of Escherichia coli O157:H7 sequences using a circulating-flow system of quartz crystal microbalance, Biosens. Bioelectron. 22 (2007) 2967–2975, https://doi.org/10.1016/j.bios.2006.12.016.
[15] A. Rahim Ruslinda, K. Tanabe, S. Ibori, X. Wang, H. Kawarada, Effects of diamond-FET-based RNA aptamer sensing for detection of real sample of HIV-1 Tat protein, Biosens. Bioelectron. 40 (2013) 277–282, https://doi.org/10.1016/j.bios.2012.07.048.
[16] J. Liskova, O. Babchenko, M. Varga, A. Kromka, D. Hadraba, Z. Svindrych, et al., Osteogenic cell differentiation on H-terminated and O-terminated nanocrystalline diamond films, Int. J. Nanomedicine. 10 (2015) 869–884, https://doi.org/10.2147/IJN.S73628.
[17] S. Koizumi, C. Nebel, M. Nesladek, Physics and Applications of CVD Diamond, Wiley, 2008. doi:10.1002/9783527623174.
[18] Y. Zhang, S. Asahina, S. Yoshihara, T. Shirakashi, Fabrication and characterization of diamond quartz crystal microbalance electrode, J. Electrochem. Soc. 149 (2002), https://doi.org/10.1149/1.1514649.
[19] O.A. Williams, V. Mortet, M. Daenen, K. Haenen, Nanocrystalline diamond enhanced thickness shear mode resonator, Appl. Phys. Lett. 90 (2007) 1–4, https://doi.org/10.1063/1.2471649.
[20] P. Krempl, G. Schleinzer, W. Wallnöfer, Gallium phosphate, gapo4: A new piezoelectric crystal material for high-temperature sensorics, Sensors Actuators, A Phys. 61 (1997) 361–363, https://doi.org/10.1016/S0924-4247(97)80289-0.
[21] K. Tsugawa, M. Ishihara, J. Kim, M. Hasegawa, Y. Koga, Large-area and low-temperature nanodiamond coating by microwave plasma chemical vapor deposition, 2006. https://www.researchgate.net/publication/236737100 (accessed 23 January 2020).
[22] Š. Potocký, O. Babchenko, K. Hruška, A. Kromka, Linear antenna microwave plasma CVD diamond deposition at the edge of no-growth region of C-H-O ternary diagram, Phys. Status Solidi Basic Res. 249 (2012) 2612–2615, https://doi.org/10.1002/pssb.201200124.
[23] A. Kromka, O. Babchenko, T. Izak, K. Hruska, B. Rezek, Linear antenna microwave plasma CVD deposition of diamond films over large areas, Vacuum 86 (2012) 776–779, https://doi.org/10.1016/j.vacuum.2011.07.008.
[24] T. Izak, O. Babchenko, M. Varga, S. Potocky, A. Kromka, Low temperature diamond growth by linear antenna plasma CVD over large area, Phys. Status Solidi Basic Res. 249 (2012) 2600–2603, https://doi.org/10.1002/pssb.201200103.
[25] M. Varga, A. Laposa, P. Kulha, J. Kroutil, M. Husak, A. Kromka, Quartz crystal microbalance gas sensor with nanocrystalline diamond sensitive layer, Phys. Status Solidi Basic Res. 252 (2015) 2591–2597, https://doi.org/10.1002/pssb.201552229.
[26] P. Kulha, J. Kroutil, A. Laposa, V. Procházka, M. Husák, Quartz Crystal Micro-Balance Gas Sensor with Ink-Jet Printed Nano-Diamond Sensitive Layer, J. Electr. Eng. 67 (2016) 61–64, https://doi.org/10.1515/jee-2016-0009.
[27] T. Zhou, K.A. Marx, M. Warren, H. Schulze, S.J. Braunhut, The quartz crystal microbalance as a continuous monitoring tool for the study of endothelial cell surface attachment and growth, Biotechnol. Prog. 16 (2000) 268–277, https://doi.org/10.1021/bp000003f.
[28] L. Nowacki, J. Follet, M. Vayssade, P. Vigneron, L. Rotellini, F. Cambay, C. Egles, C. Rossi, Real-time QCM-D monitoring of cancer cell death early events in a dynamic context, Biosens. Bioelectron. 64 (2015) 469–476, https://doi.org/10.1016/j.bios.2014.09.065.
[29] K. Kubiak-Ossowska, B. Jachimska, M. Al Qaraghuli, P.A. Mulheran, Protein interactions with negatively charged inorganic surfaces: simulation and experiment, Curr. Opin. Colloid Interface Sci. (2019), https://doi.org/10.1016/j.cocis.2019.02.001.
[30] B.K. Sah, S. Kundu, Modification of hysteresis behaviors of protein monolayer and the corresponding structures with the variation of protein surface charges, Colloids Surf. B Biointerf. 159 (2017) 696–704, https://doi.org/10.1016/j.colsurfb.2017.08.032.
[31] P. Elter, R. Lange, U. Beck, Atomic force microscopy studies of the influence of convex and concave nanostructures on the adsorption of fibronectin, Colloids Surf. B Biointerf. 89 (2012) 139–146, https://doi.org/10.1016/j.colsurfb.2011.09.021.
[32] I. Kopova, B. Rezek, S. Stehlik, E. Ukraintsev, N. Slepickova Kasalkova, P. Slepicka, S. Potocky, L. Bacakova, Growth of Primary Human Osteoblasts on Plasma-Treated and Nanodiamond-Coated PTFE Polymer Foils, Phys. Status Solidi Basic Res. 255 (2018) 1700595, https://doi.org/10.1002/pssb:201700595.
[33] B. Rezek, E. Ukraintsev, L. Michalíková, A. Kromka, J. Zemek, M. Kalbacova, Adsorption of fetal bovine serum on H/O-terminated diamond studied by atomic force microscopy, Diam. Relat. Mater. 18 (2009) 918–922, https://doi.org/10.1016/j.diamond.2009.02.009.
[34] M. Varga, T. Izák, A. Kromka, M. Veselý, K. Hruška, M. Michalka, Study of diamond film nucleation by ultrasonic seeding in different solutions, Open Phys. 10 (2012) 218–224, https://doi.org/10.2478/s11534-011-0078-4.
[35] D. Das, R.N. Singh, A review of nucleation, growth and low temperature synthesis of diamond thin films, Int. Mater. Rev. 52 (2007) 29–64, https://doi.org/10.1179/174328007X160245.
[36] A. Artemenko, T. Ižák, M. Marton, E. Ukraintsev, J. Stuchlík, K. Hruška, M. Vojs, A. Kromka, stability of the surface termination of nanocrystalline diamond and diamond-like carbon films exposed to open air conditions, Diam. Relat. Mater. 100 (2019) 107562, https://doi.org/10.1016/j.diamond.2019.107562.
[37] Q. Liu, P. Wang, Cell-based Biosensors: Principles and Applications, Artech House, 2009. https://books.google.it/books?id=nM79I9u6Zv8C (accessed 23 September 2018).
[38] S. Prawer, R.J. Nemanich, Raman spectroscopy of diamond and doped diamond, Philos. Trans. R. Soc. London, Ser. A 362 (2004) 2537–2565, https://doi.org/10.1098/rsta.2004.1451.
[39] T. Izák, V. Jirásek, G. Vanko, J. Dzuba, A. Kromka, Temperature-dependent stress in diamond-coated AlGaN/GaN heterostructures, Mater. Des. 106 (2016) 305–312, https://doi.org/10.1016/j.matdes.2016.06.006.
[40] L. Michalikova, B. Rezek, A. Kromka, M. Kalbacova, CVD diamond films with hydrophilic micro-patterns for self-organisation of human osteoblasts, Vacuum 84 (2009) 61–64, https://doi.org/10.1016/j.vacuum.2009.04.016.
[41] A.P. Sommer, D. Zhu, K. Brühne, Surface Conductivity on Hydrogen-Terminated Nanocrystalline Diamond: Implication of Ordered Water Layers, Cryst. Growth Des. 7 (2007) 2298–2301, https://doi.org/10.1021/cg070610b.
[42] M.T. Edmonds, L.H. Willems van Beveren, O. Klochan, J. Cervenka, K. Ganesan, S. Prawer, L. Ley, A.R. Hamilton, C.I. Pakes, Spin-Orbit Interaction in a Two-Dimensional Hole Gas at the Surface of Hydrogenated Diamond, Nano Lett. 15 (2015) 16–20, https://doi.org/10.1021/nl502081y.
[43] A. Härtl, J.A. Garrido, S. Nowy, R. Zimmermann, C. Werner, D. Horinek, R. Netz, M. Stutzmann, The ion sensitivity of surface conductive single crystalline diamond, J. Am. Chem. Soc. 129 (2007) 1287–1292, https://doi.org/10.1021/ja066543b10.1021/ja066543b.s001.
[44] C.E. Nebel, B. Rezek, D. Shin, H. Watanabe, Surface electronic properties of H-terminated diamond in contact with adsorbates and electrolytes, Phys. Status Solidi Appl. Mater. Sci. 203 (2006) 3273–3298, https://doi.org/10.1002/pssa.200671401.
[45] B. Rezek, M. Krátká, A. Kromka, M. Kalbacova, Effects of protein inter-layers on cell–diamond FET characteristics, Biosens. Bioelectron. 26 (2010) 1307–1312, https://doi.org/10.1016/j.bios.2010.07.027.
[46] L. Bacakova, E. Filova, M. Parizek, T. Ruml, V. Svorcik, Modulation of cell adhesion, proliferation and differentiation on materials designed for body implants, Biotechnol. Adv. 29 (2011) 739–767, https://doi.org/10.1016/j.biotechadv.2011.06.004.

8.4. Nanocrystalline diamond electrolyte-gates in field effect transistor for a prolific aptasensing HIV-1 Tat on hydrogen-terminated surface

International Journal of Nanoelectronics and Materials
Volume 13, No. 2, Apr 2020 [295-306]

Nanocrystalline Diamond Electrolyte-Gates in Field Effect Transistor for a Prolific Aptasensing HIV-1 Tat on Hydrogen-terminated Surface

Nurul Atiqah Ahmad[1], Ruslinda A. Rahim[1*], Bohuslav Rezek[3, 4], Alexander Kromka[4], Nur Syakimah Ismail[2], Subash Chandra Bose Gopinath[1], Tibor Izak[4], Václav Procházka[3], Fatin Nabilah Mohd Faudzi[1], Azrul Syafiq Zainol Abidin[1] and Nur Nasyifa Mohd Maidizn[1]

[1]*Institute of Nano Electronic Engineering (INEE), Universiti Malaysia Perlis, Kangar 01000, Perlis, Malaysia.*
[2]*School of Microelectronic Engineering, Universiti Malaysia Perlis, Arau 02600, Perlis, Malaysia.*
[3]*Faculty of Electrical Engineering, Czech Technical University, Czech Republic.*
[4]*Institute of Physics, Academy of Sciences, Czech Republic.*

Received 2 October 2019, Revised 20 January 2020, Accepted 5 February 2020

ABSTRACT

Nanocrystalline diamonds have recently gained great attention to circumvent the current hurdles, with their appealing properties such as high-surface-area to volume ratio, low-background current, wide potential window, biocompatibility, and chemical stability. The nanocrystalline diamonds electrolyte-gated field-effect transistor (NCD-EGFET) can operate directly in solution without involving gate oxides in bringing the hydrogen-tethered moieties and facilitates the p-type surface conductivity. This research investigated on Trans-activator of transcription (Tat) protein; a powerful viral gene activator that plays a pivotal role in the primary stage of the human immunodeficiency virus type 1 (HIV-1) replication. Dose-dependent interactions of HIV-1 Tat on NCD-EGFET-based RNA aptamer sensing surface were monitored and attained the detection down to 10 fM. The linear regression curve with 3σ estimation professed the sensitivity range to be 31.213 mV/log$_{10}$ [Tat Concentration]M and the limit of detection of 6.18 fM. The selectivity analysis of NCD-EGFET was conducted with different proteins from HIV (Nef and p24) and Bovine Serum Albumin. Furthermore, to practice in the clinical application, HIV-1 Tat was spiked into the human blood serum and it displayed the genuine non-fouling interaction with the aptamer. The attained high-performance signal enhancement with nanocrystalline diamond-biosensing aids to circumvent the issues in the current diagnosis.

Keywords: Aptamer, Electrolyte-gated Field Effect Transistor, HIV-1 Tat, Nanocrystalline Diamonds.

1. INTRODUCTION

Human immunodeficiency virus (HIV) has become a widespread disease throughout the world and ~70 million people were found infected. HIV predominantly comprises of 15 types of protein and ssRNA genome with two strands, which make the entire structure of the virus. HIV encodes three enzymes, namely reverse transcriptase, protease, and integrase [1]. The supplementary proteins such as trans-activator of transcription (Tat), viral protein unique (Vpu), regulator of virion (Rev), viral infectivity factor (Vif), negative regulatory factor (Nef), P6, and viral protein r (Vpr) are also present in HIV [2]. HIV disseminates throughout certain body fluids that strikes the defence system, specifically the CD4 cells, also known as T cells. These unique cells help the defence system of the body to eliminate the infections. Throughout time, HIV can demolish most of these cells causing the body unable to fight against the infections and diseases. Different screening test have been developed to identify the existence of HIV in human especially for the

*Corresponding Author: *ruslinda@unimap.edu.my*

early stage of the disease [2]. The developments of various screening test for HIV have attracted many researchers to improve the technique and quality of the device for the early detection of HIV [3].

HIV-1 Tat protein is an important component for viral replication and activation transcription of HIV-1 gene products [4]–[6]. HIV-1 Tat, a small protein consists of 86–101 amino acids which include the N-terminal, C-terminal glutamine-rich regions, basic, cysteine-rich core, and proline-rich. HIV-1 Tat experiences plentiful post-translational modifications like methylation, phosphorylation, ubiquitination, and acetylation [7], which further increase the abundance of HIV-1 Tat synergy with the host proteins by providing HIV-1 Tat with more flexible conformation changes and/or contacting interfaces. It is vital in the transcription of viral RNA and amplifies the quantity of protein produced by linking itself to the viral RNA. Although HIV-1 Tat dominates numerous functions such as controlling the cellular processes by interrelating with different cellular structures [8]–[11]; it is fundamentally included in the transcription of integrated HIV-1 proviruses [12]. In the current research, HIV-1 Tat is chosen as a target protein due to its existence during the early stage of HIV-1 infection. By detecting HIV-1 Tat, the highly risked individuals can detect virus transmission in the early disease stage regularly to reduce the risk of HIV pandemic.

Throughout this research, RNA aptamer was used as a sensing probe for the recognition of HIV-1 Tat (target). RNA aptamer is a single-stranded oligonucleotide which competent of binding to a specific target with high sensitivity, specificity and affinity. Aptamer-target interactions are based on the affinity binding and the non-covalent bonding exists between the aptamer and the target molecule (aptamer-target complex). This interaction can be caused by hydrogen bonding, electrostatic interactions, aromatic stacking, hydrophobic interaction, or van der Waals interactions [13]. The introduction of aptamer as aptasensor has built up several applications in the science, with various advantages such as more invulnerable to regeneration and degradation, hence, binding affinities and specificities can simply be controlled and promoted by rotational design or by molecular immobilization techniques on biochips. It can differentiate among chiral molecules and capable to define a target molecule site with chemical stability at stringent conditions [14]–[16]. On the other hand, merging of molecular biology and nanoelectronics has led to designate a new field known as bioelectronics. The introduction of polycrystalline diamond-based field-effect transistor (FET) as the sensing device for the detection of HIV brings a novelty due to its promising chemical stability, broad potential window, small background current, and biocompatibility [17]. Although few works have been reported on HIV-1 Tat detection, the study of HIV-1 Tat in spiked human on the nanocrystalline diamond was not yet presented.

Nanocrystalline diamond (NCD) is a carbon-based unique material for bioelectronic systems due to its above features and it is a favourable combination for optical, electrical, and mechanical properties. Regardless of the stability NCD, the surface chemistry of the diamond can be easily modified to control its physical properties, for example, surface wettability, electron affinity, and electrical conductivity. Regarding this, the hydrogen-terminated surface (H-terminated) shows a hydrophobic characteristic and displays the p-type induce surface conductivity through an intrinsic diamond. Meanwhile, the oxygen terminated (O-terminated) surface exhibits a hydrophilic and extremely resistive [18]. The prominent reasons to implement the above features into the FET are due to its promising properties such as mass production, miniaturization, standardization, low price, and its flexible configuration for simple measurement [19].

Herein, this study has demonstrated the binding activity of HIV-1 Tat protein with probe RNA aptamer in human blood serum in terms of dose-dependent analysis on hydrogen-terminated nanocrystalline diamond electrolyte-gate FET by electrical performance. It combines both the chemical stability and biocompatibility of nanocrystalline diamond surface under electrolytic condition. Furthermore, this study has shown that nanocrystalline diamond can acts as transducing channel, as it provides a large surface to volume ratio thus improving the performance of FET in terms of sensitivity, selectivity and specificity on HIV-1 Tat detection.

International Journal of Nanoelectronics and Materials
Volume 13, No. 2, Apr 2020 [295-306]

2. MATERIALS AND METHODS

2.1 Materials and Reagents

RNA aptamer used in this study has a split configuration, in which 5'-UCGGUCGAUCGCUUCAUAA-3'-NH_2 as probe aptamer and 5'-GAAGCUUGAUCCCGAA-3' is the aptamer derived as the second strand. Both aptamers were purchased from Trilink Biotechnologies, USA. The recombinant HIV-1 Tat stored at -75°C was purchased from Immuno Diagnostics, Inc. Bovine serum albumin (BSA) was purchased from Sigma Aldrich. AB male human serum was purchased from Nano Life Quest Sdn Bhd. Phosphate buffered saline solution (PBS), sodium saline citrate (SSC) and all other chemicals, unless mentioned, were purchased from Sigma Aldrich. The equipment used in this research was Keithley 6487 picoammeter and Keithley 2400 source meter.

2.2 Fabrication of the Nanocrystalline Diamond Electrolyte Gated Field-Effect Transistor (NCD-EGFET)

Nanocrystalline diamond (NCD) thin films were grown on silicon (Si) substrate for 4.5 hours by a chemical vapour deposition (CVD) process in a microwave ellipsoidal cavity reactor. The gas pressure was set at 30 mbar, microwave power of 1000 W and gas mixture as 1% methane (CH_4) in hydrogen gas (H_2) were used. The deposition temperature was in the range of 550-600°C, which led to the growth of approximately 450 nm thick nanocrystalline diamond film with grain sizes of ~250 nm [20]. NCD thin films were additionally hydrogenated in hydrogen plasma for 10 minutes at 600°C to prompt the surface conductivity giving the H-terminated NCD films. The beginning of the FET fabrication process starts with photolithographic masks were utilized on H-terminated NCD films using a positive MA-15 photoresist to specify three FET channels and three pair of gold patches that serve as source and drain with ohmic contacts of the holes accumulation layer of the FET. The gold patches were conceived by thermal evaporation [10 nm of titanium (Ti) and ~50 nm of gold (Au)] accompanied by the lift-off procedure using acetone. The samples were treated in oxygen radio frequency plasma at 300 W for one minute to achieve the insulating O-terminated areas, which surround the 20 µm wide and 60 µm long stripes H-terminated channels that connecting the source and drain contacts. The samples were cleaned by acetone and the area between contacts and channels was covered with a positive photoresist AR-P-3220 with a thickness of 4 µm. The final photolithographic step generated the aperture of 60 µm × 20 µm to clarify the active gate area.

2.3 Receptor-Target Bio-recognition for Different Concentration Detection and Selectivity of Receptor

The immobilization of chemically-modified RNA aptamer was conducted on the active gated surface of the NCD-EGFET. To trigger the carboxylic functional groups on the sample, every sample was initially treated with a mixture of 0.4 M 1-ethyl-3-(3-dimethylaminopropyl) carbodiimide hydrochloride (EDC) and 0.1 M N-hydroxysuccinimide (NHS) with ratio 1:1 for 1 hour [17], [21]. Then, the first strand of RNA aptamer was diluted with 3× SSC, 0.4 M EDC, and 0.1 M NHS to a final concentration of 10 µM. A 3 µl of the solution was manually drop-casted on the surface of the gate channel and incubated at 38°C for 2 hours in a humidified chamber, followed by a thorough cleansing with PBS. The binding of target HIV-1 Tat with the probe RNA aptamer was done at room temperature for 1 hour with various concentrations of HIV-1 Tat at different time. The concentration of the second strand aptamer used was proportional to the concentration of Tat protein used. After that, Tris–HCl buffer solution was used as a rinsing agent to avoid the nonspecific binding. An 8.3 M urea solution was used to remove the tested HIV-1 Tat from the active gate channel to achieve the regeneration process in order to test dose-dependent HIV-1 Tat. For the selectivity study, three different proteins with 100 pM concentration were used. These proteins were bovine serum albumin (BSA), negative regulatory factor (Nef), and p24. Both Nef and p24 are protein existed in HIV. For the real application of the developed aptasensor, human

serum with 100 times dilution factor was selected to study the effect of HIV-1 Tat binding to RNA aptamer. For this study, 100 nM of HIV-1 Tat was spiked in human serum and the detection procedures were carried out identical to the detection of 100 pM HIV-1 Tat in the standard solution.

3. RESULTS AND DISCUSSION

NCD-EGFET was fabricated to identify the interaction of RNA aptamer and binding activity of HIV-1 Tat protein in standard solution and spiked human serum on the active gate channel of the device. The binding of RNA aptamer on different concentration of HIV-1 Tat in standard solution was studied in details giving the sensitivity and the limit of detection of the device. Following the sensitivity study of the NCD-EGFET, the selectivity and specificity have been conducted to determine the performance of the device towards other biomolecules. In the final part of this paper, the spiking analysis was conducted. HIV-1 Tat was spiked into human blood serum to observe the interference of human blood serum on HIV-1 Tat detection.

3.1 Fabrication of the Nanocrystalline Diamond Electrolyte Gated Field-Effect Transistor (NCD-EGFET)

A fabricated NCD-EGFET device for HIV-1 Tat detection using RNA aptamer is illustrated in Figure 1(a). The NCD-EGFET biosensor detection operates based on the change with the surface charges [22]. The dominant carriers inside a nanocrystalline diamond are holes and the density of surface holes will increase or decrease in respect to the number of biomolecules charges, either positively or negatively charged ions that bind on the surface of active gate channel of NCD-EGFET. So, this characteristic defined a p-type field-effect transistor. As the surface of the gate channel is dipped in the electrolyte solution (PBS), the density carrier of the gate channel was regulated by the field effect of the biomolecules electric charge nearby the solid surface. To prove the functionality of NCD-EGFET, the measurement of I_{ds}-V_{ds} was conducted using an Ag/AgCl as a reference electrode in 1 mM PBS at pH 7.4. Figure 1(b) shows the image of 20 µm width active gate channel, observed under the scanning electron microscope (SEM) at 453× magnification, while Figure 1(c) shows the binding structure of HIV-1 Tat on the H-terminated NCD-EGFET channel with RNA aptamer as sensing probe by the activation of EDC-NHS. The RNA aptamer was immobilized on the active gate channel surface of NCD-EGFET and incubated for 2 hours in a humified chamber at 38°C. Later, HIV-1 Tat was introduced to the probe RNA aptamer accompanied by aptamer-derived second strand. These interactions form a duplex structure of aptamer in the existence of HIV-1 Tat, causing a significant change in the gate potential [21].

International Journal of Nanoelectronics and Materials
Volume 13, No. 2, Apr 2020 [295-306]

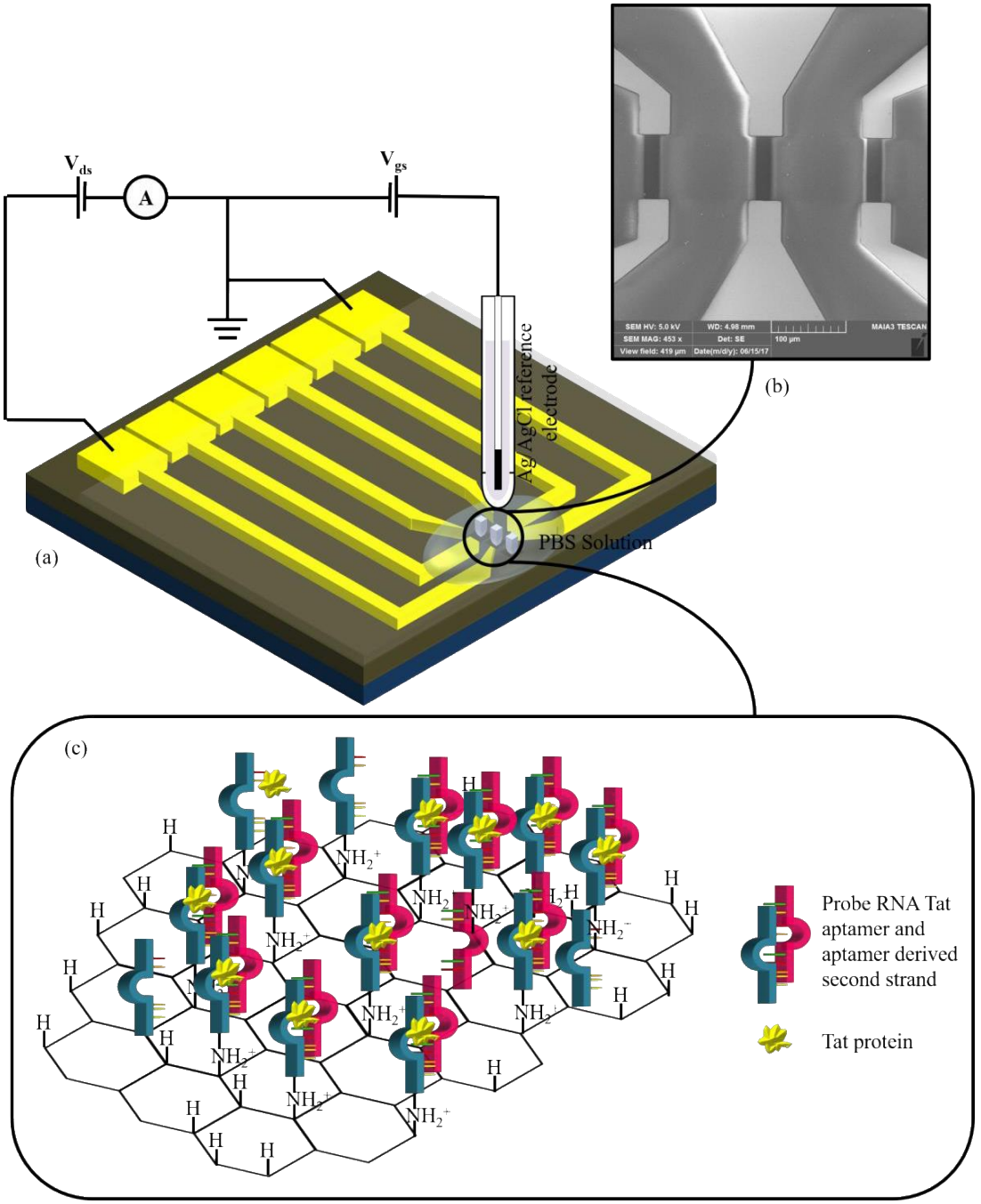

Figure 1. The fabricated NCD-EGFET: (a) in 1 cm × 1 cm dimension with three pair of source and drain contact pads for different gate channel, (b) with H-terminated gate channels of 20 µm width observed under the scanning electron microscope (SEM), and (c) the binding mechanism of HIV-1 Tat protein on NCD-EGFET via RNA aptamer as sensing probe.

3.2 Interaction of HIV-1 Tat on Split Aptamer: Dose-Dependent Binding of HIV-1 Tat and Linear Regression Analysis

The interaction of the HIV-1 Tat on split aptamer was studied in detail by observing the value of gate potential difference (ΔV_{gs}). Figure 2(b) shows a gate potential shifted by 174.80 mV when 100 pM HIV-1 Tat was introduced to RNA probe aptamer on the active gate channel surface of NCD-EGFET. This interaction caused the shift of gate potential towards the negative direction with

respect to the potential charge changes created by the biomolecular interaction. This result confirmed that the NCD-EGFET responses were only observed when specific interaction between recognition molecules (aptamer and HIV-1 Tat) takes place on the active gate surface. Based on previous studies, it has been revealed that HIV-1 Tat rich in positively charged ions [23], [24]. With the isoelectric point (pI) of 9.88, it is verified that HIV-1 Tat is positively charged at pH 7.4. The positively charge HIV-1 Tat affects the current reduction. Due to the reduction of electron transfer from source to drain, the gate potential shifted to a negative direction (M.F. Fatin *et al.,* 2019). Thus, it can be postulated that HIV-1 Tat binding cause the gate potential to deflect in the negative direction for the I_{ds}–V_{gs} transfer characteristic. Since the diagnosis of HIV-1 Tat on the NCD-EGFET biosensor is based on the modification in the charge allocation on the channel surface, the difference in molecular charges was observed, which verified the result obtained in this research. Further, when the RNA aptamers formed the duplex in the presence of HIV-1 Tat (Figure 2(a)), the fixed charge is doubled and the number of reallocation charges increases, thus the system decreases the amplitude of the current. This is primarily due to the repulsion between the positive charges of HIV-1 Tat with the positive hole carriers of the substrate within the sensing area. This work proves that the detection of HIV-1 Tat in standard solution was successfully done and the desired RNA aptamer specifically adapted for HIV-1 Tat interaction.

The binding activity between aptamer-immobilized H-terminated NCD and HIV-1 Tat was also performed in control measurement without using any probe. A 100 pM concentration of HIV-1 Tat was dropped on the bare NCD-EGFET and incubated for 1 hour at room temperature. I_{ds}-V_{gs} measurement was performed to understand the binding activity of HIV-1 Tat on the surface of an active gate channel without RNA aptamer. Only a small change in gate potential (18.52 mV) was obtained and the result was shown in Figure 2(c). The minor changes in the gate potential were insignificant thus indicated that HIV-1 Tat was not fully bound to the surface of NCD-EGFET. Weak binding of HIV-1 Tat was noticed towards the NCD-EGFET surface shows that detection of HIV-1 Tat on NCD-EGFET sample cannot be done without the existence of RNA aptamer, further indicates the specificity.

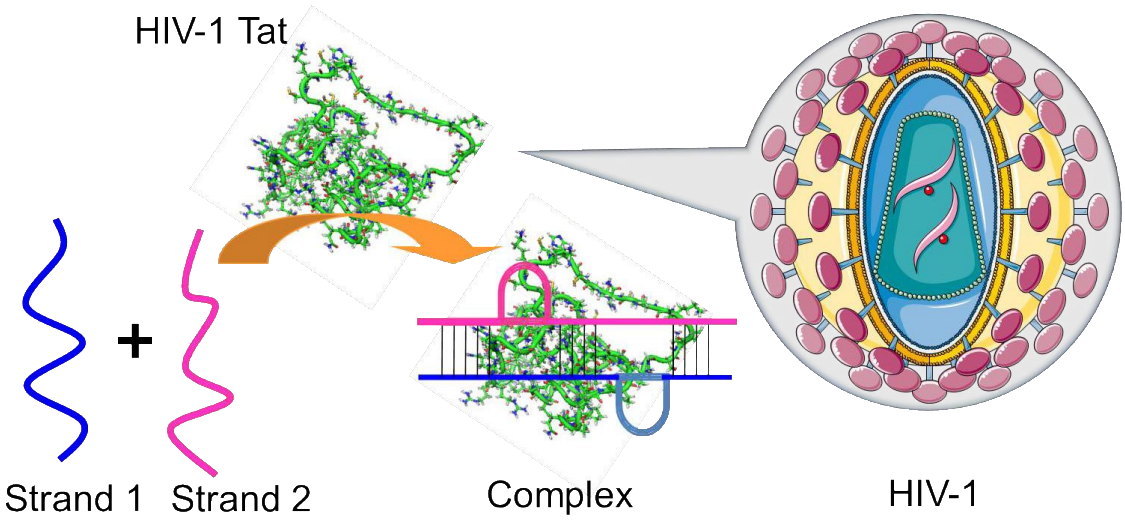

Figure 2(a). Binding mechanism of strand 1 RNA aptamer and aptamer-derived second strand with HIV-1 Tat from HIV-1 virus, forming a complex structure for detection strategy.

International Journal of Nanoelectronics and Materials
Volume 13, No. 2, Apr 2020 [295-306]

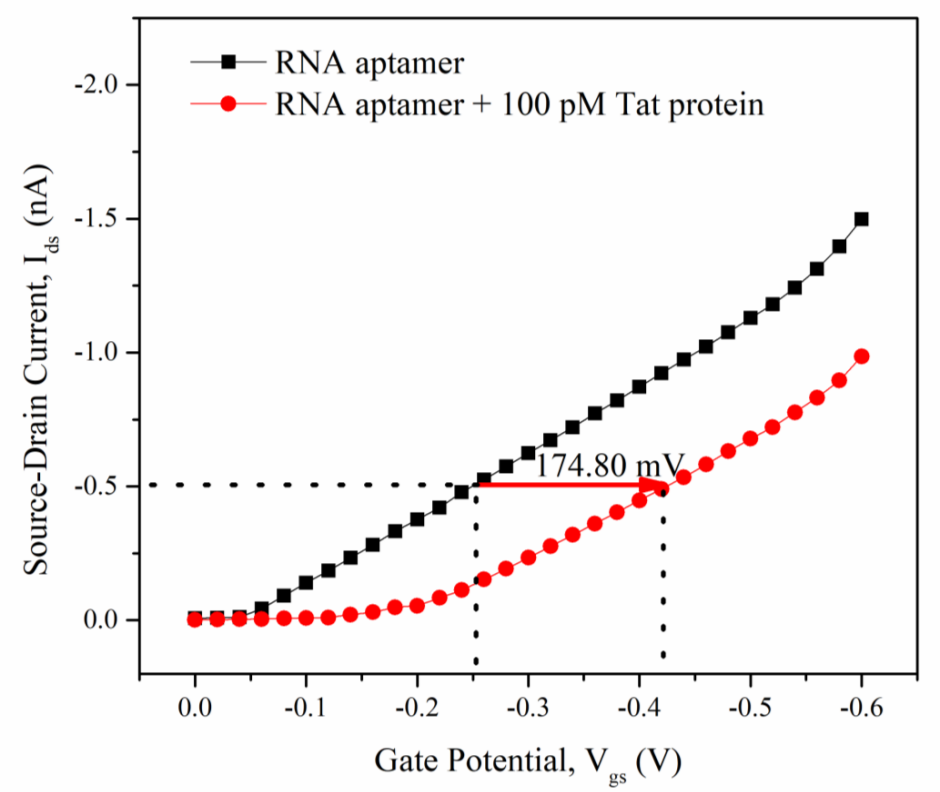

Figure 2(b). The I_{ds}-V_{gs} of NCD-EGFET with and without 100 pM HIV-1 Tat protein, measured in 1 mM PBS at pH 7.4.

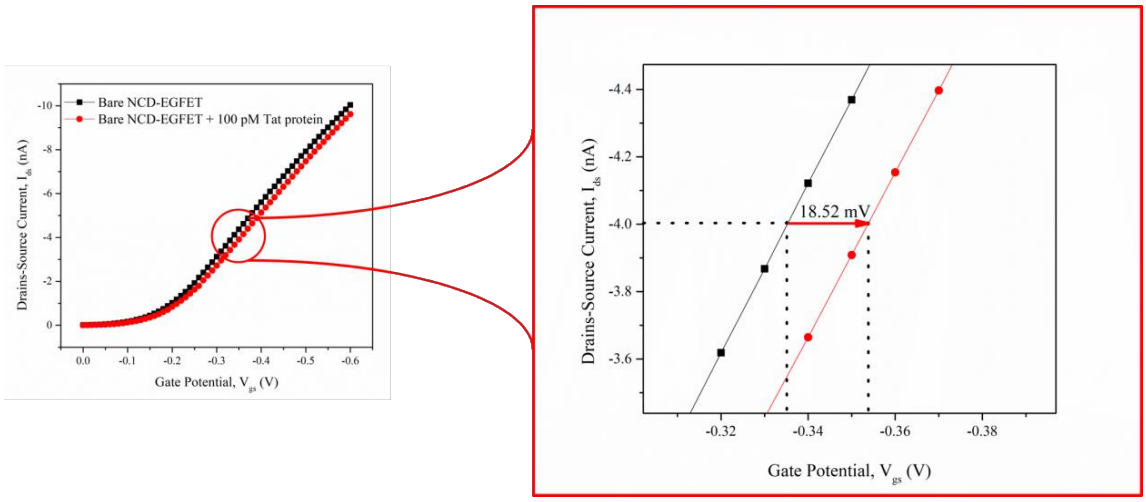

Figure 2(c). The I_{ds}-V_{gs} of NCD-EGFET with and without RNA aptamer immobilization. Small changes in gate potential show the non-specific binding of Tat protein to the active gate channel of the device.

The effect of different concentrations of the HIV-1 Tat was studied in details. Figure 3(a) and (b) displays the gate potential behaviour depending on the concentration of HIV-1 Tat protein. The concentrations of HIV-1 Tat were varied from 100 pM down to 10 fM to identify the interactions on binding activity in the standard solution. The measurement was conducted on the same device to ensure the accuracy of the shifting gate potential. When 10 pM HIV-1 Tat was introduced to the RNA probe aptamer, a 128.90 mV change in gate potential was recorded. On the other hand, a shifting of 117.10 mV was determined after the binding of 1 pM HIV-1 Tat. The shifting of gate

potential keep reducing after 100 fM and 10 fM of HIV-1 Tat were bound on RNA probe aptamer with 62.90 mV and 55.40 mV, respectively. The shifting in gate potential decline with the concentration gradient of HIV-1 Tat owing to the aspect number of charged molecules that reduce dramatically with HIV-1 Tat concentration gradient. The interaction between molecules inside the electrolytes diminished when fewer molecules interacted with the RNA probe aptamer. Furthermore, the lowest concentration for detection, which is the limit of detection (LOD) of HIV-1 Tat was analyzed as in Figure 3(c). The biosensor produced a linear response of relative change in the measured V_{gs} over the logarithmic HIV-1 Tat concentration from 10 fM to 100 pM with the LOD of 6.18 fM, based on calculation from the standard deviation of the response and the calibration curve's slope [26]. According to other researchers, the limit of detection of HIV-1 Tat was recorded at 0.6 nM using multiwall carbon nanotubes-FET based biosensor [27], 1 pM concentration when using SPR enhanced ellipsometry [28] and 10 nM using the calorimetric detection [25]. From the experiment conducted throughout this research, it can prove that the used of NCD based EGFET is much more sensitive towards HIV-1 Tat protein detection compared to other methods and materials. The calibration curve slope in Figure 3(d) was obtained from the linear response of V_{gs} with the increase of HIV-1 Tat concentration was from 10 fM to 100 pM, representing the sensitivity of the device, which is 31.213 mV/$\log_{10}$ [Tat concentration] M.

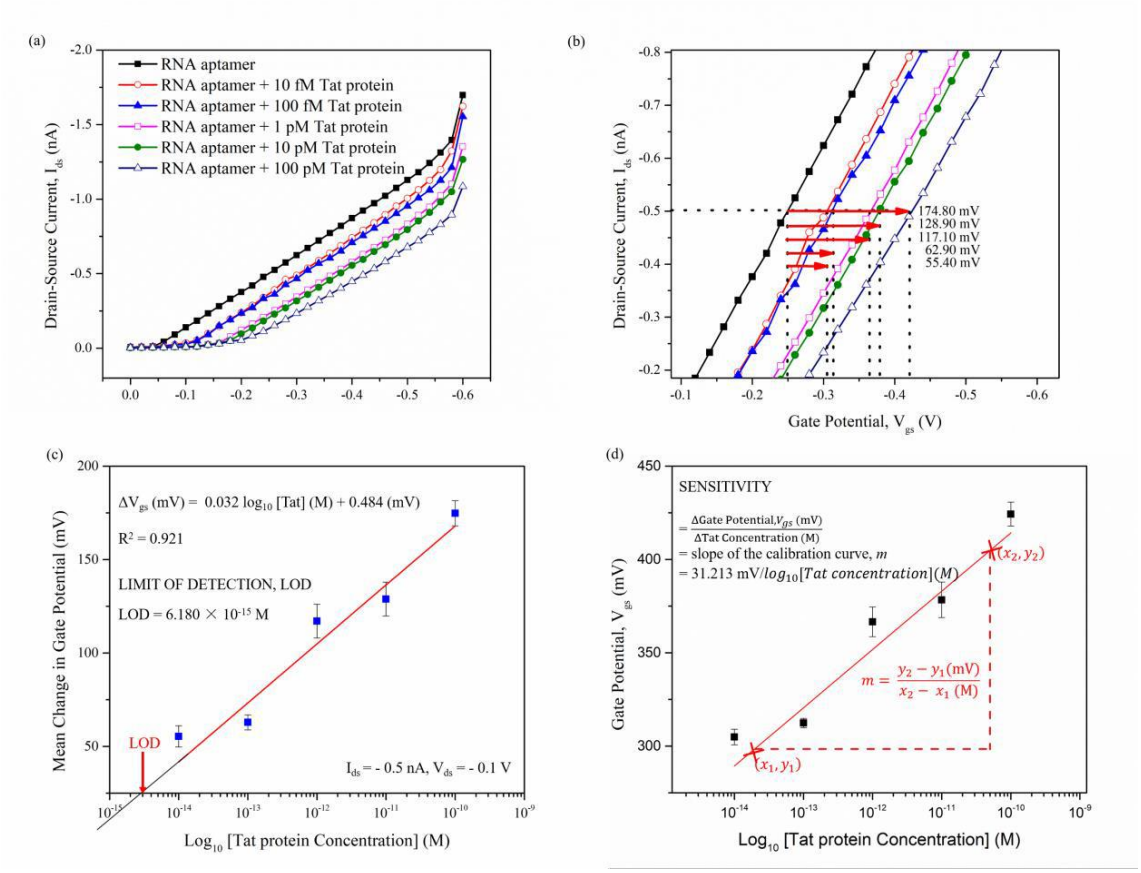

Figure 3. Detection of Tat protein target at different concentration (100 pM to 10 fM) using the NCD-EGFET biosensor at sweep V_{gs} of 0 V - -0.6 V with V_{ds} = -0.1 V. (a) I_{ds}-V_{gs} transfer characteristic at different concentration of Tat protein, (b) Enlarge of I_{ds}-V_{gs} response at different concentration of Tat protein, (c) Calibration curve of the relative change in V_{gs}, shows the LOD, (d) V_{gs} response curve of the biosensor at different Tat protein concentrations, shows the sensitivity of the device.

International Journal of Nanoelectronics and Materials
Volume 13, No. 2, Apr 2020 [295-306]

3.4 Analytical Performance of Nanocrystalline Diamond-Electrolyte Gated Field Effect Transistor

The analytical characteristics of NCD-EGFET biosensor in terms of selectivity and specificity were investigated. The selectivity of protein binding on RNA aptamer was studied in details by using different types of protein, which includes BSA, Nef, and p24. The interactions of these proteins with the RNA aptamer on the gate channel surface during the binding process were identified. The proteins were integrated on the probe RNA aptamer to replace the HIV-1 Tat and performed the experiments independently. First, BSA was integrated on the device followed by Nef and p24. The concentration of proteins tested was standardized at 100 pM.

Based on Figure 4, the shifting in gate potential was observed when biomolecules were integrated to the probe RNA aptamer. During the integration of BSA, the gate potential deflected towards the positive direction by ~38.50 mV. The shifting in gate potential was caused by the lack of BSA binding to the probe aptamer. The interaction was obstructed with the BSA molecules hence there is a hindrance in the binding with the probe [29]. A shifting of ~10.00 mV towards the positive direction was measured during the integration of Nef on the NCD-EGFET. Even though Nef was present in HIV as one of the accessory proteins, the deviation in gate potential was negligible since it was in a positive direction. In contrast, the shifted in gate potential is approximately 11.90 mV towards negative direction when p24 was introduced in the binding analysis. The fluctuation in gate potential was observed since p24 slightly binds to the probe RNA aptamer, and p24 is abundantly found in the early phase of HIV-1. Yet, the result cannot be used as the change in gate potential was insignificant compared to the shifting of gate potential obtained for HIV-1 Tat binding. This result reveals that the probe RNA aptamer is specifically and selectively binding only with HIV-1 Tat.

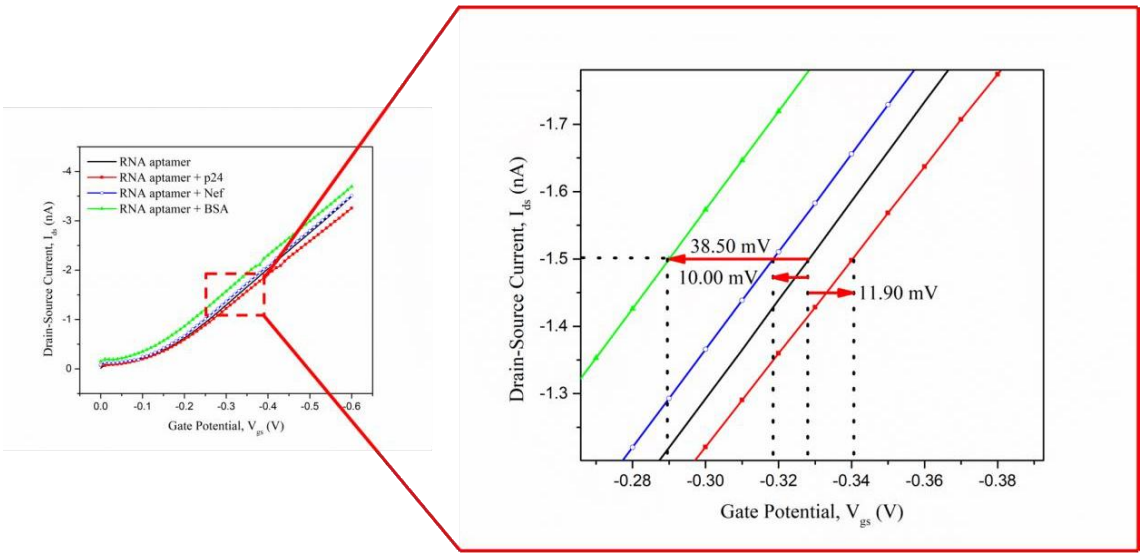

Figure 4. The I_{ds}-V_{gs} of NCD-EGFET in various proteins such as p24, Nef and BSA for the selectivity study. For p24, Nef, and BSA, the gate potential tends to shift no more than 40 mV meanwhile for Tat protein, a 174.80 mV was shifted in gate potential.

3.5 High-Performance Measurement: Spiking Analysis

Additionally, the binding of probe RNA aptamer with HIV-1 Tat in spiked human serum was studied to evaluate the interference effect from human serum in the interaction events and to practice towards the clinical sample analysis. Human serum with 100 times dilution factor was

used as a medium for the HIV-1 Tat. The binding activity was observed by measuring the gate potential shifted when HIV-1 Tat spiked in human serum passed to the RNA aptamer on the active gate channel surface. Human serum alone was used as a control experiment to investigate the binding of human serum to the probe RNA aptamer in the absence of HIV-1 Tat. Figure 5 shows the changes in gate potential on the surface channel of NCD-EGFET with and without HIV-1 Tat in human serum. There is a shift of 34.50 mV in gate potential when clear human serum bound to the RNA aptamer indicating a low interference effect of human serum in the binding event. This result was certified that the human serum contains different non-specific molecules so that a slight non-specific binding occurs during the immobilization process as shown before [30]. As soon as HIV-1 Tat was spiked in the human serum, the change in gate potential shows a significant difference (142.80 mV). The results expressed the specificity of RNA aptamer to HIV-1 Tat. From this work, we could prove that the detection of HIV-1 Tat in human serum was successfully done and the desired RNA aptamer specifically adapted for HIV-1 Tat interaction.

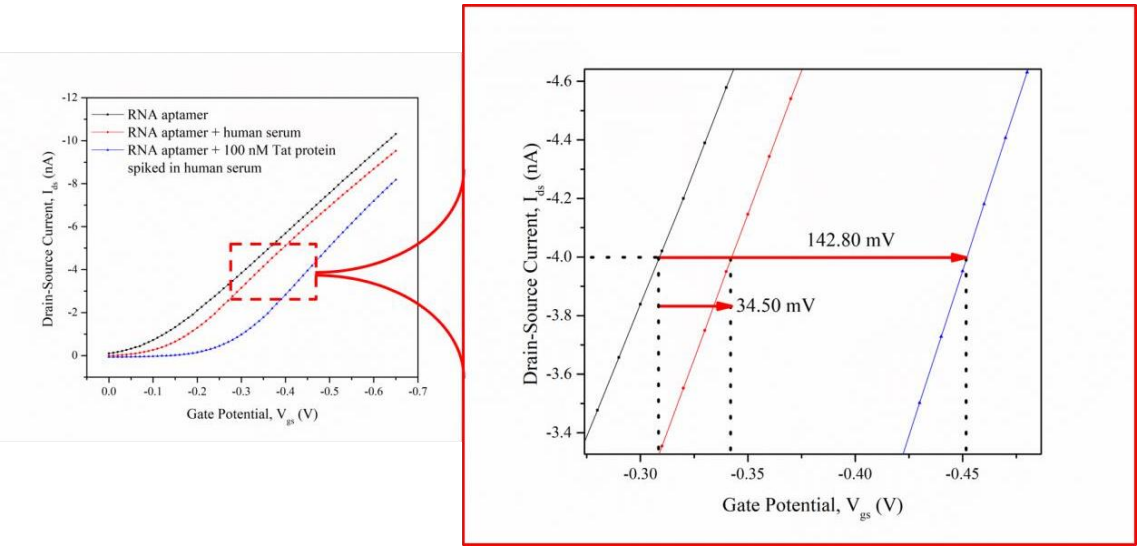

Figure 5. The I_{ds}-V_{gs} of H-terminated NCD-EGFET in human serum with and without the presence of HIV-1 Tat protein. In human serum binding activity, a small change of 34.50 mV was presented while 142.80 mV was observed when HIV-1 Tat protein spiked in human serum.

4. CONCLUSIONS

In summary, this research has successfully determined the interactions of dose-dependent HIV-1 Tat on NCD-EGFET with the limit of detection down to 10 fM. The gate voltage deviated was in a negative direction as the HIV-1 Tat approaches the active gate surface of H-terminated NCD-EGFET channel. The selectivity of RNA aptamer towards various biomolecules was examined and the RNA aptamer was specifically and selectively binds the HIV-1 Tat. The binding of 100 nM HIV-1 Tat to RNA aptamer in human serum was successfully performed by spiking experiment. The sensitivity and selectivity of the device show a successful development of a highly specific biosensor that can be adapted to clinical monitoring of biological diagnosis via nanocrystalline diamond approach for detecting HIV-1 Tat and provides the potential of nanocrystalline diamond bio-interfaces in clinical biosensor applications.

International Journal of Nanoelectronics and Materials
Volume 13, No. 2, Apr 2020 [295-306]

ACKNOWLEDGEMENTS

The authors would like to acknowledge the support from the Prototype Development Research Grant Scheme (PRGS) under a grant number of PRGS/1/2016/STG07/UNIMAP/02/1 from the Ministry of Higher Education Malaysia. This work was also financially supported by the MEYS/ERDF project CZ.02.1.01/0.0/0.0/16_019/00007660 (Solid21). The author also would like to acknowledge the support from Associate Professor Dr Bohuslav Rezek, Associate Professor Alexander Kromka and their team from the Institute of Physics, Czech Republic.

REFERENCES

[1] S.-Y. Rhee *et al.,* "HIV-1 Protease, Reverse Transcriptase, and Integrase Variation," J. Virol. **90**, 13 (2016) 6058–6070.
[2] M. F. Fatin *et al.,* "HIV-1 Tat biosensor: Current development and trends for early detection strategies," Biosens. Bioelectron. **78** (2016) 358–366.
[3] M. A. Lifson *et al.,* "Advances in biosensing strategies for HIV-1 detection, diagnosis, and therapeutic monitoring.," Adv. Drug Deliv. Rev. **103** (2016) 90–104.
[4] A. J. Fulcher & D. A. Jans, "The HIV-1 Tat Transactivator Protein: A Therapeutic Target?," IUBMB Life **55**, 12 (2003) 669–680.
[5] S. Pantano & P. Carloni, "Comparative analysis of HIV-1 Tat variants.," Proteins **58**, 3 (2005) 638–643.
[6] Y. Yamaoki, T. Nagata, T. Mashima, & M. Katahira, "Development of an RNA aptamer that acquires binding capacity against HIV-1 Tat protein: Via G-quadruplex formation in response to potassium ions," Chem. Commun. **53**, 52 (2017) 7056–7059.
[7] S. Pagans, N. Sakane, M. Schnölzer, & M. Ott, "Characterization of HIV Tat modifications using novel methyl-lysine-specific antibodies," Methods **53**, 1 (2011) 91–96.
[8] B. Romani, S. Engelbrecht, and R. H. Glashoff, "Functions of Tat: The versatile protein of human immunodeficiency virus type 1," J. Gen. Virol., vol. 91, pp. 1–12, 2010.
[9] A. Bagashev and B. E. Sawaya, "Roles and functions of HIV-1 Tat protein in the CNS: an overview.," Virol. J., vol. 10, p. 358, 2013.
[10] Y. R. Musinova, E. V. Sheval, C. Dib, D. Germini, & Y. S. Vassetzky, "Functional roles of HIV-1 Tat protein in the nucleus," Cell. Mol. Life Sci. **73**, 3 (2016) 589–601.
[11] A. T. Das, A. Harwig, & B. Berkhout, "The HIV-1 Tat protein has a versatile role in activating viral transcription.," J. Virol. **85**, 18 (2011) 9506–16.
[12] M. J. Jean, D. Power, W. Kong, H. Huang, N. Santoso, & J. Zhu, "Identification of HIV-1 tat-associated proteins contributing to HIV-1 transcription and latency," Viruses **9**, 4 (2017) 1–12.
[13] C. Acquah, M. K. Danquah, J. L. S. Yon, A. Sidhu, & C. M. Ongkudon, "A review on immobilised aptamers for high throughput biomolecular detection and screening," Anal. Chim. Acta **888** (2015) 10–18.
[14] S. Song, L. Wang, J. Li, C. Fan, & J. Zhao, "Aptamer-based biosensors," TrAC - Trends Anal. Chem. **27**, 2 (2008) 108–117.
[15] B. Strehlitz, N. Nikolaus, & R. Stoltenburg, "Protein detection with aptamer biosensors," Sensors **8**, 7 (2008) 4296–4307.
[16] Y. X. Wang, Z. Z. Ye, C. Y. Si, & Y. Bin Ying, "Application of aptamer based biosensors for detection of pathogenic microorganisms," Fenxi Huaxue/ Chinese J. Anal. Chem. **40**, 4 (2012) 634–642.
[17] A. Rahim Ruslinda, K. Tanabe, S. Ibori, X. Wang, & H. Kawarada, "Effects of diamond-FET-based RNA aptamer sensing for detection of real sample of HIV-1 Tat protein," Biosens. Bioelectron. **40**, 1 (2013) 277–282.
[18] T. Ižák, V. Procházka, T. Sakata, B. Rezek, & A. Kromka, "Real-time Monitoring of Cell Activities by Diamond Solution-gated Field Effect Transistors," Procedia Eng. **168** (2016) 469–472.

[19] K. Song & H. Kawarada, "Characteristics of Diamond Electrolyte Solution-Gate FETs (SGFETs) and Applications to Biosensor," New Diam. Front. Carbon **1** (2005) 325–335.
[20] V. Procházka, M. Cifra, P. Kulha, T. Ižák, B. Rezek, & A. Kromka, "Influence of non-adherent yeast cells on electrical characteristics of diamond-based field-effect transistors," Appl. Surf. Sci. **395** (2017) 214–219.
[21] A. Rahim Ruslinda, X. Wang, Y. Ishii, Y. Ishiyama, K. Tanabe, & H. Kawarada, "Human immunodeficiency virus trans-activator of transcription peptide detection via ribonucleic acid aptamer on aminated diamond biosensor," Appl. Phys. Lett. **99**, 12 (2011) 2–5.
[22] V. Procházka, T. Ižák, & A. Kromka, "Influence of Buffers and Culture Media on Diamond Solution-Gated Field Effect Transistors Regarding Stability and Memory Effect," in Proceedings 1st Eurosensor, Paris **1**, 4 (2017) 525.
[23] S. Shojania & J. D. O'Neil, "HIV-1 Tat is a natively unfolded protein: The solution conformation and dynamics of reduced HIV-1 Tat-(1-72) by NMR spectroscopy," J. Biol. Chem. **281**, 13 (2006) 8347–8356.
[24] R. Yamamoto, M. Katahira, S. Nishikawa, T. Baba, K. Taira, & P. K. R. Kumar, "A novel RNA motif that binds efficiently and specifically to the Tat protein of HIV and inhibits the trans-activation by Tat of transcription in vitro and in vivo," Genes to Cells **5** (2000) 371–388.
[25] F. M.F. *et al.,* "Co-ordinated split aptamer assembly and disassembly on Gold nanoparticle for functional detection of HIV-1 tat," Process Biochem. **8**, 5 (2019) 55.
[26] A. Shrivastava & V. B. Gupta, "Methods for the determination of limit of detection and limit of quantitation of the analytical methods," Chronicles Young Sci. **2**, 1 (2011) 21–25.
[27] M. F. Fatin, A. Rahim Ruslinda, S. C. B. Gopinath, & M. K. M. Arshad, "High-performance interactive analysis of split aptamer and HIV-1 Tat on multiwall carbon nanotube-modified field-effect transistor," Int. J. Biol. Macromol. **125** (2019) 414–422.
[28] M. O. Caglayan & Z. Üstündağ, "Spectrophotometric ellipsometry based Tat-protein RNA-aptasensor for HIV-1 diagnosis," Spectrochim. Acta Part A Mol. Biomol. Spectrosc. **227**, 117748 (2019).
[29] S. Cheng *et al.,* "Field effect transistor biosensor using antigen binding fragment for detecting tumor marker in human serum," Materials (Basel). **7**, 4 (2014) 2490–2500.
[30] S. Wustoni, S. Hideshima, S. Kuroiwa, T. Nakanishi, Y. Mori, & T. Osaka, "Label-free detection of Cu (II) in a human serum sample by using a prion protein-immobilized FET," Analyst **140**, 19 (2015) 6485–6488.